Doctoral Dissertation
Doctoral Program in Bioengineering and medical and surgical sciences
(33th Cycle)

Muscle Synergy Assessment during Cyclic and Non-Cyclic Movements

Methodological Issues and Application-oriented Studies

Marco Ghislieri

* * * * * *

Supervisors
Prof. M. Knaflitz, Supervisor
Prof. V. Agostini, Co-Supervisor

Doctoral Examination Committee:

Prof. Madeleine Lowery, Referee, University College Dublin
Prof. Andrea D'Avella, Referee, Università degli Studi di Messina
Prof. Silvia Conforto, Università degli Studi Roma Tre

Politecnico di Torino
July 12, 2021

I hereby declare that the contents and organization of this dissertation constitute my own original work and do not compromise in any way the rights of third parties, including those relating to the security of personal data.

Marco Ghislieri

Marco Ghislieri

Turin, July 12, 2021

Summary

Human locomotion and balance control are essential activities during daily life. Human locomotion is one of the most complex motor tasks, due to the multiple degrees of freedom of the musculoskeletal system, the several biomechanical functions carried out during each gait cycle, and the high intra-cycle variability of the muscle activation intervals. Balance control (e.g., single-leg stance) is also important during daily living activities, as a single task as well as a component of other more complex tasks, such as walking and running. It is a simple but challenging condition for balance control and for this reason it is widely used for training and rehabilitation programs.

Due to the complexity of the musculoskeletal system, the central nervous system adopts different strategies to efficiently and accurately perform movements. Even if there is no consensus regarding the neural strategies adopted by the central nervous system to perform movements, the muscle synergy theory is the most widely used in literature. According to this theory, the central nervous system controls the activation level and the synchrony of small groups of muscles, rather than controlling independently every single muscle involved in the movement.

The present doctoral thesis aims at proposing, validating, and applying novel methods for extracting muscle synergies that can be applied to achieve deeper insights into the neuromuscular control of human locomotion and balance control tasks.

Considering human locomotion, two novel approaches for extracting muscle synergies and selecting the optimal number of muscle synergies are proposed and validated considering both physiological and pathological sample populations. The novel sEMG pre-processing approach, based on the extraction of principal activation intervals before muscle synergy extraction, allows a more interpretable assessment of the modular organization of the central nervous system during

walking without any loss of information with respect to the standard pre-processing approaches. Similar results are obtained considering both physiological and pathological (patients affected by Parkinson's disease) sample populations. Moreover, the novel approach for selecting the optimal number of muscle synergies, based on a multi-criteria decision analysis model (ELECTRE III), reveals higher performance with respect to the standard threshold-dependent approaches proposed in literature, considering both simulated and real sEMG data.

Considering balance control, instead, the modular organization during single-leg stance is assessed by means of a novel approach based on the segmentation of the sEMG time-instants relative to a "*well-balanced*" single-leg stance or an "*unbalanced*" single-leg stance to be used as inputs of the muscle synergy extraction algorithm. The consolidated approach is then applied to the analysis of the modular organization of single-leg stance with and without visual feedback considering a healthy sample population. The modular organization, assessed through the novel approach, slightly changes when considering the eyes-closed condition, revealing a reorganization of the activation levels and balance control strategies.

Table of Contents

Chapter 1

Introduction

1.1 Human Motor Control

Human motor control is an outstandingly complicated system. Due to several neurophysiological (e.g., motoneurons and neuromuscular junctions), anatomical (e.g., muscles and joints), and kinematic (e.g., trajectories, accelerations, and velocities) variables that determine the execution of the same movement [1], the human motor system presents countless degrees of freedom (more than 1000). Thus, several combinations of neurophysiological, anatomical, and kinematic variables can be used to achieve the same movement, suggesting many possible ways to perform the same motor task (e.g., walking or running).

In 1967, the degrees of freedom problem was assessed for the first time by Nikolai Aleksandrovich Bernstein in his book "*The co-ordination and regulation of movements*" [1]. Bernstein formally described for the first time this problem by stating that:

"The basic difficulties for co-ordination consist precisely in the extreme abundance of degrees of freedom, with which the central nervous system [...] is not at first in a position to deal".

Moreover, he gave a very modern definition of the coordination concept that is still one of the supporting pillars of modern motor control theories:

"The co-ordination of a movement is the process of mastering redundant degrees of freedom of the moving organ, in other words its conversion to a controllable system. More briefly, co-ordination is the organization of the control of the motor apparatus".

In our body, the task of dealing with the motor system redundancy (i.e., multiple solutions for performing the same movement) is left to the Central Nervous

System (CNS). The CNS is composed of the brain and the spinal cord (**Figure 1.1**). The latter ranges from the lower region of the brain (i.e., the medulla) to the lumbar segments of the vertebral column, which encloses and protects the spinal cord. The human spinal cord is composed of 31 different segments which give rise to paired spinal nerves joined in the anterior and posterior roots. The posterior roots contain afferent fascicles and are characterized by the presence of spinal ganglia, while anterior roots contain the axons of those motor neurons (motor effector nerves) that have their bodies in the ventral grey horns of the spinal cord. Finally, the interneurons create reflex arcs between sensory and motor nerves, modulating the information between the anterior and the posterior roots. **Figure 1.1** shows a graphical representation of the central nervous system and the spinal reflex arc.

More specifically, 31 pairs of spinal nerves are present in the spinal cord: 8 pairs of cervical nerves (from C1 to C8), 12 pairs of thoracic nerves (from T1 to T12), 5 pairs of lumbar nerves (from L1 to L5), 5 pairs of sacral nerves (from S1 to S5), and 1 pair of coccygeal nerves. Cervical nerves are used to control muscles involved in respiration and the movement of the head, neck, and arms. Thoracic

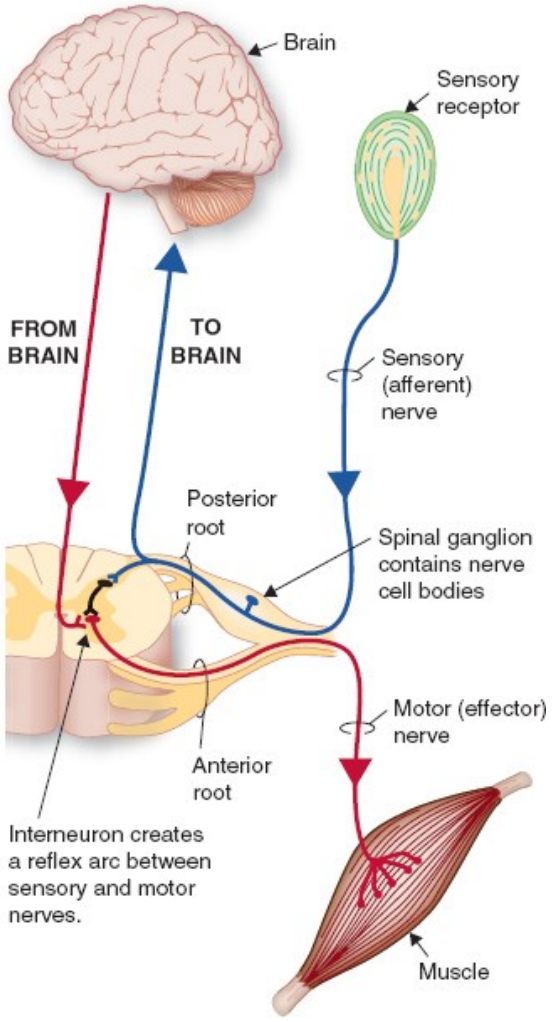

Figure 1.1 Schematic representation of the central nervous system and the spinal reflex arc. Sensory receptor generates an input signal which travels through the afferent pathway from the sensory receptor to the posterior root of the spinal cord. The motor output, instead, travels through the efferent pathway from the anterior root of the spinal cord to the muscle. The connection between the afferent (input) and efferent (output) pathways is mediated by the interneuron.

nerves are used to control muscles involved in finger and trunk movements. Lumbar and sacral nerves are used to control locomotion, intestinal, and reproductive functions.

Accordingly, how our CNS manages such complexity and selects only one solution (i.e., a combination of neurophysiological, anatomical, and kinematic variables) from all the other possibilities? How can we rapidly and accurately perform movements having an outstanding amount of degrees of freedom to choose from? What if our CNS, instead of choosing over multiple degrees of freedom, reduces the motor control complexity by using a few combinations of low-dimensional elements?

1.2 Muscle Synergy Theory

Theoretical Background

Despite several theoretical models (e.g., spinal force field, neuromotor synergies, and unit burst generators) [2–5] have been proposed in literature over the last decades, the muscle synergy theory is the one that achieved the greatest consensus across researchers [6]. According to this theory, the CNS controls the activation level (spatial component) and the synchrony (temporal component) of all the muscles involved in a specific movement through the combination of a small number of low-dimensional elements (called muscle synergies), rather than controlling independently every single muscle. Moreover, some muscle synergies have been demonstrated to be task-specific, while others may be shared among different motor behaviors, such as walking and running [7].

Figure 1.2 shows a schematic representation of the muscle synergy theory. The CNS manages the multiple degrees of freedom of the motor system by controlling small sets of muscles (called muscle synergies), rather than controlling every single muscle involved in a specific movement, separately.

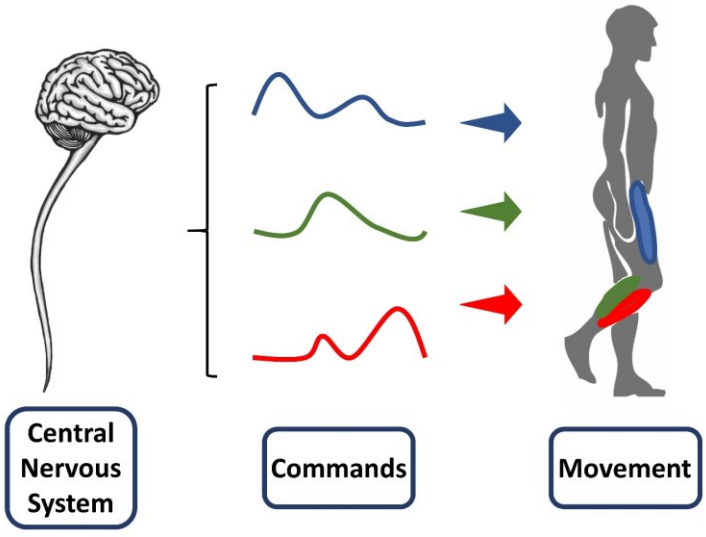

Figure 1.2 Schematic representation of the muscle synergy theory.

More specifically, two different definitions of the muscle synergy theory have been proposed in literature: the "*time-invariant*" muscle synergies and the "*time-varying*" muscle synergies [8]. Considering the "*time-invariant*" muscle synergies, all the muscles within a specific muscle synergy are synchronously activated (i.e., there is no temporal modulation of the muscle activation levels), while, considering the "*time-varying*" muscle synergies, each muscle within a specific muscle synergy shows a temporal modulation over the task duration. In the present thesis, only the "*time-invariant*" muscle synergy definition was considered, allowing for the assessment of the temporal patterns of each muscle synergy.

Even if there is no consensus on the neural origin of muscle synergies [7,9,10], several studies have supported the muscle synergy theory in several motor tasks, both in animals and humans. Considering animal studies, several authors have demonstrated a modular organization in the spinal cords and brainstems (in particular in the medulla) of rats, frogs, and cats [2,6,11–14]. These studies have shown that the spinal cord and brainstem express most of the muscle synergies for motor behavior [3,15]. However, the job of activating and coordinating these low-level motor structures (i.e., weight vectors) is left to the primary motor cortex and other non-primary motor areas of the brain, such as the supplementary motor cortex and premotor cortex [3]. These high-level motor structures (i.e., activation coefficients) may contribute to the activation and coordination of the low-level motor structures by selecting the best subset of muscle synergies for the execution of a specific motor task.

Considering human studies, the assessment of patients affected by neuromuscular or neurodegenerative diseases has contributed to the understanding of muscle synergies in humans, revealing results that are in line with those found considering animals. In particular, mildly-to-moderate impaired stroke survivors with motor cortical lesions have shown, during voluntary arm movements, similar muscle synergies between the affected and the unaffected arm, suggesting the preservation of the low-level motor structures (i.e, weight vectors) [16]. However, differences between the affected and the unaffected arm have been detected in the temporal coordination of the muscle synergies, suggesting the presence of disrupted high-level motor structures (i.e., activation coefficients) due to stroke-related lesions [16].

The effectiveness of the muscle synergy theory in modeling the human modular organization of the CNS during different motor tasks has been demonstrated in several studies and research areas, such as clinics, robotics, and sport [17,18]. Among all the possible motor tasks, human locomotion is one of the most widely studied movement to assess muscle synergies in humans. Several are the reasons explaining why human locomotion is the most widely investigated motor task:

- the high number of muscles and joints involved
- the biomechanical functions carried out during each gait cycle
- is one of the most important Activities of Daily Living (ADL)
- it is easier with respect to other movements thanks to its cyclic nature
- the high cycle-by-cycle variability of the muscle activation intervals

- it can be easily performed by patients, children, and elderly that are able to independently walk without walking aids or external supports.

According to several studies, human locomotion can be modeled by a small set of muscle synergies characterized by specific biomechanical functions [19–22]. Besides inter-subject variability, the number of muscle synergies extracted and their biomechanical functions may vary depending on the type and number of muscles considered [23], the sEMG pre-processing techniques, and the factorization algorithm implemented. Nevertheless, the number of muscle synergies characterizing human locomotion is usually found equal to 4 or 5 [19,24].

Moreover, the muscle synergy theory has been recently used to gain a deeper understanding of human postural control [25–27]. The control of balance requires sensorimotor transformations that allow CNS to rapidly interpret multiple sensory input signals from all segments of the body to produce context-dependent muscle activation patterns that stabilize the body. According to several studies, the variations in muscle activation patterns evoked in response to different "controlled" perturbations (e.g., support-surface movements in the horizontal plane) could be described by a limited set of muscle synergies [25–29]. Muscle synergies that contribute to balance control have been demonstrated to be highly consistent across different balance tasks and levels of difficulty [26,30,31], suggesting that increasing the task complexity there should be only slight modifications to the basic motor control strategies involved in postural balance control. Depending on the type and the number of muscles acquired and the factorization algorithm implemented, the number of muscle synergies extracted during postural control ranges between 4 and 6.

Numerical Approaches

Muscle synergies are usually extracted from surface electromyographic (sEMG) signals acquired, during a specific motor activity, from a set of muscles that are mainly involved in the analyzed movement [6]. The factorization approach aims at identifying common sEMG patterns recorded from multiple muscles during specific motor activity.

Figure 1.3 shows the schematic representation of the muscle synergy extraction process. **Figure 1.3A** represents the sEMG signals acquired during a specific motor activity, e.g., walking, while **Figure 1.3B** shows the weight vectors and the activation coefficients extracted from the sEMG signals through factorization approaches. Finally, **Figure 1.3C** represents the activation coefficients and weight vectors that are used by the CNS to generate a specific motor activity (as described in **Figure 1.3A**).

In the last years, the modular organization of the CNS has been modeled as the linear combination of synergies as weight vectors in the space of muscle activations as defined by the following equation [32,33]:

$$M(t) = \sum_{k=1}^{N} C(t)_k \cdot W_k + e \qquad \textbf{(1.1)}$$

where $M(t)$ is a matrix containing the original sEMG signals acquired from the observed muscles at a specific time point (t) [8], N is the number of synergies, W_k is a time-independent vector of non-negative weights (called weight vector [34]), $C(t)_k$ is a time-dependent set of non-negative muscle activation coefficients (called activation coefficients [34]), and e is the model reconstruction error [6]. According to this model, high-dimensional data, such as sEMG signals acquired from multiple muscles (**Figure 1.3A**), can be compactly represented by the linear combination of low-dimensional elements (i.e., weight vectors and activation coefficients) (**Figure 1.3B**).

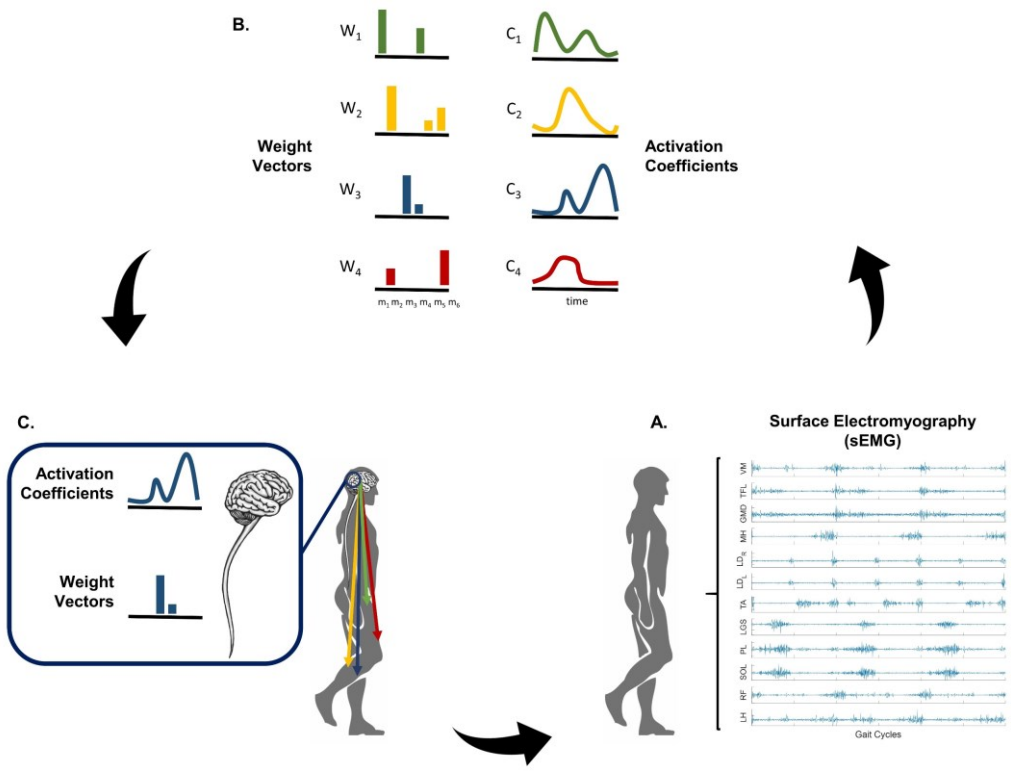

Figure 1.3 Schematic representation of the muscle synergy extraction process.

Several factorization methods for muscle synergy extraction have been proposed in literature. Some of the most widely used methods are the Principal Component Analysis (PCA), the Independent Component Analysis (ICA), the inverse Gaussian, and the Non-Negative Matrix Factorization (NNMF) [4,6,17,32,33,35–40]. The comparison among different factorization approaches for muscle synergy extraction reveals a high similarity in the computed muscle synergies [32,41]. However, since the nature of muscle activation is undeniably non-negative, the Non-Negative Matrix Factorization (NNMF) is one of the most widely used factorization approaches, as it does not allow for negative values.

According to the original definition of the NNMF approach by Daniel D. Lee and Sebastian H. Seung [41], a matrix of observations V can be decomposed in the product of two non-negative matrixes W and C as it follows (**1.2**):

$$V_{m\times t} \approx V_R = W_{m\times r}\, C_{r\times t} \qquad \textbf{(1.2)}$$

where V_R represent the model reconstruction of the original observation matrix V containing the sEMG data, W is a matrix of dimension $m \times n$, and C is a matrix of dimension $n \times t$, with m being the number of observed muscles, t the number of recorded time-instants, and r the rank of factorization (i.e., the number of muscle synergies) [41].

Figure 1.4 shows a schematic representation of sEMG data factorized using the NNMF approach. The matrix of observations V is graphically represented for six different muscles. Then, V can be approximated (V_R) through the linear combination of W (weight vector matrix) and C (activation coefficient matrix). Since the weight vectors are time-independent constants, W is usually represented through a bar diagram. Instead, since the activation coefficients describe the temporal modulation of the muscle synergies, C is usually represented as time-dependent curve. By multiplying and summing synergy-by-synergy the elements of W and C, it is then possible to reconstruct the matrix of observations V (representing the original sEMG data).

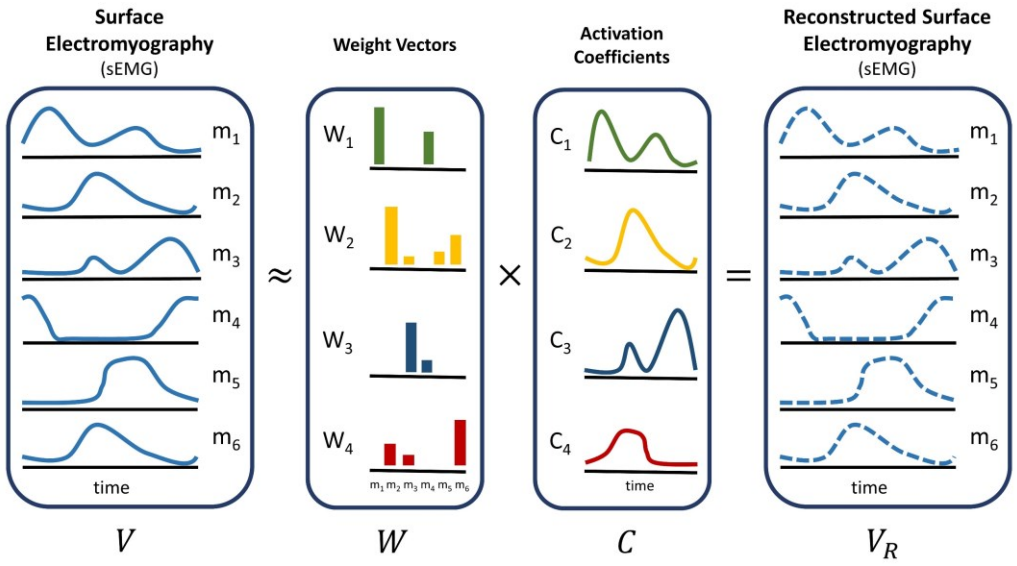

Figure 1.4 Schematic representation of sEMG data factorized through Non-Negative Matrix Factorization (NNMF) approach. Muscle activations of six different muscles (***V***) are compactly represented with four muscle synergies. Each weight vector (***W***) describes the time-independent contribution of each muscle to a specific muscle synergy. Each activation coefficient (***C***), instead, describes the time-dependent modulation of a specific muscle synergy. The multiplication of W and C gives an approximate reconstruction of the original sEMG data (***V***).

More specifically, the NNMF approach is an iterative process that aims at computing the W and C values that minimize the model reconstruction error (e). This optimization problem is solved by the NNMF approach by minimizing a cost function for measuring the divergence between the matrix of observations (V) and

the reconstructed matrix of observations (V_R) that was originally defined by Lee and Seung [42]. One of the most commonly used cost functions is the squared error (or Frobenius Norm), defined as follows:

$$F(W, C) = \|V - WC\|_F^2 \quad \textbf{(1.3)}$$

where V represents the observation matrix, W represents the weight vector matrix, and C the activation coefficient matrix.

An important consideration on factorization approaches is that, since none of them can automatically define the best factorization rank r (i.e., the optimal number of muscle synergies necessary to reconstruct the original sEMG data), a further step is needed to define the factorization rank that best models the original matrix of observations. To assess the reconstruction quality of the extracted muscle synergies, two metrics have been commonly used in literature: the Variance Accounted For (VAF) and the coefficient of determination R^2. These metrics indicate to what extent the reconstructed sEMG data (obtained by multiplying W and C matrixes) are similar to the acquired sEMG signals (V). Both metrics are defined as follows:

$$VAF = \left(1 - \frac{RSS}{SST}\right) \cdot 100 = \left(1 - \frac{\sum_{i=1}^{n}(y_i - \hat{y}_i)^2}{\sum_{i=1}^{n}(y_i)^2}\right) \cdot 100 \quad \textbf{(1.4)}$$

$$R^2 = \left(1 - \frac{RSS}{SST}\right) \cdot 100 = \left(1 - \frac{\sum_{i=1}^{n}(y_i - \hat{y}_i)^2}{\sum_{i=1}^{n}(y_i - \bar{y}_i)^2}\right) \cdot 100 \quad \textbf{(1.5)}$$

where RSS represents the Residual Sum of Squares (or the sum of squared errors), SST the Sum of Squares Total (or the total sum of squares), y_i the observed data, $\bar{y}_i$ the average of the observed data, and $\hat{y}_i$ the estimate of the observed data through the factorization algorithm. Therefore, both metrics quantify the fraction of data variation accounted for by the muscle synergy reconstruction, but they differ in the data variation definition used for their computation. Considering R^2 metric, the data variation is computed with respect to the mean, while, for the VAF metric, the mean is not subtracted before data variation computation and, thus, the data variation is computed with respect to zero. High values of VAF or R^2 (i.e., close to 100%) indicate an accurate reconstruction of the original sEMG data, while low values (i.e., close to 0%) indicate that muscle synergies do not explain a large part of the sEMG variance. The minimum number of muscle synergies necessary to reconstruct the original sEMG data is then selected by analyzing the plot of the VAF (or R^2) versus all the tested number of muscle synergies (called VAF or R^2 curve) [16,23,32,43–47]. One of the most widely used criteria is the selection of the first point where the VAF or R^2 curve reaches a threshold that is commonly set equal to 90% [24,43,44,46].

Figure 1.5 shows an example of non-negative matrix factorization outcomes extracted from sEMG signals of a healthy subject during walking, where non-negative weight vectors are represented through bar diagrams and activation coefficients through curves. A large number of muscle activities (i.e., 12 muscle activities) can be modeled by a lower number of activation coefficients (C) and

weight vectors (W). In particular, during walking, foot plantar flexors (e.g., Lateral Gastrocnemius, Peroneus Longus, and Soleus) are used for propulsion in the second part of the stance phase, when their weight (or contribution) is highest (i.e., W1 in **Figure 1.5**). However, during the swing phase, their activity is not as "important" and thus their contribution is close to zero (i.e., W2, W3, W4, and W5 in **Figure 1.5**).

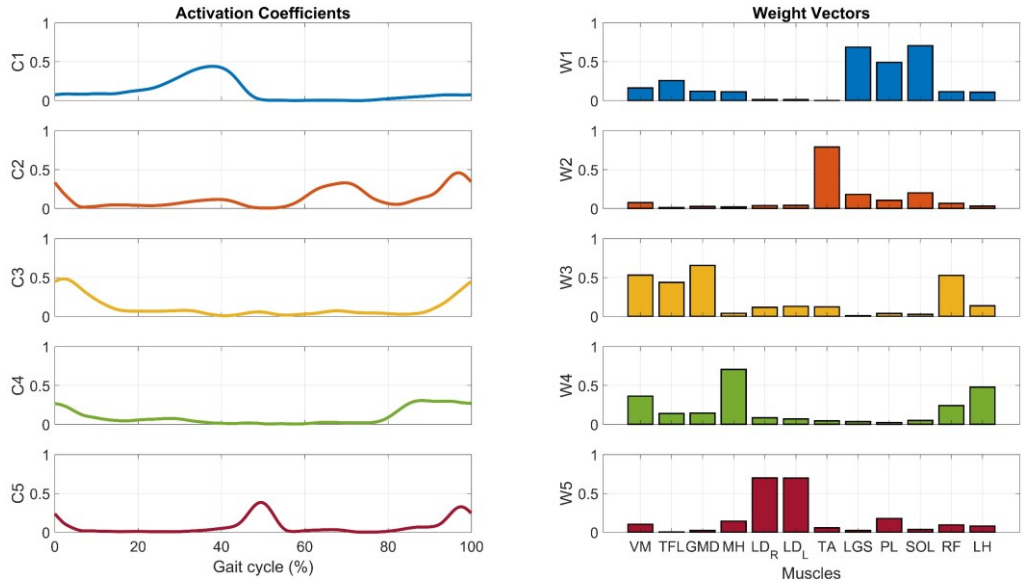

Figure 1.5 Example of muscle synergies extracted via Non-Negative Matrix Factorization (NNMF) from a set of muscles of a healthy subject during walking. Weight vectors ($\boldsymbol{W}$) are represented through bar diagrams on an amplitude-normalized y-axis, while activation coefficients ($\boldsymbol{C}$) are represented through curves on an amplitude-normalized y-axis. Muscle abbreviations: LD_R = right Longissimus Dorsii, LD_L = left Longissimus Dorsii, TFL = Tensor Fasciae Latae, GMD = Gluteus Medius, RF = Rectus Femoris, LH = Lateral Hamstring, MH = Medial Hamstring, VM = Vastus Medialis, LGS = Lateral Gastrocnemius, PL = Peroneus Longus, SOL = Soleus, and TA = Tibialis Anterior.

Another important consideration on factorization approaches is that each of them can be applied in many different ways and their outputs may vary depending on the initial data conditions. For example, several NNMF algorithms have been proposed in the last years based on different mathematical models [41,48]. Additionally, the way initial random values of the NNMF approach are selected plays a role in the number and quality of the calculated muscle synergies [37].

The number and choice of the muscles to be acquired, the number of task repetitions, and the necessary sEMG pre-processing steps before factorization are other factors that can strongly influence the factorization output. Several studies have provided methodological recommendations to allow a more comprehensive muscle synergy analysis and guarantee comparability of the results [23,36,38,39,44,49–53]. The study by Steele *et al.* [23] demonstrated that the number and the structure of muscle synergies are dependent upon the number and choice of muscles included in the analysis. Indeed, due to constraints on time, experimental setup, and subject comfort, sEMG signals are usually measured only from a subset of muscles involved in the observed movement. In particular, researchers typically include the larger muscles thought to contribute to the observed movement and from which it is easier to acquire sEMG signals. Depending on the limb and movement observed, different numbers of muscles,

ranging from five to twenty-four muscles, have been measured to model motor control strategies [31,54–59]. Results revealed that the average similarity of synergies to the master set (e.g., muscle synergies calculated from all the acquired muscles) dropped below 0.8 when fewer than eleven muscles were included in the analysis. Moreover, analyses that included small subsets of muscles also overestimated the variance accounted for by the synergies compared to the analysis computed considering larger subsets of muscles.

The study by Oliveira *et al.* [38], instead, investigated the influence of data structure (i.e., sEMG averaging, concatenation, and number of task repetitions) on the extracted muscle synergies, providing practical guidelines on the methodological aspects of muscle synergy extraction from sEMG signals during locomotion. The same number of muscle synergies was extracted by NNMF from all the acquired gait cycles separately, from averaging 2, 3, 5, 10, 20, and 40 consecutive gait cycles, and from the concatenation of the same sets of consecutive gait cycles. However, the muscle synergies extracted considering the concatenation of gait cycle subsets revealed a slightly reduced reconstruction accuracy compared to the other two tested conditions. Nevertheless, muscle synergies extracted from all the gait cycles separately or from averaging subsets of gait cycles did not account for step-to-step variability.

Finally, in the work by Kieliba *et al.*[49], the effect of different low-pass filter cut-off frequencies and amplitude-normalization techniques on muscle synergies extracted from the upper limb muscles of healthy subjects during point-to-point 3D reaching movements was assessed. Four different low-pass filter cut-off frequencies (i.e., 0.5 Hz, 4 Hz, 10 Hz, and 20 Hz) and two different amplitude-normalization techniques (i.e., maximum voluntary contraction and maximum amplitude of the recorded sEMG signal) were tested. In terms of filter cut-off frequencies, results showed that increasing the low-pass filter cut-off frequency had the effect of decreasing the amount of variance accounted for and, perhaps, the selected number of muscle synergies. Muscle synergies, instead, were not significantly altered by the amplitude-normalization techniques.

1.3 Aim of the Thesis and Organization

The present doctoral thesis aims at proposing, validating, and applying novel methods for extracting muscle synergies. These methods can be useful to provide deeper insights into the neuromuscular control of human locomotion and single-leg stance tasks. More specifically, this thesis is divided into two different sections aimed at assessing the modular organization of the central nervous system during cyclic (locomotion) and non-cyclic (single-leg balance) movements. In this thesis, both methodological and application-oriented studies are presented and discussed.

Chapter 2 - A Deep Learning Approach for Muscle Activity Detection aims at proposing a novel approach for extracting muscle activation intervals (onset/offset time instants) from raw surface electromyographical (sEMG) signals by using a deep learning approach based on Long Short-Term Memory (LSTM)

neural networks. Then, the proposed muscle activity detector will be used, in the following chapter (**Chapter 3 - Motor Control Strategies during Cyclic Movements**), as an sEMG pre-processing step before muscle synergy extraction.

Chapter 3 - Motor Control Strategies during Cyclic Movements aims at assessing human motor control strategies during cyclic movements (i.e., locomotion) in both patients affected by Parkinson's Disease and healthy subjects. More specifically, two methodological studies are described. Those studies aim at presenting and validating novel methods for extracting muscle synergies by extracting principal activations (**Methodological Issue - Muscle Synergies Extracted Using Principal Activations**) and for selecting the optimal number of muscle synergies by applying a multi-criteria decision analysis approach (**Methodological Issue – Multi-Criteria Decision Analysis for Selecting the Optimal Number of Muscle Synergies**).

Chapter 4 - **Motor Control Strategies during Non-Cyclic Movements** aims at assessing human motor control strategies during non-cyclic movements (i.e., single-leg stance). More specifically, one methodological and one application-oriented study are described. The first one aims at presenting and validating a novel method for extracting muscle synergies by distinguishing between the sEMG time-instants relative to a "*well-balanced*" and an "*unbalanced*" single-leg stance (**Methodological Issue – Muscle Synergy Assessment during Single-Leg Stance**). The application-oriented study, instead, aims to assess the influence of visual feedback on the modular organization of the central nervous system during single-leg stance considering healthy subjects (**Application - Influence of Visual Feedback on Muscle Synergies**).

Chapter 5 - Conclusions and Perspectives aims at summarizing the results described in the previous chapters highlighting the advantages of the proposed methodologies and the future perspectives.

Finally, in **Appendix A - Extraction of Principal and Secondary Activations through CIMAP** chapter, a brief introduction to the Clustering for Identification of Muscle Activation Patterns (CIMAP) algorithm is provided.

To improve the readability of the present thesis, at the beginning of each chapter the muscle synergy theory, the factorization approach adopted, and the sample population enrolled are briefly introduced.

Figure 1.6 shows a graphical representation of the doctoral thesis's contents.

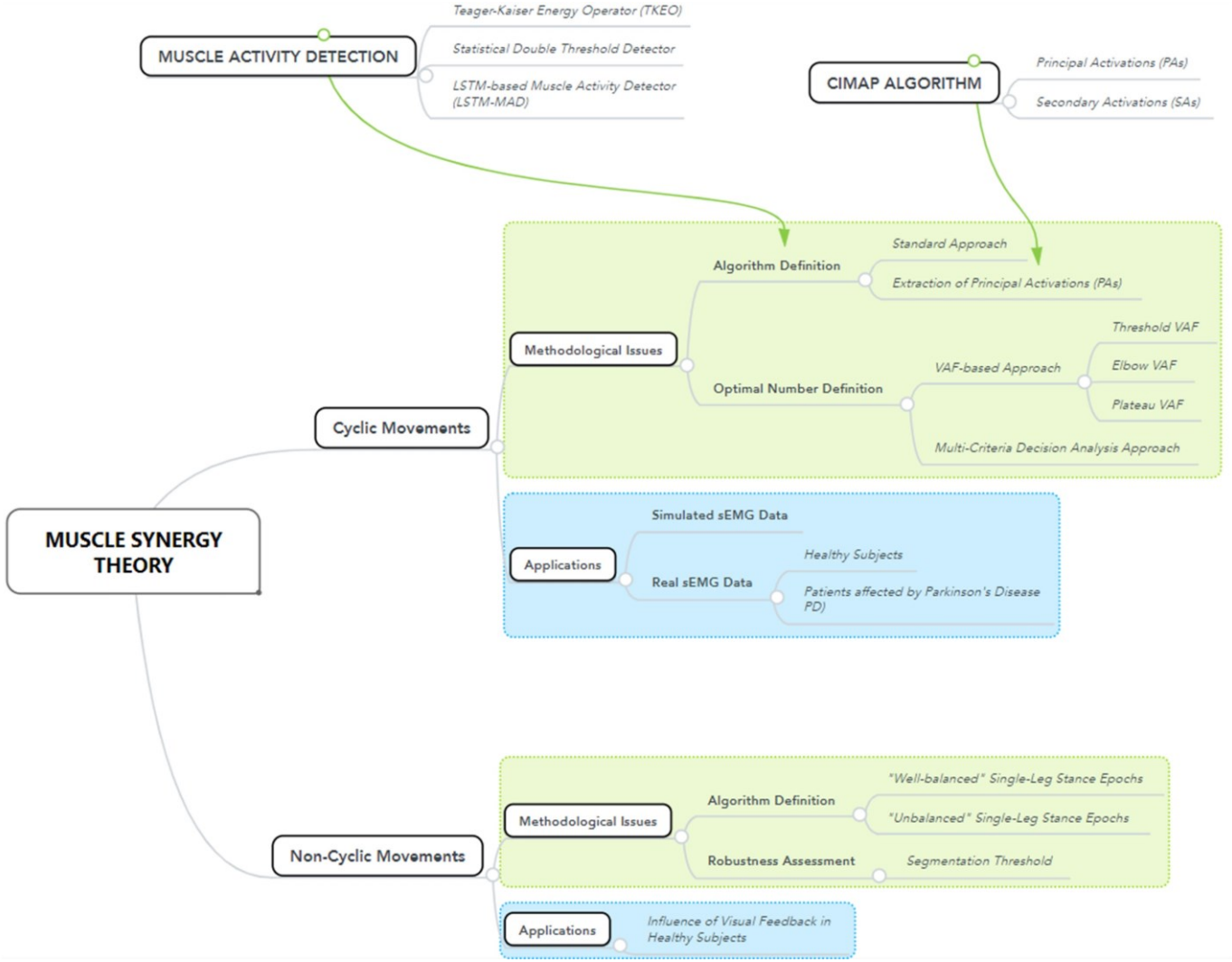

Figure 1.6 Graphical representation of the doctoral thesis's contents.

1

Chapter 2

A Deep Learning Approach for Muscle Activity Detection

Determining muscle activation intervals (onset/offset time-instants) during human movements is of great interest in different research fields, such as gait analysis, myoelectric control of prostheses, and pre-processing of muscle synergy extraction.

In the following chapter, the methodological issues related to muscle activation interval detection are presented and discussed. More specifically, a novel approach for muscle activity detection, based on LSTM neural networks, is proposed and its performance is compared against two of the most widely used approaches: the Teager-Kaiser Energy Operator (TKEO) detector and the statistical double threshold detector.

2.1 Introduction

Dynamic muscle activity can be non-invasively investigated by means of surface electromyography (sEMG). Determining the start (onset) and end (offset) instants of muscle activations during human movements is of great interest in different research fields including gait analysis [60], motor rehabilitation and sport science [61], myoelectric control of prostheses [62], human-machine interaction [63], design of biofeedback systems [64], and pre-processing of muscle synergy extraction [46,65,66]. In particular, the accurate temporal analysis of muscle activation in terms of burst onset, duration of the activation interval, and burst offset, can be useful in the assessment of the altered locomotion patterns of orthopedic and neurological patients [67].

A classical way to detect the timing of muscle activations from sEMG signals is using a double threshold detector, such as the statistical detector by Bonato *et al.* [68], specifically developed for gait analysis. However, this detector requires, as a necessary input parameter, to set the first (amplitude) threshold that depends on the

background noise level. Furthermore, to fine-tune the second threshold, it is important to estimate the signal-to-noise ratio (SNR), e.g., through the algorithm described in Ref. [69].

Alternative methods, such as deep learning approaches, are being explored to perform sEMG-based pattern recognition [70–79]. Muscle activity detection is somewhat easier with respect to a pattern-recognition problem. Indeed, the focus is not on classifying different movements, but simply detecting the presence or absence of muscle activation. Exploiting artificial intelligence, such as a Recurrent Neural Network (RNN), has been a winning strategy in a wide variety of different applications and might be explored also for our problem. RNN is a powerful learning algorithm inspired by the biological neural networks that constitute the human brain, and it is trained to present to the network a large number of labeled "examples" [80]. Long Short-Term Memory (LSTM) neural networks are a widely used type of RNNs specifically designed to recognize patterns and time-dependencies in sequential data, such as numerical time series, texts, and audio tracks [81]. These neural networks were first introduced by Hochreiter and Schmidhuber in 1997 [82] and represent an extension of the Recurrent Neural Networks (RNNs), allowing for a better assessment of the time-dependencies in long sequential data. Actually, LSTM neural networks represent the state of art in natural language processing and speech recognition problems [83].

The aim of this chapter is to assess the applicability of a novel approach for muscle activity detection, based on LSTM neural networks, specifically developed to overcome the limitations of the standard approaches. The performance of the LSTM-based Muscle Activity Detector (LSTM-MAD) are evaluated and compared against a standard approach (Teager-Kaiser Energy Operator, TKEO) [84,85], and a statistical approach (Statistical Double Threshold Detector) [68] in terms of Precision, Recall, F1-score, and Jaccard similarity index, both on simulated and real sEMG signals.

2.2 Materials and Methods

First, a dataset of simulated sEMG signals was built to assess the applicability of the LSTM-based approach to muscle activity detection and to compare its performance with respect to a standard and a statistical approach. For the standard approach, the Teager-Kaiser Energy Operator (TKEO) followed by the linear envelope extraction was implemented [85], while for the statistical approach it was implemented the double threshold statistical detector proposed in Ref. [68]. **Figure 2.1** represents the block diagram of the procedure followed in this chapter.

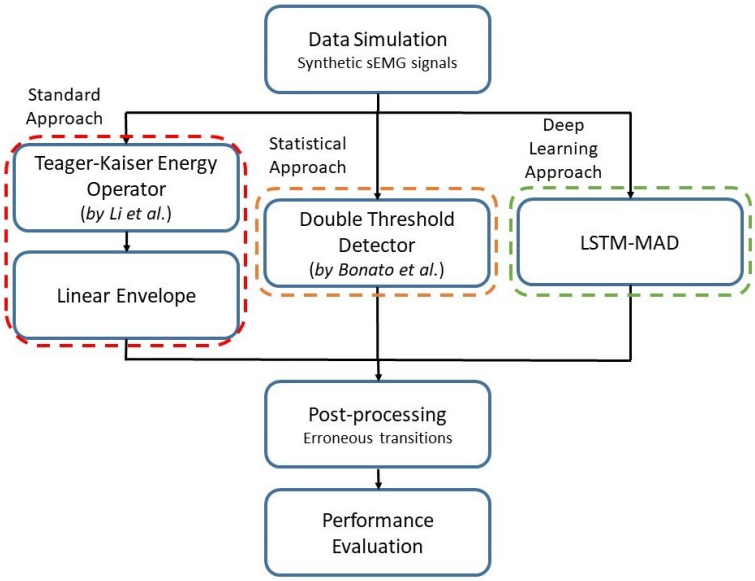

Figure 2.1 Schematic representation of the procedure followed to assess the performance of the new LSTM-MAD (LSTM-based Muscle Activity Detector) with respect to standard and statistical approaches for muscle activity detection.

Second, the LSTM-based approach was optimized on real sEMG signals, acquired in previous studies from lower limb and trunk muscles during gait, to emphasize its advantages in gait analysis.

1. Simulated Data

The sEMG signals acquired during cyclic movements, such as gait, can be modeled by the superimposition of two different contributions: (*i*) the electrical activity ($s(t)$) generated by each muscle during the contraction and (*ii*) the background noise ($n(t)$) mainly generated by the neighboring muscles and, to a lesser extent, by the acquisition system electronics. Under the hypothesis of cyclic contractions, the sEMG signal can be defined as a cyclostationary process [86] and, therefore, described through the superimposition of two different stationary processes [69]:

i. The muscle activity ($s(t)$) modeled as a Gaussian process with zero-mean and variance σ_s^2, as described in (**2.1**):

$$s(t) \in N(0, \sigma_s^2) \quad \textbf{(2.1)}$$

where σ_s was set equal to $10^{(SNR/20)} \cdot 1\mu V$.

ii. The background noise ($n(t)$) modeled as a zero-mean Gaussian process with variance σ_n^2, as described in (**2.2**):

$$n(t) \in N(0, \sigma_n^2) \quad \textbf{(2.2)}$$

where σ_n was set equal to $1\mu V$.

Each simulated sEMG signal was finally modeled as the superimposition of two stationary processes: the background noise process only in correspondence of the time-instants in which the muscle is non-active (OFF state) and a second stationary process $x(t)$ in correspondence of the time-instants in which the muscle is active (ON state) given by the superimposition of the muscle activity **(2.1)** and the background noise **(2.2)** Gaussian processes as follows **(2.3)**.

$$x(t) = n(t) + s(t) \quad \textbf{(2.3)}$$

Each realization of the muscle activity process $s(t)$ was simulated assuming a time period of 1s (gait cycle) and a sampling frequency of 1 kHz. Physiological muscle activity was modeled by time-windowing the Gaussian process $s(t)$ through a single truncated Gaussian function centered at 50% of the gait cycle. Different standard deviations (σ), and time supports ($2\alpha\sigma$) of the truncated Gaussian function have been considered to simulate sEMG signals similar to those observed in leg, thigh, and trunk muscles during gait. More specifically, three different values of the standard deviation ($\sigma = 50, 100, 150\ ms$) and four different values of the time support $2\alpha\sigma$ (with $\alpha = 1, 1.5, 2, 2.4$) have been tested [68]. Each muscle activity was then band-pass filtered through a 4th order Butterworth digital filter with a lower cut-off frequency of 10 Hz and a higher cut-off frequency of 450 Hz to simulate the frequency spectrum of real sEMG signals [87].Then, the background noise process ($n(t)$) was superimposed. Nine different values of Signal-to-Noise Ratio (SNR) were simulated ($SNR = 3, 6, 10, 13, 16, 20, 23, 26, 30\ dB$) [68]. For each triplet of σ, α, and SNR values, 100 different realizations (N) have been simulated and, therefore, a dataset composed by 10800 different realizations (3 standard deviations × 4 time supports × 9 $SNRs$ × 100 realizations) was built.

Figure 2.2 represents an example of a simulated sEMG signal with the superimposition of the truncated Gaussian function used to model a physiological muscle activity.

The time-instants relative to each simulated muscle activity ($s(t)$) were defined by a binary mask (BM_{sim}) that was set equal to 1 in correspondence of the time-

instants in which the truncated Gaussian assumed values higher than 0, and it was set equal to 0 otherwise.

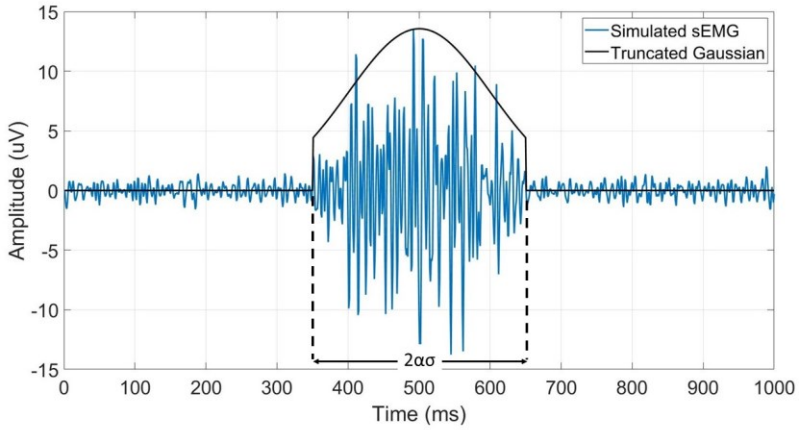

Figure 2.2 Example of a simulated sEMG signal (blue line) with the indication of the truncated Gaussian function (black line) used for the simulation of the muscle activity. The ***SNR*** is set equal to 20 dB, the standard deviation of the truncated Gaussian (σ) is equal to 100 ms, and the time support (2ασ) is obtained for α=1.5.

2. Real Data

Gait data were acquired from 20 subjects at PoliToBIOMed Lab (Politecnico di Torino, Turin, Italy) to test the performance of the three different approaches when applied to real sEMG signals. Subjects were randomly selected from our database to include both healthy individuals, and patients affected by neurological or orthopedic pathologies. This non-homogeneous group of subjects was specifically chosen to verify that the algorithm works under different conditions. In particular, 8 out of 20 subjects were healthy adults (age: 38.0 ± 13.1 years, height: 164.9 ± 5.4 cm, weight: 65.4 ± 21.2 kg) [46], 6 were patients with unilateral total hip prosthesis (age: 73.8 ± 8.4 years, height: 175.5 ± 7.6 cm, weight: 86.8 ± 16.3 kg) [88], and the other 6 were patients affected by idiopathic normal pressure hydrocephalus (age: 75.7 ± 6.3 years, height: 170.5 ± 6.3 cm, weight: 72.5 ± 10.4 kg) [89].

Signals were recorded through a multichannel acquisition system (STEP32, Medical Technology, Italy), specifically developed for statistical gait analysis [46,90,91]. Surface electromyographic (sEMG) signals were acquired through active probes (configuration: single differential, size: 19 mm × 17 mm × 7 mm, Ag-disks diameter: 4 mm, interelectrode distance: 12 mm, gain: variable in the range from 60 dB to 86 dB) placed over the following 4 muscles of the lower limb: Rectus Femoris (RF), Lateral Hamstring (LH), Lateral Gastrocnemius (LGS), and Tibialis Anterior (TA). The dominant lower limb was analyzed for healthy subjects, while the most affected limb was selected for pathological subjects.

For each subject, 5 gait cycles were randomly selected from the whole walking task to build the real dataset. Therefore, a dataset composed of 400 different sEMG signals (20 subjects × 5 gait cycles × 4 muscles) was obtained. The time-instants relative to each real-muscle activity were manually segmented by three expert operators. More specifically, a binary mask (BM_{real}) was set equal to 1 in

correspondence of the time-instants in which the majority of the expert operators (at least two out of three) detected a muscle activity and to 0 otherwise.

The real dataset described and used in this chapter to train and test the LSTM-MAD can be freely found online at Zenodo (doi: 10.5281/zenodo.4391062) in MAT and CSV format.

3. Standard Approach: TKEO and Linear Envelope

One of the most commonly applied standard approaches for muscle activity detection is the Teager-Kaiser Energy Operator (TKEO) followed by the linear envelope extraction. This approach has been demonstrated to increase the accuracy of the simple linear envelope approach [84,85].

More specifically, a single threshold was applied to the filtered sEMG signals after the computation of the TKEO (ψ), defined as in (**2.4**):

$$\psi_{x(n)} = x(n)^2 - x(n+1)x(n-1) \quad \textbf{(2.4)}$$

where x represents the sEMG time-series and n the sample number. The single threshold (Thr) was defined as described in (**2.5**):

$$Thr = \mu_n \pm j \cdot \sigma_n \quad \textbf{(2.5)}$$

where μ_n, σ_n and j represent the mean of the background noise, the standard deviation of the background noise, and a multiplicative constant, respectively. In this chapter, the constant j was set equal to 7 as suggested in Ref. [84],[92]. Since the average (μ_n) and the standard deviation (σ_n) of the background noise are required as inputs of this approach, time-instants corresponding to the background noise were automatically selected considering a 100-ms window before the onset of the simulated and segmented muscle activities, for the simulated and real sEMG signals, respectively.

The output of this detector was finally defined as a binary mask ($\text{Output}_{\text{TKEO}}$) as it follows:

- $\text{Output}_{\text{TKEO}} = 1$, if $\psi_{x(n)} \geq Thr$
- $\text{Output}_{\text{TKEO}} = 0$, if $\psi_{x(n)} < Thr$.

4. Statistical Approach: Double Threshold Statistical Detector

The statistical approach used in this chapter is the double threshold statistical detector proposed in Ref. [68]. The algorithm, specifically developed for statistical gait analysis, operates on raw sEMG signals and, hence, it does not require any pre-processing step (e.g., envelope or TKEO computation). The computation steps used for the double threshold detector are the following:

i. An auxiliary sequence z_i is computed from the raw sEMG signals as the sum of the squared values of two successive samples (**2.6**):

$$z_i = x_i^2 + x_{i+1}^2 \quad \textbf{(2.6)}$$

where x_i and x_{i+1} represent two consecutive samples of the sEMG time series

ii. A first threshold ζ is applied on a sliding detection window defined by *m* consecutive samples of the auxiliary sequence z_i

iii. A muscle activation is detected if at least r_0 (second threshold) out of *m* consecutive samples of the detection window are above the first threshold ζ.

Considering the computation steps above mentioned, the double threshold statistical detector has a more elaborate structure compared to single threshold approaches. In particular, muscle activations are detected when at least r_0 (second threshold) out of *m* consecutive values of the auxiliary sequence (z_i) cross the first threshold (ζ). Accordingly, this detector is defined by three different input parameters: (*i*) the first (or amplitude) threshold (ζ), (*ii*) the length of the observation window (*m*), and (*iii*) the second (or temporal) threshold. As suggested in Ref. [68], the length of the observation window (*m*) and the second threshold r_0 were set equal to 5 and 1, respectively.

The output of this detector was finally defined as a binary mask ($\text{Output}_{\text{Stat}}$) as it follows:

- $\text{Output}_{\text{Stat}} = 1$, if $z_i \geq \zeta$ for at least r_0 out of *m* samples
- $\text{Output}_{\text{Stat}} = 0$, otherwise.

5. Deep Learning Approach: LSTM-MAD

An LSTM model is generally composed by the following architecture:

i. An *input sequence layer*
ii. One or more *LSTM layers* used to learn the time-dependencies within the sequential data
iii. A *fully connected layer* used to convert the output size of the previous layers into the number of classes to be recognized
iv. A *softmax layer* used to compute the belonging probability to each class
v. A *classification output layer* used to compute the cost function.

In this chapter, several LSTM neural network models were tested to assess the applicability of this approach for muscle activity detection during gait, considering sEMG data without any pre-processing step. To define the best LSTM model for

muscle activity detection, the entire dataset of simulated (and real) sEMG signals was divided into 3 different sets: training set (70%), validation set (15%), and test set (15%), respectively. The training set was used to train the LSTM model, while the validation set (or "development" set) was used to evaluate the network performances and to avoid the overfitting of the training data. More specifically, the validation set was used to stop training automatically when the validation accuracy stopped increasing to avoid overfitting [80]. Finally, the test set was used for the final validation and the comparison of LSTM-MAD with the other two detectors.

Using the Deep Learning Toolbox of MATLAB® release R2020b (The MathWorks Inc., Natick, MA, USA), 720 different LSTM neural networks were tested. All the LSTM models had a sequence *input layer* consisting of 1 unit (dimension of a single simulated sEMG signal), and a *fully connected output layer* consisting of 2 units (number of classes to be recognized). Different numbers of LSTM layers (n), numbers of hidden units for each layer (n_{units}), values of learning rate (α), and values of drop period (δ) were tested to achieve the LSTM architecture with the highest performance. More specifically, two different numbers of LSTM layers ($n = 1, 2$), nine different numbers of hidden units in each LSTM layer (n_{units} = 100, 125, 150, 175, 200, 225, 250, 275, and 300), five different learning rates (α = 0.01, 0.015, 0.02, 0.025, and 0.03), and eight different drop rate values (δ = 10, 15, 20, 25, 30, 35, 40, and 45) were tested [80]. The adaptive moment (ADAM) optimization algorithm was adopted in this work to train all the tested LSTM models [93]. The performance of each LSTM model was assessed considering the simulated (or real) test set by computing the overall classification accuracy, defined as the number of correctly classified sEMG samples normalized to the total number of sEMG samples within the test set.

The training process was performed on a workstation with a 3.2 GHz six-core CPU, 32 GB of RAM memory, and a 64-bit Windows operating system.

The BM_{sim}, extracted from the truncated Gaussian functions, and the BM_{real}, manually defined by the expert operators, were used to compute the target (ground truth) of the LSTM model for the simulated and real datasets, respectively.

The output of the LSTM approach was computed as a binary mask ($Output_{LSTM\text{-}MAD}$) that was defined as it follows:

- $Output_{LSTM\text{-}MAD}$ = 1, if the sEMG time-instant was classified as muscle activity (class 1)
- $Output_{LSTM\text{-}MAD}$ = 0, if the sEMG time-instant was classified as background noise (class 0).

6. Post-processing

A post-processing step was applied to the output of each detector (standard, statistical, and deep learning approach) to reject the erroneous transitions due to the stochastic nature of the sEMG signal. Since it is generally accepted that a muscle activation shorter than 30 ms does not affect the kinetics and the kinematics of gait [94], all the muscle activations lasting less than 30 ms were discarded [68]. This concept is illustrated in **Figure 2.3**. In particular, **Figure 2.3A** shows a sample realization of a simulated sEMG signal modulated by a truncated Gaussian function (SNR = 16 dB, σ = 100 ms, and α = 1.5). **Figure 2.3B** represents the output of the standard approach ($Output_{TKEO}$) without any post-processing step, while **Figure 2.3C** shows the effect of the post-processing on the detector's output.

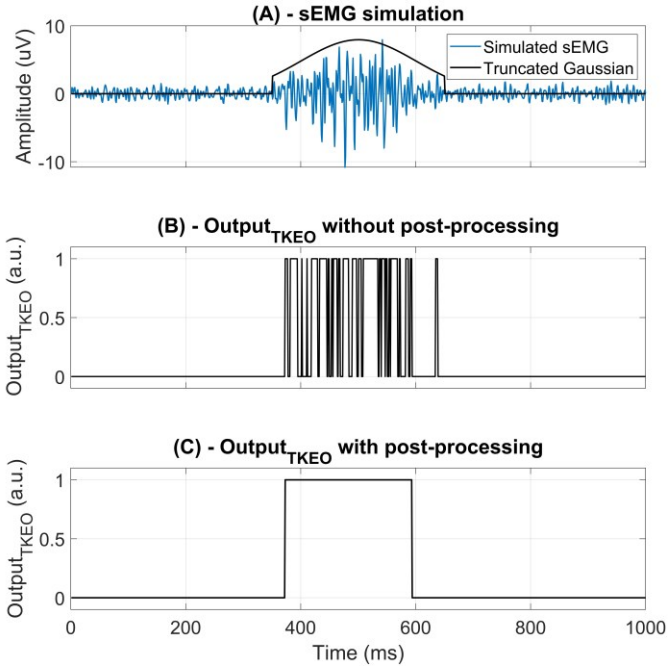

Figure 2.3 Example of post-processing applied to the standard approach output ($Output_{TKEO}$). (A) Sample realization of a simulated sEMG signal (blue line) with the superimposition of the truncated Gaussian function used to modulate the muscle activity (black line). The ***SNR*** is set equal to 20 dB, standard deviation of the truncated Gaussian (σ) is 100 ms and the multiplicative constant (α) of the time support is 1.5. (B) Output of the standard approach ($Output_{TKEO}$) without any post-processing. (C) Output of the standard approach after rejecting all the activations shorter than 30 ms (post-processing step).

7. Performance Evaluation

The muscle activations detected by the three different approaches ($Output_{TKEO}$, $Output_{Stat}$, and $Output_{LSTM\text{-}MAD}$) were quantitatively compared in terms of (*i*) Precision, (*ii*) Recall, (*iii*) F1-score, and (*iv*) Jaccard similarity index. More specifically, the indexes were defined as it follows:

$$Precision = \frac{TP}{TP + FP} \quad (\mathbf{2.7})$$

$$Recall = \frac{TP}{TP + FN} \quad (\mathbf{2.8})$$

$$F1\ score = \frac{2 \times (Recall \times Precision)}{(Recall + Precision)} \quad (\mathbf{2.9})$$

$$Jaccard = \frac{|Output_i \cap BM|}{|Output_i \cup BM|} \quad (\mathbf{2.10})$$

where TP represents the True Positive (i.e., number of sEMG time-instants correctly classified by the detectors as muscle activity), FN describes the False Negative (i.e., number of sEMG time-instants incorrectly classified by the detectors as background noise), and FP represents the False Positive (i.e., number of sEMG time-instants incorrectly classified by the detectors as muscle activity). Finally, $Output_i$ represents the binary mask computed by the i-th detector (i = 1: Standard approach with TKEO, i = 2: Statistical approach with the double-threshold detector, i = 3: New approach with LSTM-MAD), and BM represents the ground truth of the simulated (or real) data.

8. Effect of SNR on Muscle Activity Detection

To assess the effect of the SNR on the performance of the three muscle activity detectors, the performance parameters described above were computed on the simulated test set, separately for each of the nine SNR values ($SNR = 3, 6, 10, 13, 16, 20, 23, 26, 30\ dB$).

9. Statistical Analysis

A one-way repeated-measures analysis of variance (ANOVA) followed *by post-hoc* analysis with Bonferroni adjustment for multiple comparisons was performed to assess significant differences in the performance of the three approaches, setting the significance level (α) equals to 0.05.

2.3 Results

First, the results supporting the applicability of the LSTM approach for muscle activity detection (LSTM-MAD) are presented, considering simulated sEMG signals. Second, the performance of the three detectors (standard TKEO, double-threshold statistical detector, and the newly introduced LSTM-MAD) on simulated sEMG signals are compared, highlighting the effect of the SNR. Finally, LSTM-MAD is validated on real data.

1. Simulated Data - LSTM Model Definition

The best LSTM model was selected among all the tested networks as the one with the highest overall classification accuracy on the test set, discarding those networks with a difference between the training and validation accuracy higher than 4% (to avoid overfitting of the training data).

TABLE 2.1 shows the properties of the LSTM model that achieved the highest overall classification accuracy (96.8% ± 4.3%) on the test set.

TABLE 2.1
PROPERTIES OF THE BEST LSTM MODEL

LSTM Layers	*PROPERTIES*
Sequence input layer	1 input feature
LSTM layer #1	275 hidden units, Bi-directional sequence-to-sequence architecture
LSTM layer #2	138 hidden units, Bi-directional sequence-to-sequence architecture
Fully connected layer	2 units
Softmax layer	Softmax activation function (threshold = 0.5)
Classification output layer	2 classes (1 = muscle activity, 0 = background noise)

2. Simulated Data – Performance Evaluation

The performances of the three different muscle activity detectors were assessed and compared in terms of (*i*) Precision, (*ii*) Recall, (*iii*) F1-score, and (*iv*) Jaccard similarity index:

i. *Precision:* An average precision of 0.92 ± 0.10, 0.98 ± 0.09, and 0.95 ± 0.08 was found on the simulated test set, considering the standard, the statistical, and the deep learning approach, respectively. One-way ANOVA followed by *post-hoc* analysis revealed significant differences between each pair of detectors ($p < 0.0001$)

ii. *Recall:* On average, a recall of 0.86 ± 0.20, 0.53 ± 0.39, and 0.96 ± 0.08 was found on the simulated test set, considering the standard, the statistical, and the deep learning approach, respectively. One-way ANOVA followed by *post-hoc* analysis revealed significant differences between each pair of detectors ($p < 0.0001$)

iii. *F1-score:* On average, an F1-score of 0.87 ± 0.14, 0.76 ± 0.25, and 0.95 ± 0.06 was found on the simulated test set, considering the standard, the statistical, and the deep learning approach, respectively. One-way ANOVA followed by *post-hoc* analysis revealed significant differences between each pair of detectors ($p < 0.0001$)

iv. *Jaccard similarity index:* An average Jaccard index of 0.80 ± 0.19, 0.52 ± 0.38, and 0.91 ± 0.10 was found on the simulated test set, considering the standard, the statistical, and the deep learning approach, respectively. One-way ANOVA followed by *post-hoc* analysis revealed significant differences between each pair of detectors ($p < 0.0001$).

Figure 2.4A compares the performance of the three detectors tested (standard TKEO [84], statistical double-threshold detector [68], and LSTM-MAD), based on the four parameters introduced above. The average values and standard errors of the parameters were estimated on the simulated dataset. Asterisks highlight statistical differences between each pair of detectors.

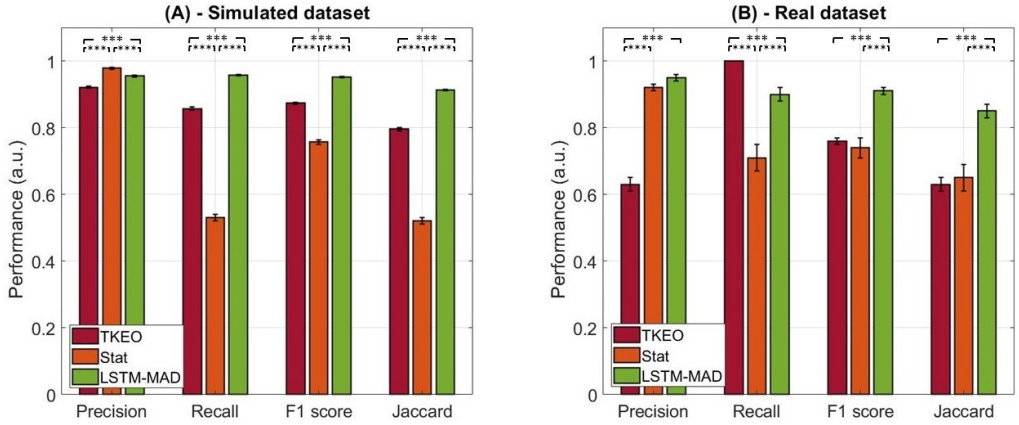

Figure 2.4 Comparison of the performance of the three muscle activity detectors (standard TKEO by Li *et al.* [24], statistical double-threshold detector by Bonato *et al.* [10], and LSTM-MAD) estimated considering (A) the simulated and (B) the real dataset. Average values and standard errors are represented. Statistically significant differences are indicated by asterisks (***p < 0.0001).

3. Simulated Data – Effect of SNR on Muscle Activity Detection

The effect of the SNR on the detectors' performance was assessed by computing the performance parameters (Precision, Recall, F1-score, and Jaccard similarity index), separately for each simulated SNR-value.

Figure 2.5 represents, for each muscle activity detector, the average values (and standard errors) of Precision (**Figure 2.5A**), Recall (**Figure 2.5B**), F1-score (**Figure 2.5C**), and Jaccard similarity index (**Figure 2.5D**), for each simulated SNR-value.

For all the parameters, LSTM-MAD revealed a higher performance consistency across the different SNR values, suggesting a lower effect of SNR on muscle activity detection with respect to the other two approaches. The approach more affected by the SNR was the statistical double threshold detector, with an evident decrease of the performances for simulated sEMG signals with SNR-values lower than 20 dB.

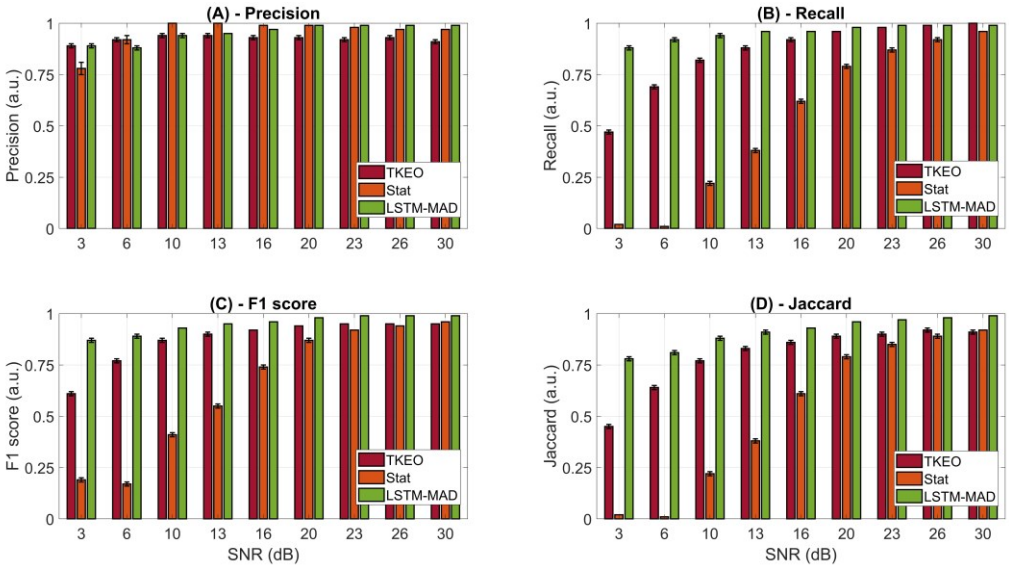

Figure 2.5 Values of (A) Precision, (B) Recall, (C) F1 score, and (D) Jaccard similarity index, averaged on the simulated test set, for each value of ***SNR*** and for each muscle activity detector. Each colored bar represents the average performance of a specific detector (TKEO by Li *et al.* [24] in red, double-threshold statistical detector by Bonato *et al.* [10] in orange, and LSTM-MAD in green). Error bars represent the standard errors.

4. Real Data

The same procedure described for the simulated dataset was followed to determine the best LSTM model considering real sEMG data. In the following, the results obtained from the real dataset for the three different approaches are detailed.

5. Real Data – LSTM Model Definition

The same 720 different LSTM neural networks considered for the simulated dataset were tested. The best LSTM model that achieved the highest overall classification accuracy (90.1% ± 14.28%) on the test set had the same architecture and properties as the one selected considering the simulated data (see **TABLE 2.1**). **Figure 2.6** shows an example of a real sEMG signal acquired from the TA muscle of a healthy subject with the superimposition of the ground truth (BM_{real}) and the outputs of the three detectors ($\text{Output}_{\text{TKEO}}$, $\text{Output}_{\text{Stat}}$, and $\text{Output}_{\text{LSTM-MAD}}$).

6. Real Data – Performance Evaluation

The performance of the three different muscle activity detectors on real sEMG signals were assessed considering the same four parameters described for the simulated dataset:

i. Precision: An average precision of 0.63 ± 0.15, 0.92 ± 0.11, and 0.95 ± 0.11 was found on the real test set, considering the standard, the statistical, and the

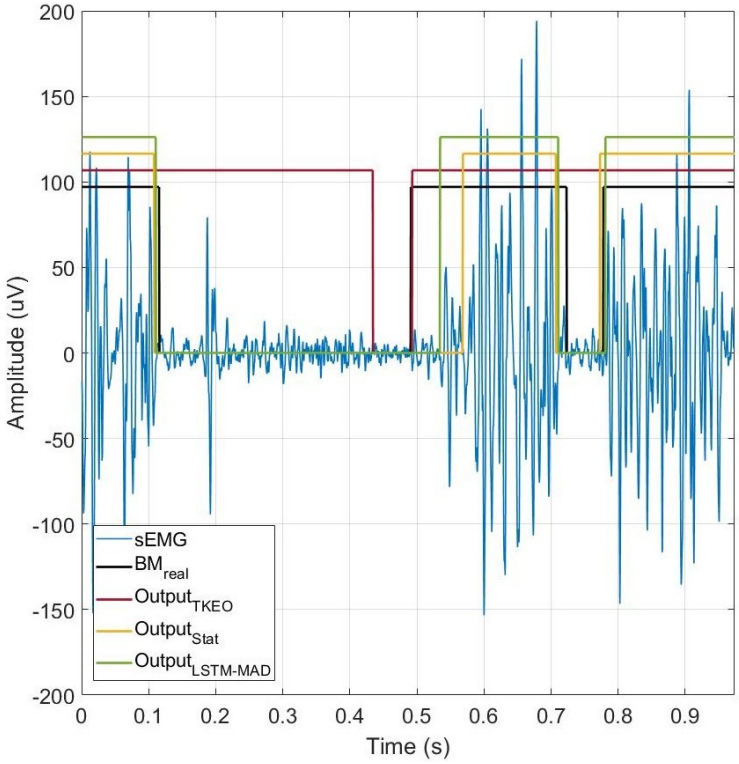

Figure 2.6 Example of a real sEMG signal (blue line) acquired from the Tibialis Anterior (TA) muscle of a healthy subject of the sample population. The output of the standard (red line), statistical (orange line), and LSTM-MAD approach (green line) are represented along with the indication of the ground truth (black line) manually segmented by expert operators. All the muscle activity shorter than 30 ms are rejected by means of the post-processing step for all the approaches.

deep learning approach, respectively. One-way ANOVA followed by *post-hoc* analysis revealed significant differences between the standard and the statistical approach ($p < 0.0001$), and between the standard and the deep learning approach ($p < 0.0001$), while no difference was found between the statistical and the deep learning approach

ii. *Recall:* On average, a recall of 1.00 ± 0.00, 0.71 ± 0.31, and 0.90 ± 0.15 was found on the real test set, considering the standard, the statistical, and the deep learning approach, respectively. One-way ANOVA followed by *post-hoc* analysis revealed significant differences between each pair of detectors ($p < 0.0001$)

iii. *F1-score:* On average, an F1-score of 0.76 ± 0.11, 0.74 ± 0.26, and 0.91 ± 0.11 was found on the real test set, considering the standard, the statistical, and the deep learning approach, respectively. One-way ANOVA followed by *post-hoc* analysis revealed significant differences between the standard and the deep learning approach ($p < 0.0001$), and between the statistical and the deep learning approach ($p < 0.0001$), while no difference was found between the standard and the statistical approach

iv. *Jaccard similarity index:* An average Jaccard index of 0.63 ± 0.15, 0.65 ± 0.27, and 0.85 ± 0.16 was computed from the real test set, considering the standard, the statistical, and the deep learning approach, respectively. One-way ANOVA followed by *post-hoc* analysis revealed significant differences

between the standard and the deep learning approach ($p < 0.0001$), and between the statistical and the deep learning approach ($p < 0.0001$), while no difference was found between the standard and the statistical approach.

Considering the real test set, **Figure 2.4B** compares the performance of the three detectors, based on the four parameters introduced above. The average values and standard errors of the parameters are reported, as well as asterisks to highlight statistical differences between each pair of detectors.

2.4 Discussion and Conclusions

This chapter demonstrates that the detection of muscle activity during gait can be successfully performed by means of a novel approach, based on a Long Short-Term Memory (LSTM) Recurrent Neural Network (RNN). The newly introduced muscle activity detector (LSTM-MAD) is able to effectively separate muscle activation intervals from background noise, with an overall classification accuracy of 97% (considering simulated data).

Results showed that the proposed detector outperforms current methods used to discern muscle activity. In particular, LSTM-MAD clearly exhibits better performance than both the alternative approaches tested (standard approach using the Teager-Keiser Energy Operator (TKEO) [84], and statistical double-threshold detector [68]). Indeed, improved performance was demonstrated both on simulated and real sEMG signals.

Considering simulated signals, all the four "performance" parameters introduced (Precision, Recall, F1-score, and Jaccard similarity index) showed remarkably higher values for LSTM-MAD when compared to the statistical detector. Furthermore, three out of four parameters (Recall, F1-score, and Jaccard similarity index) displayed greater values for LSTM-MAD when compared to the TKEO detector, and only a slightly worst precision was found. However, it should be noticed that while LSTM-MAD shows an excellent balance between Precision and Recall, the same cannot be said for the TKEO detector, which displays a very high Precision (i.e., low number of false positive), but a very low Recall (i.e., a high number of false-negative). In other words, the TKEO detector demonstrates a reduced probability of detection and an increased number of false-negative compared to the LSTM-MAD. By the way, the "optimal balance" between Precision and Recall is incorporated in the definition of the F1-score, which is broadly used in literature specifically to take into account the balance between Precision and Recall by considering both the number of false-positive and the number of false-negative.

Considering real signals, all the four "performance" parameters showed remarkably higher values for LSTM-MAD with respect to the TKEO detector. Furthermore, three out of four parameters (Precision, F1-score, and Jaccard similarity index) displayed greater values for LSTM-MAD when compared to the TKEO detector. Only the Recall was higher in the TKEO detector with respect to our approach. Again, it should be noted that LSTM-MAD is characterized by an

excellent balance between Precision and Recall, while this is not true for the TKEO detector, which is characterized by a higher probability of detection and, hence, by a higher number of false-positive (i.e., lower precision) compared to the LSTM-MAD. Indeed, the TKEO detector shows a very good Recall to the detriment of a very poor Precision. The statistical detector, instead, shows different behavior, revealing a very high Precision (similar to the Precision obtained considering the LSTM-MAD approach) to the detriment of a very poor Recall. In other words, the statistical detector demonstrates a reduced probability of detection and an increased number of false-negative compared to the LSTM-MAD.

Overall, LSTM-MAD revealed a smaller variability in the detector's performance, especially compared to the TKEO approach. Although a thorough analysis of this aspect is beyond the scope of this work, this reduced variability can be qualitatively appreciated in **Figure 2.4**, when comparing the small error bars obtained for LSTM-MAD compared to those obtained for TKEO.

Furthermore, the novel approach introduced in this chapter revealed increased robustness of the detector's performance with respect to the effect of the signal-to-noise ratio (SNR), suggesting the applicability of the LSTM-MAD to a wider range of noise conditions compared to the other two tested approaches. Indeed, while it is evident that decreasing SNR inevitably diminishes the detection performance of each approach, LSTM-MAD is the least affected one (see **Figure 2.5**). In particular, focusing on the parameters Recall, F1-score, and Jaccard similarity index, we found a conspicuous worsening of the performance of the statistical double-threshold detector with decreasing SNR. The situation is even more dramatic considering the TKEO detector. On the contrary, our detector LSTM-MAD shows a limited worsening of the performance with decreasing SNR. Indeed, even at very low SNR values (e.g., 3 or 6 dB), the performance of LSTM-MAD never degrade too much (Recall is always greater than 0.88, F1-score is always greater than 0.87, and Jaccard similarity index is always greater than 0.78). For what concerns the parameter Precision, none of the three detectors showed a drastic decrease of the performance with decreasing SNR ratio. The analysis about how a poor SNR can eventually degrade detectors' performance was carried out on simulated signals only. This was chosen to study the above-described phenomenon in a more controlled condition, i.e., to have a precise knowledge (*a priori*) about the SNR itself (since sEMG signals were simulated at each specific SNR level). Indeed, considering real signals one would have needed to apply some additional algorithm to estimate the SNR.

A further valuable attribute and distinctive quality of the LSTM-MAD approach is that it does not require any additional input parameter. The proposed algorithm directly works on "raw" sEMG signals, the only pre-processing step being the usual passband filtering (e.g., between 10 Hz and 450 Hz), applied to all the three approaches, in the same manner. On the contrary, the statistical double-threshold detector requires, as a necessary input parameter, the knowledge of the background-noise power. Furthermore, the estimation of the SNR is also usually required to properly fine-tune the algorithm parameters. The estimation of

background-noise power and SNR-ratio is usually obtained by analyzing 30 s-windows of sEMG signal. However, since LSTM-MAD does not require any additional input parameter (e.g., background-noise power or SNR estimation), it is intrinsically more adaptable to eventual SNR variations arising during signal acquisition. Furthermore, differently from the TKEO approach, it does not require the computing of a linear envelope.

In conclusion, a Long-Short-Term-Memory approach for muscle activity detection was proposed and validated (both on simulated and real sEMG signals). The presented approach clearly outperforms previous detectors, and it is robust even when applied to signals with low to medium signal-to-noise ratio. Therefore, it may be considered a valuable tool, in all the applications requiring an accurate and effective recognition/distinction of muscle activity from background noise.

Chapter 3

Motor Control Strategies during Cyclic Movements

In this chapter, two fundamental methodological issues in the assessment of motor control strategies through the muscle synergy theory are discussed: the sEMG pre-processing technique used to extract muscle synergies and the criterion used to select the optimal number of muscle synergies. First, an innovative sEMG pre-processing approach for muscle synergy extraction during gait is presented and compared with respect to a "standard" pre-processing approach (**Methodological Issue - Muscle Synergies Extracted Using Principal Activations**). Then, to overcome the limitations of the VAF- or R^2-based methods for the selection of the optimal number of muscle synergies, a novel approach, based on Multi-Criteria Decision Aiding (MCDA), is assessed and validated considering both simulated and real data (**Methodological Issue – Multi-Criteria Decision Analysis for Selecting the Optimal Number of Muscle Synergies**).

Methodological Issue - Muscle Synergies Extracted Using Principal Activations

Some of the results presented in this paragraph are reproduced and modified from an article published in *IEEE Transactions on Neural Systems and Rehabilitation Engineering* (Volume: 28, Issue: 2, Feb. 2020) by Ghislieri *et al*. The final authenticated version of the manuscript is available online at http://dx.doi.org/10.1109/TNSRE.2020.2965179.

3.1 Introduction

According to the muscle synergy theory, the Central Nervous System (CNS) controls small groups of muscles (called *muscle synergies*) rather than coordinating and activating every single muscle involved in a specific motor task. The

effectiveness of the muscle synergy theory in modeling the modular organization of the CNS during different motor tasks has been demonstrated in several studies and research areas, such as clinics, robotics, and sport [17,18,27,47,95,96].

More specifically, human locomotion is one of the most widely studied and complex motor tasks, due to the multiple degrees of freedom of the skeletal muscle system, the several biomechanical functions carried out during each gait cycle [97], and the high intra-cycle variability of the muscle activation intervals [98]. Previous studies demonstrated that human locomotion can be modeled by a small set of muscle synergies characterized by specific biomechanical functions [19–22]. The number of muscle synergies extracted and their biomechanical functions may vary depending on the type and the number of muscles acquired [23], the sEMG pre-processing techniques, and the factorization algorithm implemented. On average, five muscle synergies are needed to properly describe human locomotion [19,24].

Muscle synergies during human locomotion are often extracted from surface electromyography (sEMG) signals by applying the Non-Negative Matrix Factorization (NNMF) algorithm [28,41]. Before computing the factorization, the acquired sEMG signals are usually pre-processed to extract their envelopes. In the last years, several pre-processing approaches were proposed in literature for muscle synergy extraction during cyclic movements [19,23,27,28,41,55,99]. For example, in the study by Clark *et al.* [55] the acquired sEMG signals were previously high-pass filtered at 40 Hz through a zero-lag 4^{th}-order digital Butterworth filter, demeaned, full-cycle rectified, and smoothed by means of a zero-lag 4^{th}-order Butterworth digital filter with a cut-off frequency of 4 Hz. Finally, to facilitate the comparison among different muscles and different motor conditions, the filtered sEMG signals were amplitude-normalized with respect to the global maximum of the signal acquired from each recorded muscle. In the work by Steele *et al.* [23] sEMG data were band-pass filtered with a lower cut-off frequency of 20 Hz and a higher cut-off frequency of 400 Hz, rectified and low-pass filtered at 10 Hz.

The application of these *standard* pre-processing techniques may not be sufficient to fully understand the motor control mechanism due to the high intra-cycle variability of the sEMG activation intervals [100]. Statistical Gait Analysis (SGA) [60] was introduced to deal with this issue by selecting only the representative gait patterns. It was successfully applied to the study of the frequency-of-occurrence of muscle activation modalities [100], muscle activation timing [101], and co-contractions [102]. Moreover, through the application of the Clustering for Identification of Muscle Activation Patterns (CIMAP) algorithm [103], [104], it is possible to define the principal and secondary muscle activations. Principal activations (PAs) are defined as those activations that are strictly necessary to accomplish the motor task, while secondary activations (SAs) may have an auxiliary function, such as providing corrections to motion and body segment posture. The CIMAP algorithm was successfully applied to the study of gait asymmetry of healthy, orthopedic, and neurological patients [67,105,106].

The aim of this work is to assess how the combined application of the SGA and CIMAP (i.e., extraction of PAs) techniques can be used to overcome the limitations of the *standard* pre-processing algorithms in terms of intra-subject consistency,

robustness, and interpretability of muscle synergies during gait in both physiological and pathological populations.

3.2 Materials and Methods

1. Sample Population and Experimental Protocol

Gait data from twenty-two patients affected by Parkinson's disease (7 females and 15 males, age: 58.9 ± 8.1 years, height: 174.4 ± 9.4 cm, weight: 76.5 ± 13.1 kg) and twenty-two healthy subjects (18 females and 4 males, age: 39.2 ± 17.0 years, height: 165.2 ± 8.2 cm, weight: 60.9 ± 17.5 kg) were acquired and analyzed at PoliToBIOMed Lab (Politecnico di Torino, Turin, Italy). Patients affected by Parkinson's Disease (PD) were enrolled from those eligible for Deep Brain Stimulation (DBS) at the Stereotactic and Functional Neurosurgery Unit of the University of Turin (Italy). The inclusion criteria were:

i. Diagnosis of PD, according to the UK Brain Bank guidelines
ii. Good response to Levodopa
iii. Age at surgery below 70 years
iv. Absence of freezing of gait and postural instability unresponsive to pharmacological therapy
v. Ability to walk independently for a few minutes without walking aids or external supports, at least within the best-on pharmacological time-window.

PD patients affected by other co-morbidities that could potentially affect gait performance were excluded from the study.

Gait and balance performance were rated using the Unified Parkinson's Disease Rating Motor Subscale (UPDRS-III) [107]. For the enrolled PD population, the average UPDRS-III score was equal to 17.1 ± 0.2 and 44.6 ± 12.3 considering ON and OFF condition, respectively.

Considering the healthy subjects, none of them reported lower limb injuries or had neurological or musculoskeletal disorders that could compromise their gait performance.

The experimental protocol consisted of a 5-minute walk at self-selected speed, back and forth on a 9-m straight walkway. PD patients were acquired during their best-on conditions. **Figure 3.1** shows a schematic representation of the walking path. The protocol conformed to the Helsinki declaration on medical research

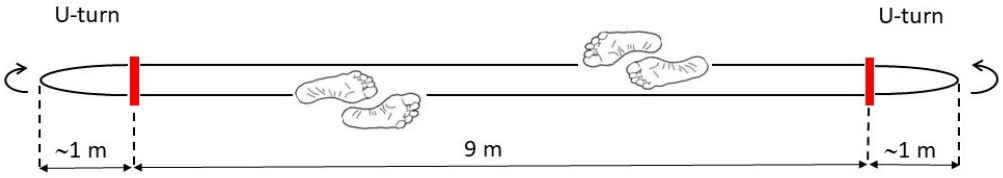

Figure 3.1 Schematic representation of the walking path. Subjects walked back and forth, without interruptions, along a straight path of 9 m, for approximately 5 minutes. U-turns were excluded by the analysis.

involving human subjects and was approved by the Ethics Committee of the A.O.U. Città della Salute e della Scienza di Torino - A.O. Ordine Mauriziano - A.S.L. "Città di Torino" (No. 0092029).

TABLE 3.1 represents the anthropometric characteristics of the PD and healthy populations analyzed in this chapter.

TABLE 3.1
ANTHROPOMETRIC CHARACTERISTICS OF PD AND HEALTHY POPULATIONS.

	Age (years)	Weight (kg)	Height (cm)	UPDRS-III (ON condition)	UPDRS-III (OFF condition)	Disease duration (years)
PD	58.9 ± 8.1	76.5 ± 13.1	174.4 ± 9.4	17.1 ± 0.2	44.6 ± 12.3	12.8 ± 3.7
Healthy	39.2 ± 17.0	60.9 ± 17.5	165.2 ± 8.2	N/A	N/A	N/A

Values of parameters are reported as mean ± standard deviation over the population.
UPDRS-III: Unified Parkinson's Disease Rating Motor Subscale
N/A: Not Applicable

2. Data Acquisitions

A multichannel system specifically developed for statistical gait analysis (STEP32, Medical Technology, Italy) was used to acquire gait data. The following signals were simultaneously recorded:

i. Surface electromyographic (sEMG) signals, by means of active probes (configuration: single differential, size: 19 mm × 17 mm × 7 mm, Ag-disks diameter: 4 mm, interelectrode distance: 12 mm, gain: variable in the range from 60 dB to 86 dB)
ii. Foot-switch signals (size: 10 mm × 10 mm × 0.5 mm, activation force: 3 N) to detect gait phases
iii. Knee joint kinematics signals in the sagittal plane by means of electro-goniometers (accuracy: 0.5°).

The sEMG active probes were placed over the following 12 muscles of the dominant lower limb and trunk (bilaterally): right and left Longissimus Dorsii (LD_R, LD_L), Tensor Fasciae Latae (TFL), Gluteus Medius (GMD), Rectus Femoris (RF), Lateral Hamstring (LH), Medial Hamstring (MH), Vastus Medialis (VM), Lateral Gastrocnemius (LGS), Peroneus Longus (PL), Soleus (SOL) and Tibialis Anterior (TA). Foot-switches were positioned beneath the heel, the first, and fifth metatarsal heads, bilaterally. Electro-goniometers were positioned on the lateral aspect of the knee joint, bilaterally.

An example of sensor placement is shown, for a representative healthy subject of the sample population, in **Figure 3.2**.

Signals were acquired with a sampling frequency of 2000 Hz, converted by a 12-bit analog to digital converter, and sent to a PC for real-time representation. The acquired signals were then imported into the MATLAB® release 2020b (The MathWorks Inc., Natick, MA, USA) to be processed by means of custom routines.

3. Data Processing

Before muscle synergy extraction, the acquired sEMG signals were pre-processed considering two different approaches:

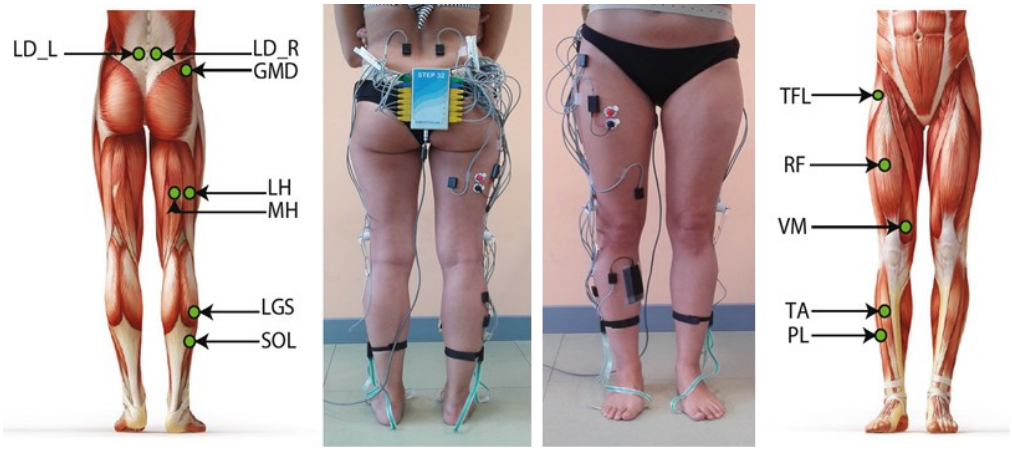

Figure 3.2 Sensor placement for a healthy subject of the sample population. sEMG active probes are placed over the principal muscle of the dominant lower limb and the trunk (bilaterally). Foot-switches are place beneath the heel, the first, and the fifth metatarsal heads to detect gait phases and time-segment gait cycles. Electro-goniometers are positioned on the lateral aspect of the knee joint.

i. the *standard* approach, in which all sEMG time-instants were considered for muscle synergy extraction

ii. the *novel* approach in which only the principal activation intervals of the sEMG signal were considered.

Figure 3.3 shows the workflow of the two approaches implemented for the extraction of the muscle synergies.

Gait Cycle Segmentation and Normalization

In the last years, several approaches have been proposed to time-segment sEMG signal [108–110]. In this study, the foot-switch signals were used to time-segment and classify the gait cycles according to the foot-floor contact sequence. Only the HFPS gait cycles, defined as the physiological sequence of Heel Contact (H), Flat Foot Contact (F), Push Off (P), and Swing (S), were considered, discarding those characterized by atypical gait cycles [108]. Only the gait cycles belonging to the rectilinear path (see **Figure 3.1**) were analyzed, removing those corresponding to direction changes at the beginning and at the end of the walkway (including deceleration before and acceleration after the U-turn) [11]. Finally, each segmented gait cycle was normalized in amplitude with respect to its global maximum, time-normalized to 1000 samples [55], and all gait cycles selected were concatenated in a single vector [111].

Extraction of Principal Activations (PAs) through CIMAP algorithm

The muscle activation onset/offset timing was computed from the sEMG signals by means of a muscle activity detector based on LSTM neural networks (LSTM-MAD). See **A Deep Learning Approach for Muscle Activity Detection** chapter for further details on the LSTM-MAD approach. The optimized version of the CIMAP (Clustering for Identification of Muscle Activation Patterns) [104] algorithm was then applied to the muscle activation intervals to select PAs.

Briefly, PAs are defined as those muscle activations that are strictly necessary to accomplish a specific biomechanical task and describe the fundamental

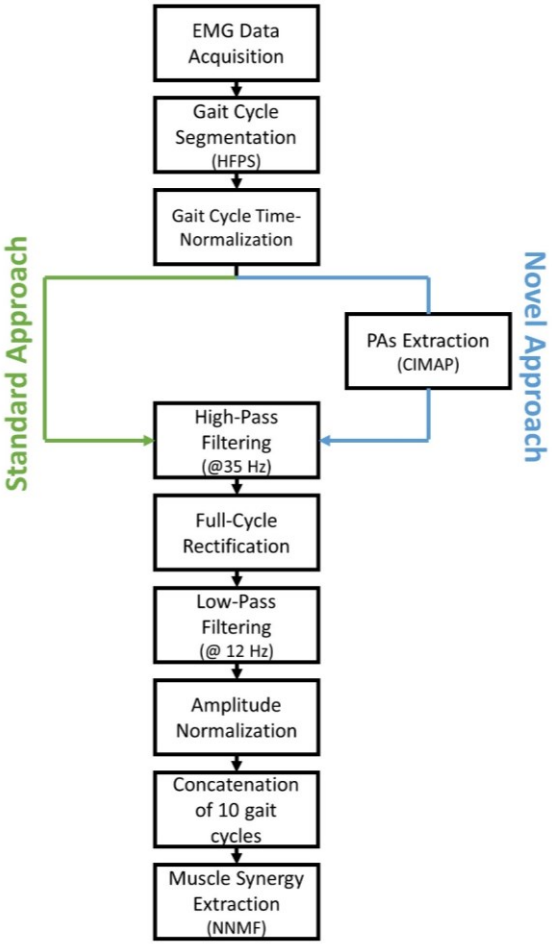

Figure 3.3 Workflow of the two approaches implemented for the muscle synergy extraction. Reprinted from "*Muscle Synergies Extracted Using Principal Activations: Improvement of Robustness and Interpretability*" by Ghislieri *et al.* (2020).

activation intervals of a specific muscle. The CIMAP algorithm, based on hierarchical clustering, groups together the gait cycles sharing similar sEMG onset-offset patterns. For each cluster, the cluster prototype is defined as the median timing pattern. Considering only the most representative clusters (i.e., those containing a significant number of elements compared to the total number of gait cycles acquired during the task), PAs are computed as the intersection of the representative clusters' prototypes [104]. Then, for each observed muscle, a single PA was obtained. PA was defined as a 1000-samples binary mask that was set to 1 in correspondence of the time-instants in which a principal activation was detected and to 0 otherwise.

Figure 3.4 represents an example of application of the CIMAP algorithm to sEMG gait data acquired during the walking task of a healthy subject of the sample population from the PL and GMD muscles. **Figure 3.4A** represents normalized activation intervals for the various gait cycles, grouped in clusters sharing similar activation timings. Each orange interval represents the prototype of a representative cluster. **Figure 3.4B** depicts how PAs are obtained from the intersection of the cluster prototypes.

The extraction of the PA intervals from the original sEMG signals of a specific

muscle was performed by windowing all the time-normalized gait cycles through the correspondent binary mask.

See **Extraction of Principal and Secondary Activations through CIMAP** chapter for additional details on the optimized version of the CIMAP algorithm.

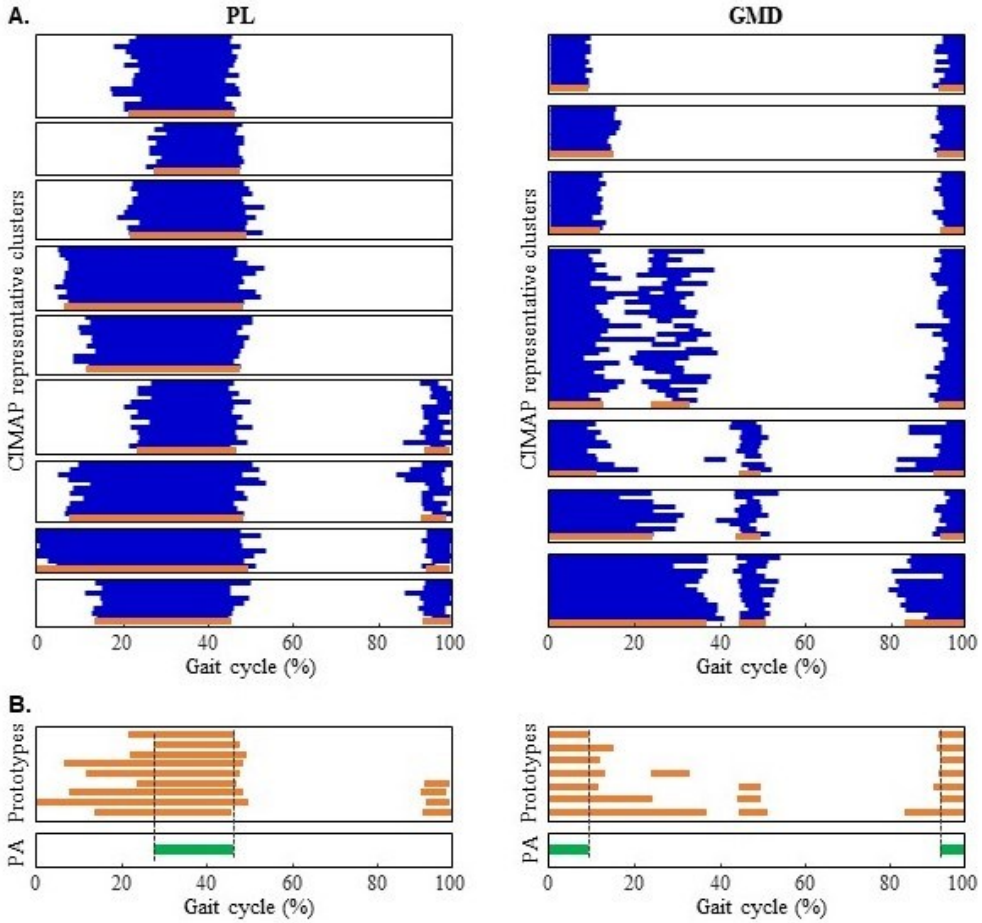

Figure 3.4 Application of the optimized version of the CIMAP algorithm to sEMG signals acquired from the PL (left) and GMD (right) muscles of a healthy subject of the sample population during a walking task. (A) Blue lines represent the cluster elements (muscle activation intervals computed through LSTM-MAD algorithm) normalized into 1000 time points with respect to the gait cycle duration, while orange intervals represent the prototypes of each cluster (computed as median of the elements that belong to the same cluster). (B) Principal activation (PA) is represented in green and is defined as the intersection of all the cluster's prototypes. Reprinted from "*Muscle Synergies Extracted Using Principal Activations: Improvement of Robustness and Interpretability*" by Ghislieri *et al.* (2020).

Muscle Synergies Extraction and Sorting

The sEMG signals were high-pass filtered at 35 Hz by means of an 8th-order Butterworth digital filter to remove motion artifact, demeaned, and full-cycle rectified to obtain a non-negative signal. Then, the rectified signals were low-pass filtered by means of a 5th order digital Butterworth filter with a cut-off frequency of 12 Hz to obtain the sEMG envelope. The signals were then normalized in amplitude with respect to the global maximum of each muscle to ensure an equally weighted contribution of each acquired muscle in the muscle synergy extraction process.

The normalized envelopes were divided into groups of 10 concatenated gait

cycles (called subgroups) allowing for muscle synergy assessment over the entire walk duration [112]. For each subgroup, muscle synergies were extracted from the filtered sEMG signals by means of the Non-Negative Matrix Factorization (NNMF) algorithm. This algorithm models the original sEMG signals (M) as the linear combination of the time-independent muscle synergy weights (W) and the time-dependent activation coefficients (C) [34] as described in (**3.2**):

$$M(t) = \sum_{k=1}^{N} C(t)_k \cdot W_k + e \qquad \textbf{(3.2)}$$

where N represents the optimal number of muscle synergies needed to properly model the original sEMG data. The weight vector W_k describes the contribution of each observed muscle to the *k*-synergy, the activation coefficient vector $C(t)_k$ represents the time-dependent modulation of the muscles recruited in the *k*-synergy and e represents the prediction error of the factorization algorithm. The MATLAB® function "*nnmf*" was used to apply the NNMF algorithm, setting the routine's input parameters as follows: multiplicative update as factorization algorithm, $1e^{-6}$ as function and search tolerance, 50 as the number of factorization replicates, and 1000 as the maximum number of factorization iterations.

The first algorithm initialization was performed differently for the weight vector W_k and the activation coefficient vector $C(t)_k$. The C matrix was initialized with values randomly selected from a uniform distribution in the range [0, 1]. To improve the performance of the factorization algorithm and the accuracy in the reconstruction of the original sEMG data, a sparseness constraint was imposed in the initialization of the W matrix [37]. In particular, W matrix was first initialized with values randomly chosen from a uniform distribution in the range [0, 0.05], then one random element of each W_k vector was set to a value selected from a uniform distribution in the range [0.7, 0.8]. Therefore, only one muscle for each *k*-synergy has a significant contribution, obtaining an extremely sparse NNMF initialization [37].

To explore different solutions of the NNMF algorithm, the factorization process was run many times on the same gait data, changing the number of muscle synergies (N) in the range [1, 8]. For each value of *N*, the reconstruction quality was assessed by means of the total Variance Accounted For ($tVAF$), defined as the uncentered Pearson's correlation coefficient expressed in percentage (**3.3**):

$$tVAF = \left(1 - \frac{\sum_{k=1}^{m}(M_k - M_k^R)^2}{\sum_{k=1}^{m} M_k^2}\right) \cdot 100 \qquad \textbf{(3.3)}$$

where m represents the number of muscles observed, $\sum_{k=1}^{m}(M_k - M_k^R)^2$ describes the sum of the squared errors between the original (M_k) and reconstructed (M_k^R) sEMG signals of the *k*-synergy, and $\sum_{k=1}^{m} M_k^2$ represents the total sum of squared M_k values with respect to zero. The optimal number of muscle synergies needed to properly model the sEMG signals of the *i-th* subgroup ($N_{90,i}$) was selected by choosing the smallest number of synergies (N) granting a $tVAF$ value equal to or

greater than 90% [55]. Since each subgroup could be described by a different number of muscle synergies, the final number of synergies (N_{90}) was then selected, for each subject, as the mode of the numbers of muscle synergies computed on each 10-gait-cycle subgroup ($N_{90,i}$).

To represent the synergy output in the range [0, 1], the weight vectors W_k were normalized in amplitude with respect to their global maximum. Then, the activation coefficient vectors $C(t)_k$ were multiplied by the correspondent normalized values.

To sort the muscle synergies in the same order for each subgroup and for each subject, the *k*-means algorithm was applied to the W matrix [22]. Clustering was performed by means of the MATLAB® routine "*kmeans*" using the following input parameters: N_{90} as number of *k*-means clusters, 1000 as maximum number of iterations, 15 as number of replicates, and cosine as distance metric. The activation coefficients matrix C was ordered accordingly.

Muscle Synergy Analysis

The number of muscle synergies, the intra-subject consistency, the robustness, and the interpretability were used in the following to quantitatively compare the muscle synergies extracted from the PD and healthy populations considering the *standard* and the novel approach.

i. Number of Muscle Synergies

As stated above, the optimal number of muscle synergies needed to properly reconstruct the sEMG signals of the *i*-th subgroup ($N_{90,i}$) was selected by choosing the smallest number of synergies (N) granting a $tVAF \geq 90\%$. The final number of synergies (N_{90}) was then selected, for each subject, as the mode of the number of muscle synergies computed on each 10-gait-cycle subgroup.

ii. Intra-Subject Consistency

The intra-subject consistency of the muscle synergies among the 10-gait-cycle subgroups was evaluated by computing the Cosine Similarity (CS) [30] of the previously sorted weight vectors W_k and activation coefficient vectors $C(t)_k$, separately. The CS between the previously sorted weight vectors belonging to the *i*- and *j-th* subgroup of the *k*-synergy was defined as the normalized scalar product between the vectors expressed in percentage, as described in (**3.4**) and (**3.5**):

$$CS_{W,k}^{i,j} = \left(\frac{W_k^i \cdot W_k^j}{\|W_k^i\| \, \|W_k^j\|} \right) \cdot 100 \qquad (\mathbf{3.4})$$

$$CS_{C,k}^{i,j} = \left(\frac{C_k^i \cdot C_k^j}{\|C_k^i\| \, \|C_k^j\|} \right) \cdot 100 \qquad (\mathbf{3.5})$$

where $CS_{W,k}^{i,j}$ and $CS_{C,k}^{i,j}$ represent the cosine similarity computed between the weight vectors W_k and the activation coefficients $C(t)_k$ of the *i*- and *j-th* subgroup, respectively. The CS values range between 0 (no similarity) and 1 (complete similarity).

iii. Robustness

The robustness of the muscle synergies among different subgroups of 10 gait cycles was assessed through the Cross-Variance Accounted For [111] defined as in (**3.6**):

$$CrossVAF^{i,j} = \left(1 - \frac{\sum_{k=1}^{m}(M_k^i - M_k^{R,j})^2}{\sum_{k=1}^{m}(M_k^i)^2}\right) \cdot 100 \qquad (\mathbf{3.6})$$

where M_k^i and $M_k^{R,j}$ represent the original and the reconstructed sEMG signals of the *k*-muscle for the *i*- and *j-th* subgroup, respectively.

This parameter assesses how well the muscle synergies extracted for the *i-th* subgroup reconstruct the sEMG signals that belong to the *j-th* subgroup. For each subject, the average $CrossVAF$ value was computed over all the possible couples of 10-gait-cycle subgroups without considering the main diagonal of the $CrossVAF$ matrix. The average $CrossVAF$ can assume values ranging from 0% to 100%, corresponding to a low or high correlation between the reconstructed and the original sEMG signals from different subgroups, respectively.

iv. Interpretability

Previous studies demonstrated that five muscle synergies are usually needed to properly describe human locomotion [19,24]. Each of these muscle synergies can be characterized by a specific biomechanical function. These biomechanical functions were generally assigned to each muscle synergy by applying an amplitude threshold to the weight vectors (W_k> 0.5) in order to define the prevailing muscles contributions [24]. Moreover, the profile of the activation coefficients $C(t)_k$ was usually observed to define the gait cycle phase in which the muscle synergy is mainly activated, according to the functional gait cycle phases proposed by Perry *et al.* [97]. In the study by Rimini *et al.* [24] 5 biomechanical functions common to all the analyzed subjects during the walking task were discovered. **TABLE 3.2** reports the description of each biomechanical function and the muscles mainly involved in each function (W_k> 0.5).

TABLE 3.2
BIOMECHANICAL FUNCTIONS OF THE MUSCLE SYNERGIES DURING GAIT.

Function	Involved muscles	Biomechanical function
F1	TFL, GMD	Hip joint stabilization during heel strike and load acceptance phase.
F2	LGS, PL, SOL	Propulsion at the mid and terminal stance.
F3	TA	Forefoot clearance control during the swing phase and foot control during the first rocker.
F4	MH, LH	Leg deceleration at the end of the swing phase.
F5	LD_R, LD_R	Control of the trunk position in the frontal plane at heel strike.

Reprinted from "*Muscle Synergies Extracted Using Principal Activations. Improvement of Robustness and Interpretability*" by *Ghislieri et al., 2020*

For example, the biomechanical function F2 is used to generate the propulsion and requires, among the observed muscles, the involvement of the LGS, PL, and SOL muscles (the other acquired muscles are not directly involved during propulsion).

The muscle synergy Interpretability (I) was evaluated considering the average of the muscle synergy weights that are not directly involved in the k-synergy biomechanical function as described in (**3.7**):

$$I = \frac{1}{N}\sum_{k=1}^{N}((1 - \overline{W_k'}) \cdot 100) \quad (\mathbf{3.7})$$

where N represents the final number of muscle synergies needed to describe the motor task and $\overline{W_k'}$ is the average contribution of the muscles not directly involved in the biomechanical task described by the k-synergy. A muscle synergy can be considered more easily interpretable when the averages of the muscle synergy weights not directly involved in the specific biomechanical function are close to zero ($\overline{W_k'} \cong 0$), while it can be considered less interpretable when they have values comparable with the weights of the muscles directly involved in the biomechanical function ($\overline{W_k'} \cong 1$). The I values are expressed in percentage, and range between 0% and 100%, suggesting low and high interpretability, respectively.

Statistical Analysis

To determine if there is a statistically significant difference, in the walking speed, between healthy and PD subjects, the Wilcoxon signed-rank test was used, setting the significance level (α) at 0.05. Two-way repeated measures analysis of variance (ANOVA) followed by *post-hoc* analysis with Tukey's adjustment for multiple comparisons was used to test differences in muscle synergy results between Group (Healthy and PD) and Approach (Standard and PAs). The effect size of the statistically significant differences was calculated by means of the Hedges' g including the correction for small sample sizes [113]. The significance level (α) was set equal to 0.05. The statistical analysis was carried out using the Statistical and Machine Learning Toolbox of MATLAB®.

3.3 Results

During the experimental sessions, an average speed of 1.2 ± 0.1 m/s and 1.0 ± 0.2 m/s and a dataset of 156 ± 25 and 129 ± 37 *typical* gait cycles (i.e., gait cycles characterized by the HFPS foot-floor contact sequence) were assessed for the healthy and PD population, respectively. On average, the Wilcoxon test revealed a slightly significant decrease (p = 0.04) in the walking speed of PD patients with respect to the healthy subjects.

In the following, the results obtained using the *standard* and the novel approach (entailing the extraction of PAs) were compared in terms of (*i*) number of muscle synergies, (*ii*) intra-subject consistency, (*iii*) robustness, and (*iv*) interpretability.

i. Number of Muscle Synergies

On average, an optimal number of muscle synergies of 4.8 ± 0.1 and 5.0 ± 0.1 was found on the healthy population, considering the *standard* and the novel

approach, respectively. Considering the PD population, an average number of 4.7 ± 0.1 and 5.1 ± 0.1 muscle synergies was computed considering the *standard* and the novel approach, respectively. Two-way repeated measures ANOVA revealed a statistically significant increase (p = 0.002, g = 0.69) in the optimal number of muscle synergies computed considering the novel approach with respect to the *standard* one, while no statistically significant differences (p = 0.83) were assessed between healthy and PD populations. No significant interaction effects were detected between Group and Approach.

The average number of muscle synergies values are reported in **TABLE 3.3**, with the indication of the statistically significant differences ($p < 0.05$).

TABLE 3.3
MUSCLE SYNERGY RESULTS ON HEALTHY SUBJECT AND PARKINSON DISEASE (PD) PATIENTS

	HEALTHY SUBJECTS		*PD PATIENTS*		*2-WAY ANOVA (P-VALUE)*	
	Standard	***PAs***	***Standard***	***PAs***	***Group***	***Approach***
Number of muscle synergies	4.8 ± 0.1	5.0 ± 0.1	4.7 ± 0.1	5.1 ± 0.1	0.83	**0.002**
Intra-subject consistency						
• **Weight vectors**	0.99 ± 0.01	0.99 ± 0.01	0.98 ± 0.02	0.98 ± 0.02	**0.003**	0.13
• **Activation coefficients**	0.99 ± 0.01	0.99 ± 0.01	0.98 ± 0.01	0.98 ± 0.02	**0.005**	0.24
Robustness (%)	80.7 ± 0.7	80.6 ± 1.2	79.1 ± 0.7	79.6 ± 0.7	0.13	0.82
Interpretability (%)	90.6 ± 4.4	93.6 ± 3.9	90.1 ± 2.6	93.7 ± 1.7	0.79	**< 0.0001**

Values of parameters are reported as mean ± standard deviation over the population.
Statistically significant differences (p < 0.05) between Group or Approach are represented in bold.

Figure 3.5 and Error! Reference source not found. report the weight vectors and the activation coefficients extracted from a representative healthy subject and PD patient of the sample population, respectively, using the two pre-processing techniques: (

Figure 3.5A and Error! Reference source not found.**A**) *standard* approach and (

Figure 3.5B and Error! Reference source not found.**B**) the novel approach (extraction of PAs). No significant differences both in the final number of muscle synergies and in their composition were revealed.

ii. Intra-Subject Consistency

Considering the activation coefficients $C(t)_k$, two-way repeated-measures ANOVA revealed a statistically significant decrease (p = 0.005, g = 0.83) in the intra-subject consistency of the PD population with respect to the healthy population. No statistically significant differences (p = 0.24) between Approach and no significant interaction effects between Group and Approach were detected.

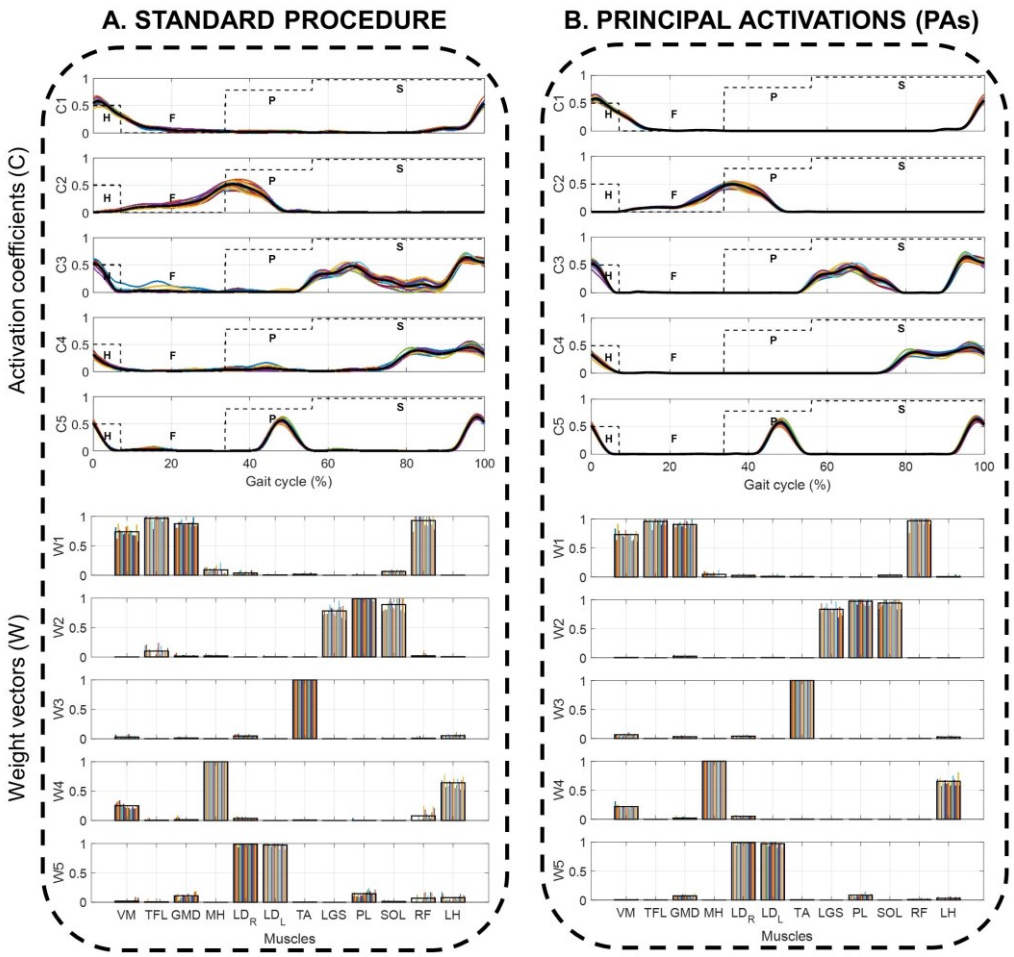

Figure 3.5 Example of activation coefficients C_k and weight vectors W_k extracted from a representative healthy subject of the sample population using the two different processing techniques: (A) standard approach, and (B) novel approach (extraction of PAs). Each colored line (or colored vertical bar) represents C_k (or W_k) extracted from a single 10-gait-cycle subgroup, while black lines (or top of black rectangles) represent the average C_k (or W_k) computed over subgroups. The dotted lines, in the C_k-plots, represent the mean foot-switch signal with the indication of the 4 gait phases: Heel contact (H), Flat foot contact (F), Push off (P) and Swing (S).

Considering the weight vectors W_k, two-way ANOVA revealed a statistically significant decrease ($p = 0.003$, $g = 0.66$) in the intra-subject consistency of the PD population with respect to the healthy population. No statistically significant differences ($p = 0.13$) between Approach and no significant interaction effects between Group and Approach were detected.

The average intra-subject consistency values are reported in **TABLE 3.3**, with the indication of the statistically significant differences ($p < 0.05$).

Figure 3.7A shows the boxplots of the intra-subject consistency computed on the healthy and PD populations using the two approaches.

iii. Robustness

On average, a robustness value of 80.7% ± 0.7% and 80.6% ± 1.2% was found on the healthy population, considering the *standard* and the novel approach, respectively. Considering the PD population, instead, an average robustness value of 79.1% ± 0.7% and 79.6% ± 0.7% was computed considering the *standard* and

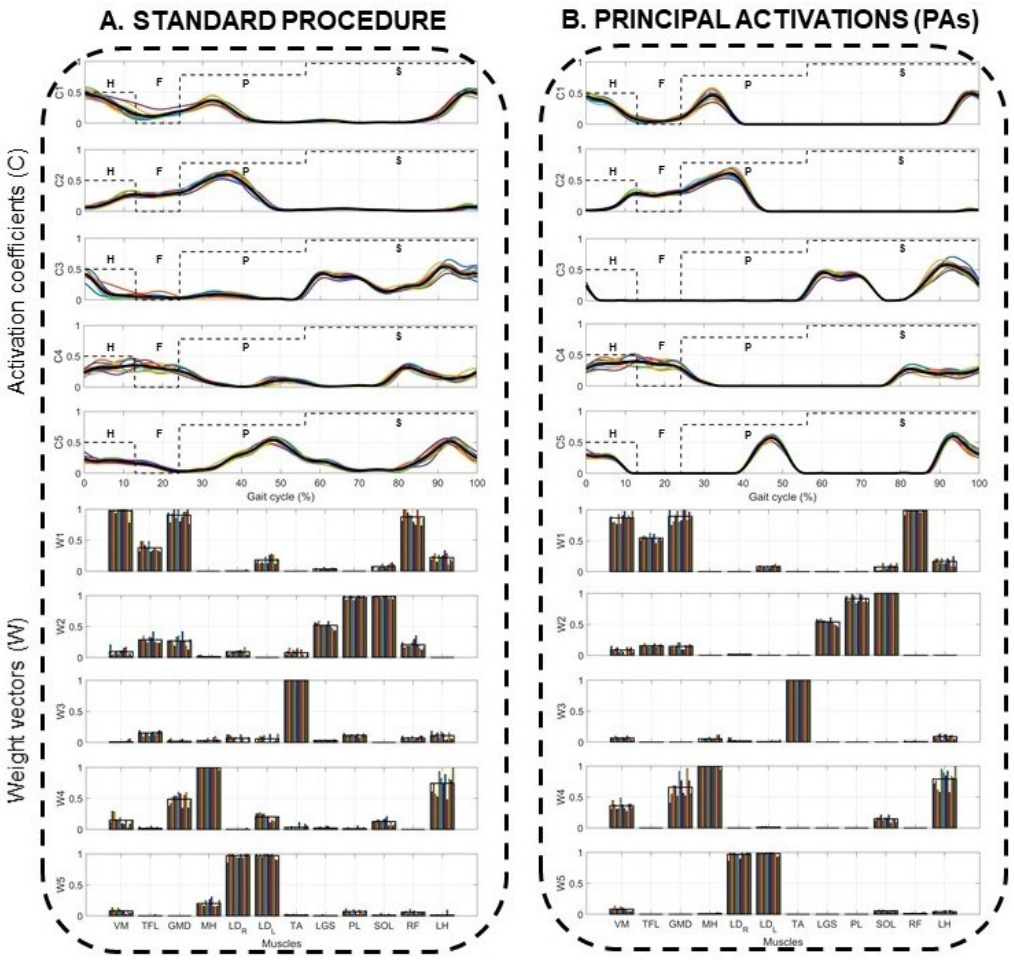

Figure 3.6 Example of activation coefficients $\boldsymbol{C_k}$and weight vectors $\boldsymbol{W_k}$ extracted from a representative PD patient of the sample population using the two different processing techniques: (A) standard approach, and (B) novel approach (extraction of PAs). Each colored line (or colored vertical bar) represents $\boldsymbol{C_k}$ (or $\boldsymbol{W_k}$) extracted from a single 10-gait-cycle subgroup, while black lines (or top of black rectangles) represent the average $\boldsymbol{C_k}$ (or $\boldsymbol{W_k}$) computed over subgroups. The dotted lines, in the $\boldsymbol{C_k}$-plots, represent the mean foot-switch signal with the indication of the 4 gait phases: Heel contact (H), Flat foot contact (F), Push off (P) and Swing (S).

the novel approach, respectively. Two-way repeated-measures ANOVA revealed no statistically significant differences in the muscle synergy robustness between Group (p = 0.13) and between Approach (p = 0.82). No significant interaction effects were detected between Group and Approach.

The average robustness values are reported in **TABLE 3.3**, with the indication of the statistically significant differences ($p < 0.05$).

Figure 3.7B represents the boxplots of the $CrossVAF$ computed on the healthy and PD populations considering the two processing approaches.

iv. Interpretability

On average, a muscle synergy interpretability value of 90.6% ± 4.4% and 93.6% ± 3.9% was found on the healthy population, considering the *standard* and the novel approach, respectively. Considering the PD population, instead, an average interpretability value of 90.1% ± 2.6% and 93.7% ± 1.6% was computed considering the *standard* and the novel approach, respectively. Two-way repeated-

measures ANOVA reveals a statistically significant increase ($p < 0.0001$, $g = 1.01$) in the interpretability of the muscle synergies extracted considering the novel approach with respect to those extracted considering the *standard* one. No statistically significant differences ($p = 0.79$) were assessed between Group (healthy and PD) and no significant interaction effects were detected between Group and Approach.

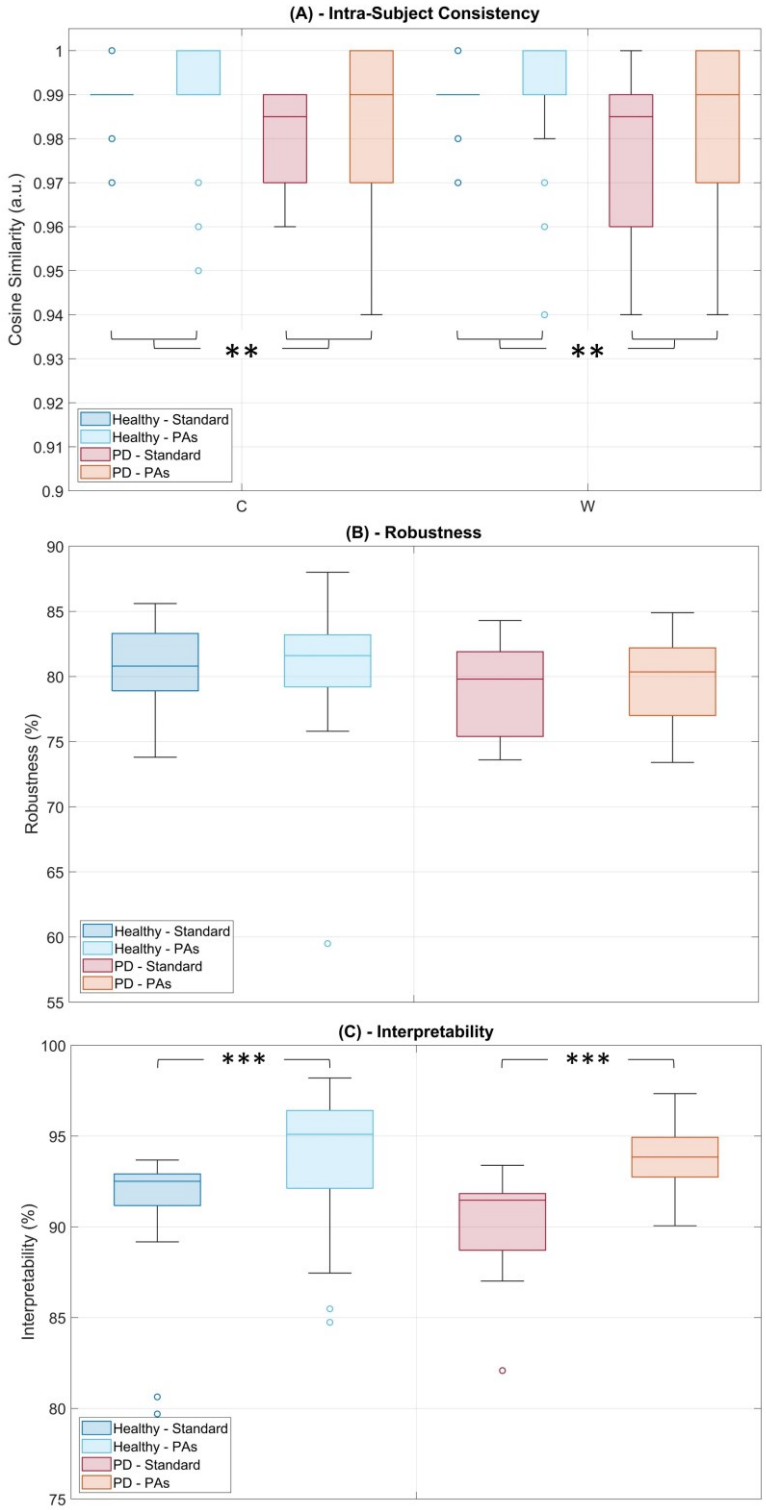

Figure 3.7 Boxplots of (A) intra-subject consistency, (B) robustness, and (C) interpretability used to compare the standard and the novel approach for muscle synergy extraction. Outliers are indicated by circles. Single and double asterisks represent *p*-values lower than 0.05 and 0.01, respectively.

The average interpretability values are reported in **TABLE 3.3**, with the indication of the statistically significant differences ($p < 0.05$).
Figure 3.7C shows the boxplots of muscle synergy interpretability computed on the healthy and PD populations considering both the pre-processing techniques.

3.4 Discussion and Conclusions

Although the effectiveness of the muscle synergy theory in modeling the modular organization of the CNS during motor tasks is well known in literature [7,24,27,30,47,55], there are no shared standards for sEMG pre-processing before muscle synergy extraction. The pre-processing techniques previously used in literature (*"standard"* approaches) for muscle synergy extraction generally considered the whole sEMG time-instants as input of the factorization algorithm [19,23,28,55]. However, these standard approaches may be influenced by the high cycle-by-cycle variability of the sEMG activation patterns [100]. Therefore, these approaches may not be sufficient to fully understand the motor control strategies during human locomotion.

The combination of SGA and CIMAP (with the extraction of the principal and secondary muscle activation intervals) algorithms as a pre-processing step before muscle synergy extraction may provide a valuable tool to understand how a set of muscle synergies are recruited and modulated by the central nervous system under different conditions. In particular, the ability to distinguish between the principal and the secondary muscle activation intervals allows for separately assessing human motor control strategies adopted during gait cycle phases characterized by highly consistent and repeatable activation intervals (PAs) and during gait cycle phases characterized by extemporary and lowly repeatable activation intervals (SAs), respectively. Moreover, the selection of the PAs from the whole sEMG signal may help the interpretation of muscle activation patterns by reducing the intra-subject variability of the activation intervals. In this chapter, only the applicability of the selection of PAs as a pre-processing step before muscle synergy extraction was tested, leaving the study of motor control strategies during secondary muscle activations to future studies.

As stated before, the extraction of the PAs allows evaluating only the "*necessary*" muscle activations, discarding those with auxiliary function [105], such as those providing corrections to cyclic motion and body segment posture (whose muscle synergies can be investigated through the selection of the SAs from the whole sEMG signals). According to this approach, only the sEMG time-instants in correspondence of PAs are considered as inputs of the factorization algorithm [24,104], while the remaining sEMG time-instants are set to zero.

To assess the differences in muscle synergies between the newly proposed approach and the standard one, the muscle synergies extracted from 22 healthy subjects and 22 patients affected by Parkinson's disease during a walking task have been compared in terms of number of muscle synergies, intra-subject consistency, robustness, and muscle synergy interpretability.

In terms of the number of muscle synergies, both approaches accurately

reconstruct the original sEMG signals acquired from both the sample populations through five muscle synergies. These muscle synergies are very similar both in their composition (temporal modulation of the activation coefficients and weighted contribution of the observed muscles) and in the biomechanical functions described by each of them. In particular, the same five biomechanical functions described in Ref. [24] can be associated with the muscle synergies extracted considering both the standard and the novel approach. Even if a statistically significant difference in age between PD patients and control subjects was detected, a few studies, such as those published by Monaco *et al.*[20,114], demonstrated that neither temporal patterning of activation coefficients nor muscles' contribution to each muscle synergy were significantly affected by aging. Moreover, the purpose of this chapter was to assess the applicability and the performance of the novel approach considering both physiological and pathological conditions rather than assess the difference in motor control strategies between the two sample populations.

In terms of intra-subject consistency and robustness, the standard and the novel approach reveal similar average values of intra-subject consistency and robustness of muscle synergies considering both healthy and pathological subjects, suggesting high repeatability of the motor control strategy among the 10-gait-cycle subgroups and high robustness of muscle synergy results, independently from the pre-processing technique used. However, statistically significant ($p < 0.05$) differences in weight vector and activation coefficient intra-subject consistencies between the PD patients and healthy controls have been detected considering both the standard and the novel approach. This finding is consistent with a previous study by Allen *et al.* [115] focused on assessing the improvement of gait and balance function in PD patients after short-term rehabilitation through the muscle synergy theory. Results revealed that muscle synergies were more consistently recruited immediately after rehabilitation, suggesting more reliable and repeatable motor output. Furthermore, intra-subject consistency has been demonstrated to be a more sensitive marker of improved motor performance compared to the number of muscle synergies. Indeed, only a modest reduction in muscle synergy number has been detected in the PD population compared to the control subjects.

In terms of interpretability of the muscle synergies, the novel approach outperforms the standard one. Indeed, results suggest that the extraction of the PAs allows for obtaining higher interpretability of the muscle synergies considering both healthy (90.6 % ± 4.4 % vs. 93.6 % ± 3.9 %) and pathological patients (90.1% ± 2.6% vs. 93.7 % ±1.7 %) compared to the standard approach, thus providing a more clear assessment of the modular organization of the CNS during gait. Moreover, the possibility to extract more distinctly organized (or interpretable) muscle synergies may be useful to make easier the assignment of a specific biomechanical function to each muscle synergy.

The analysis of the final number and the composition of the obtained muscle synergies revealed no loss of information due to the extraction of the PAs, compared to the standard approach. Moreover, the higher performance in terms of muscle synergy interpretability obtained considering the novel approach demonstrates that the extraction of the PAs may successfully improve the muscle

synergy analysis during gait in both healthy and pathological subjects.

The number and composition of muscle synergies can also be strongly influenced by other steps of the muscle synergy extraction process [23,36,38,39,44,49–53], such as the sEMG pre-processing (e.g., low-pass filtering techniques) [38,49–51,53] and the number and choice of muscles acquired [23]. However, the focus of this chapter was on developing and validating an approach for muscle synergy extraction based on the combined application of SGA and CIMAP (with the extraction of PAs) algorithms, and not on evaluating the effect of different filtering techniques or subsets of acquired muscles on the extraction of the muscle synergies. Indeed, the same number of acquired muscles (i.e., 12 lower limb and trunk muscles) and filtering steps (i.e., high-pass filter at 35 Hz, full-cycle rectification, and low-pass filter at 12 Hz) were considered for both the tested approaches (standard and novel approach), following the common recommendations and guidelines for muscle synergy extraction.

In this chapter, an innovative pre-processing technique for muscle synergy extraction was proposed combining Statistical Gait Analysis (SGA) and a clustering algorithm (CIMAP) that allows for obtaining the principal activations (PAs). To properly compute PAs, sEMG signals must be recorded for at least 3 minutes during gait. More specifically, sEMG signals used in this chapter for muscle synergy extraction were acquired during 5-minute walking tasks. Signal recording during a "long" physiological walk is needed to be able to collect at least 100 - 200 typical gait cycles required for PAs computation. This requirement does not limit the feasibility and applicability of the proposed methodology to pathological populations. Indeed, gait analysis is commonly used to quantitatively assess patients' locomotion performance only in those patients able to independently walk, for some minutes, without walking aids or external supports. In the past, several studies demonstrated the feasibility of gait data acquisition, during recording sessions lasting 3 minutes, in patients suffering from different neurological conditions, e.g., Normal Pressure Hydrocephalus [89], mild ataxia [116], and cerebral palsy [117].

In this chapter, the CIMAP algorithm was used to select PAs and discard secondary activations, suggesting that muscle synergies are better understood when considering only PAs. This is in line with a previous work in which the selection of PAs was used to define a robust asymmetry index, based on sEMG activity during locomotion [67]. In particular, the study by Castagneri *et al.* [67] provided a validation both on healthy and pathological populations.

The approach proposed in this chapter was validated considering both healthy and pathological populations, for whom the assessment of motor control through muscle synergies may be of the uttermost importance [45,115]. However, when considering pathological populations, also secondary activations (SAs) might be fundamental in the interpretation of the results. Indeed, discarding the effect of auxiliary functions included in the secondary activations might bias the interpretation of pathological types of behavior, instead of improving it. Nevertheless, it should be noticed that the opportunity to separate principal from secondary activations, provided by the CIMAP algorithm, does not preclude

studying also secondary (auxiliary) activations. Therefore, future developments of the proposed approach will include the analysis of muscle synergies extracted from a pathological sample population considering the principal and the secondary activations, separately.

In conclusion, the results presented in this chapter demonstrate that the extraction of the principal activations can be successfully used as a pre-processing step before muscle synergy extraction, allowing a more interpretable assessment of the modular organization of the CNS during a walking task without any loss of information.

Methodological Issue – Multi-Criteria Decision Analysis for Selecting the Optimal Number of Muscle Synergies

3.5 Introduction

One of the main challenges for researchers and clinicians interested in human motion control is to understand how the CNS controls a complex system, such as the musculoskeletal system, during different movement tasks. The complexity of the musculoskeletal system lies in its redundancy, due to the countless number of muscles and joints involved and the many different ways that muscles can be enrolled to execute the same motor task.

One of the most widely accepted theory for the assessment of human motor control is the muscle synergy theory. Muscle synergies are a valuable tool to quantitatively and non-invasively assess how the CNS can manage the high complexity and redundancy of the motor control system. Applications range from the medical field (e.g., monitoring of patients suffering from neurological, neurodegenerative diseases [18,43], or joint disorders [118]), to the rehabilitation field (e.g., pre-/post-treatment comparisons [119]), to the robotic field (e.g., control of robotic devices or exoskeletons [17,120]). According to this theory, muscles involved in a specific movement are activated in small groups, commonly referred to as muscle synergies [121]. Therefore, the CNS can reduce the complexity of the motor control system thanks to the activation of multiple muscles with a single control signal. Previous studies have demonstrated that muscle activity during a variety of movement tasks, such as walking, running, and cycling, can be successfully described through a small set of muscle synergies responsible for specific biomechanical functions [19]. In these studies, muscle synergies are extracted from surface electromyography (sEMG) signals acquired from sets of muscles during a variety of motor tasks, using different matrix factorization algorithms, such as "standard" Non-Negative Matrix Factorization (NNMF) [41,122], Gaussian NNMF (GNNMF), inverse Gaussian NNMF (IGNNMF) [36,123], and principal or independent component analysis. Among all the factorization algorithms, NNMF is the most widely used algorithm for muscle synergy extraction, even if it was demonstrated that similar results can be obtained by applying other approaches [32,40]. The NNMF algorithm models the original sEMG data as a linear combination of muscle synergy weight vectors and activation coefficients, whose dimensions depend on the number of muscle synergies needed to properly reconstruct the motor task.

In the last years, the optimal number of muscle synergies (N_{opt}) has been proposed as a meaningful feature for the analysis of motor control strategies in pathological populations. In the study by Allen *et al.* [124], a reduced number of muscle synergies has been demonstrated in patients affected by brain injury with respect to a healthy population while executing walking tasks. Similar results have been obtained in the work of Rodriguez *et al.* [45], in which a decreased

neuromuscular complexity during gait has been assessed in patients affected by Parkinson's disease. These studies suggest that the number of muscle synergies and their composition could be correlated with the motor control capacity and its reduction in pathological conditions [33,55].

Despite the growing interest in the assessment of muscle synergy number, there is a lack of standardized criteria or shared guidelines for computing the optimal number of muscle synergies (N_{opt}) from sEMG recordings, revealing a low reproducibility and comparability of muscle synergy results obtained from different studies. One of the most widely used methods is the application of a cut-off threshold based on the Variance Accounted For (VAF) [23,24,43–46,112,118,120,125,126], defined as the uncentered Pearson's correlation coefficient between the original and the reconstructed sEMG signals. More specifically, according to this method, N_{opt} is defined as the smallest number of synergies that ensures a VAF value above a cut-off threshold (threshold criterion). The VAF threshold is commonly set equal to 90% [23,24,43,44,46,112,118,120,125,126] , but several other studies considered threshold values in the range from 80% to 95% [45]. Discordance over the VAF threshold values significantly intensifies the confusion over the selection of the optimal number of muscle synergies and reduces the comparability with other studies. To a lesser extent, N_{opt} was selected by means of the coefficient of determination R^2 [16,31,34,47,121,122,127,128], setting a cut-off threshold for the mean squared error between the R^2 curve and the linear fit. In the studies by Sawers *et al.* [129] and by Cheung *et al.* [31], bootstrapping techniques have been used to resample multiple times the sEMG data and compute VAF and R^2 curves, respectively. The optimal number of muscle synergies was then selected as the value at which the 95% confidence interval exceeds 90% VAF (or R^2).

To the best of the author's knowledge, only a few works have already explored alternatives to VAF or R^2 curves, using the variability of muscle synergies among task cycles [130], a task decoding-based metric [131], likelihood ratio tests, Bartlett Akaike, Bayesian, and Laplacian information criteria [32,132–135].

In the last years, Multi-Criteria Decision Analysis (MCDA) or Multi-Criteria Decision-Making (MCDM) approaches have been proposed in the field of operational research, in addition to Cost-Benefit Analysis (CBA), to support rigorous decision-making by explicitly taking into account multiple criteria [136]. Applications range from the medical field [137,138] to the transport field [139,140], to the environment and water management [141,142]. The selection of the optimal number of muscle synergies can be considered itself a multi-criteria approach, where several criteria (e.g., reconstruction accuracy and muscle synergy consistency) should be addressed to obtain the best representation of the motor system.

This chapter aims at assessing the applicability of a novel approach for the selection of the optimal number of muscle synergies (N_{opt}), based on an MCDA approach, specifically developed to overcome the limitations of the standard VAF-based approaches. The performance of the MCDA-based approach is evaluated and

compared against standard approaches (Threshold VAF, Elbow VAF, and Plateau VAF) in terms of estimation bias and mean absolute error (MAE), both on simulated and real sEMG signals.

3.6 Materials and Methods

A dataset of simulated and real sEMG signals was used to assess the applicability of the MCDA-based approach for selecting the optimal number of muscle synergies (N_{opt}) and to compare its performance to the principal VAF-based approaches [23,24,43–46,112,118,120,125,126].

1. Real Data

Gait data acquired from 12 subjects were retrospectively analyzed to test the performance of the four different approaches (Threshold VAF, Elbow VAF, Plateau VAF, and MCDA-based approach) when applied to real sEMG signals. Subjects were randomly selected from the PoliToBIOMed Lab (Politecnico di Torino, Turin, Italy) database to include both healthy individuals and patients affected by Parkinson's Disease (PD). This non-homogeneous group of subjects was specifically chosen to verify that the algorithm could work under different conditions.

In particular, 6 out of 12 subjects were patients affected by PD (age: 55.5 ± 5.7 years, height: 171.1 ± 9.1 cm, weight: 76.7 ± 13.2 kg, UPDRS-III [96] during OFF condition: 45.8 ± 13.1, UPDRS-III during ON condition: 16.2 ± 6.5), while the remaining 6 subjects were healthy controls (age: 52.3 ± 10.0 years, height: 171.3 ± 7.2 cm, weight: 73.0 ± 8.7 kg). PD patients were enrolled from those eligible for Deep Brain Stimulation (DBS) at the Stereotactic and Functional Neurosurgery Unit of the University of Turin (Italy). Moreover, none of the healthy subjects reported lower limb injuries or had neurological or musculoskeletal disorders that could compromise their gait performance.

Gait data were recorded through the STEP32 system (Medical Technology, Italy)[46,90,91]. Surface electromyographic (sEMG) signals were acquired through active probes (configuration: single differential, size: 19 mm × 17 mm × 7 mm, Ag-disks diameter: 4 mm, interelectrode distance: 12 mm, gain: variable in the range from 60 dB to 86 dB) placed over the following 12 muscles of the lower limb: right and left Longissimus Dorsii (LD_R, LD_L), Tensor Fasciae Latae (TFL), Gluteus Medius (GMD), Rectus Femoris (RF), Lateral Hamstring (LH), Medial Hamstring (MH), Vastus Medialis (VM), Lateral Gastrocnemius (LGS), Peroneus Longus (PL), Soleus (SOL) and Tibialis Anterior (TA). The dominant lower limb was analyzed for healthy subjects, while the most affected limb was selected for pathological subjects. **Figure 3.2** shows an example of sensor placement for a representative subject of the healthy population.

Subjects were asked to perform a 5-minute walk at a self-selected speed, back and forth on a 9-m straight walkway (**Figure 3.1**). The protocol conformed to the Helsinki declaration on medical research involving human subjects and all the

volunteers signed a written informed consent to participate in the study before each experimental session.

The reconstructed sEMG envelopes were computed, for each subject and each number of muscle synergies in the range [1, 8], as the linear combination of the weight vectors (W) and the activation coefficients (C) extracted from the real data through the NNMF algorithm (**Equation 1.2**).

2. Simulated Data

The sEMG signal during cyclic contractions, such as those observed during walking, can be modeled as the superimposition of two different contributions: (*i*) the muscle activity and (*ii*) the background noise generated by the activity of the neighboring muscles and electronics. Thus, the sEMG signal can be defined as a cyclostationary process [86] and modeled as the superimposition of two different stationary processes [69]:

i. Muscle activity (s) defined as a zero-mean Gaussian process with variance σ_s^2:

$$s(t) \in N(0, \sigma_s^2) \quad \textbf{(3.8)}$$

where $\sigma_s = 10^{(\frac{SNR}{20})} \cdot 1\ \mu V$.

ii. Background noise (n) defined as a Gaussian process with zero-mean and variance σ_n^2:

$$n(t) \in N(0, \sigma_n^2) \quad \textbf{(3.9)}$$

where $\sigma_n = 1\ \mu V$.

Similarly to what was performed in previous studies[37,125,143], simulated sEMG signals were generated starting from real data, defining *a priori* the optimal number of muscle synergies (N_{opt}). More specifically, the muscle activity of twelve muscles was simulated by time-windowing twelve Gaussian processes (s) by means of different time supports. Each time support was defined as the reconstructed sEMG envelope calculated from the muscle synergies extracted from the real data[143], selecting *a priori* the number of muscle synergies (N_{opt}) in the range between 4 and 6 synergies (i.e., numbers of muscle synergies usually selected during walking in healthy subjects). Then, twelve background noise processes (n) were superimposed to simulate the crosstalk of the neighboring muscles. Eight different values of SNR were simulated (SNR = 6, 10, 13, 16, 20, 23, 26, 30 dB) to assess the impact of SNR on the approaches' performance.

The simulated sEMG signals were then band-pass filtered through a 4th order Butterworth digital filter with a lower cut-off frequency of 10 Hz and a higher cut-off frequency of 450 Hz. The steps for the computation of the simulated sEMG signals are represented in **Figure 3.8** for the Tibialis Anterior (TA) muscle. First, muscle synergies (W and C) were extracted from the real data of a representative PD subject of the sample population (**Figure 3.8a**). Second, the reconstruction of the TA envelope was calculated as $W_{TA} \cdot C$ (**Figure 3.8b**). Third, a simulated sEMG signal without additive noise is generated by time-windowing a Gaussian process through the TA envelope (**Figure 3.8c**). Finally, noise is superimposed to the

previous signal to simulate the crosstalk from the neighboring muscles (**Figure 3.8d**).

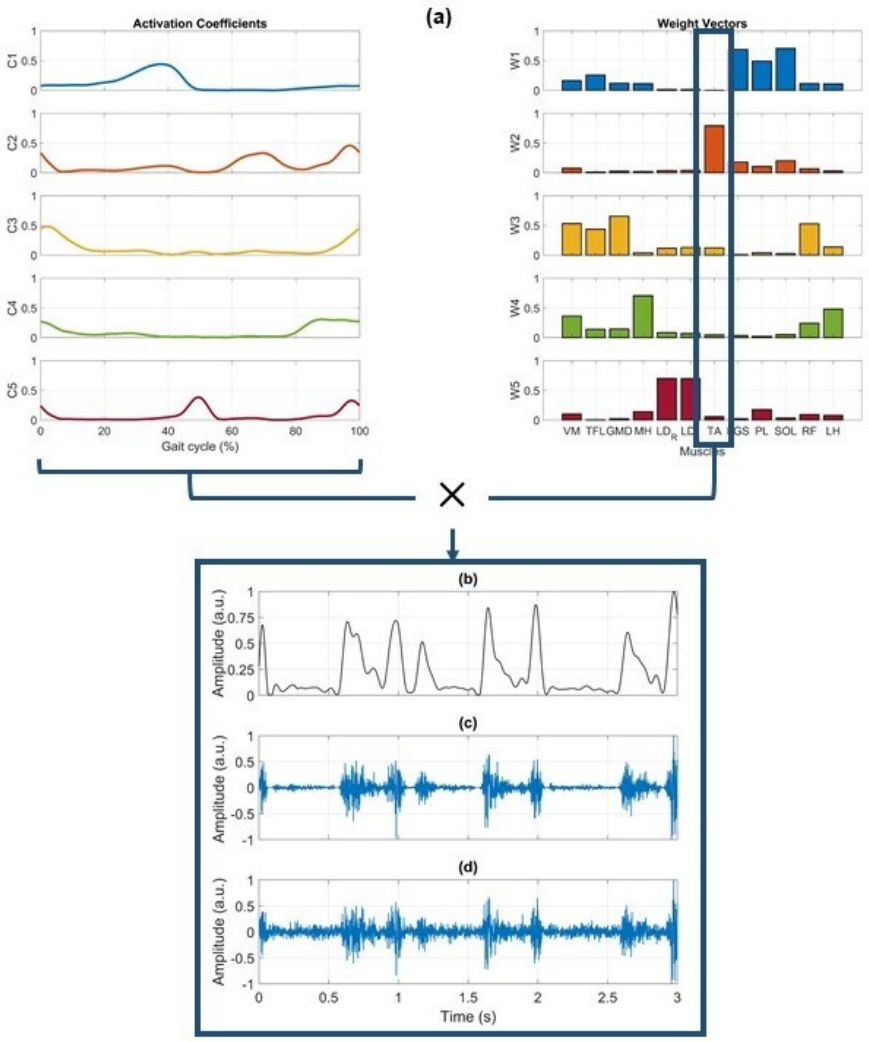

Figure 3.8 Example of the generation of simulated sEMG signal for the Tibialis Anterior (TA) muscle: the first step is (a) the extraction of muscle synergies (W and C) from the real data of a representative subject, the second is (b) the reconstruction of the TA envelope (obtained as W_{TA}*C). Then, (c) a simulated sEMG signal without additive noise is generated. Finally, noise is added to the previous signals. An example of a simulated sEMG signal with $\boldsymbol{SNR}$ = 16 dB is shown in (d).

Therefore, for each of the 12 muscles mentioned above, a dataset composed of 288 simulated sets (12 subjects × 8 $SNRs$ × 3 N_{opt}) was built.

3. Muscle Synergy Extraction

Before muscle synergy extraction, both the simulated and real sEMG signals were pre-processed to obtain the sEMG envelopes.

Considering the real data, sEMG signals were first time-segmented into gait cycles, according to the foot-floor contact sequence. Second, only the HFPS gait cycles, defined as the physiological sequence of Heel Contact (H), Flat Foot Contact (F), Push Off (P), and Swing (S), were considered, discarding those characterized by atypical gait cycles (i.e., non-HFPS gait cycles) [108]. Third only the gait cycles belonging to the rectilinear path (see **Figure 3.1**) were analyzed,

removing those corresponding to direction changes at the beginning and at the end of the walkway (including deceleration before and acceleration after the U-turn) [24]. Finally, each segmented gait cycle was time-normalized to 1000 samples [55], and all gait cycles selected were concatenated in a single vector [24].

Both simulated and real sEMG signals were then high-pass filtered through an 8^{th} order Butterworth digital filter with a cut-off frequency of 35 Hz, demeaned, full-cycle rectified, and low-pass filtered at 12 Hz through a 5^{th} order Butterworth digital filter to obtain the sEMG envelopes. Each sEMG envelope was then normalized in amplitude with respect to its global maximum to ensure an equally weighted contribution of each acquired muscle in the muscle synergy extraction process. The amplitude-normalized envelopes were divided into groups of 10 concatenated gait cycles (called subgroups) allowing for muscle synergy assessment over the entire walk duration [24,112].

Muscle synergies were then extracted for each subgroup of 10 gait cycles [24,46,112] by means of the NNMF algorithm [32,41]. The NNMF algorithm describes the original sEMG signals as a linear combination of muscle synergy weight vectors (W_k) and activation coefficients ($C(t)_k$), as detailed in (**3.2**). More specifically, the weight vector W_k describes the time-independent contribution of each observed muscle to the *k*-synergy, while the activation coefficient vector $C(t)_k$ represents the time-dependent modulation of the muscles recruited in the *k*-synergy. The MATLAB® function *"nnmf"* was used to apply the NNMF algorithm, setting the routine's input parameters as follows: multiplicative update as factorization algorithm, $1e^{-6}$ as function and search tolerance, 50 as the number of factorization replicates, and 1000 as the maximum number of factorization iterations.

The first algorithm initialization was performed differently for the weight vector W_k and the activation coefficient vector $C(t)_k$. The C matrix was initialized with values randomly selected from a uniform distribution in the range [0, 1]. To improve the performance of the factorization algorithm and the accuracy in the reconstruction of the original sEMG data, a sparseness constraint was imposed in the initialization of the W matrix [37]. In particular, W matrix was first initialized with values randomly chosen from a uniform distribution in the range [0, 0.05], then one random element of each W_k vector was set to a value selected from a uniform distribution in the range [0.7, 0.8]. Therefore, only one muscle for each *k*-synergy has a significant contribution, obtaining an extremely sparse NNMF initialization [37].

To sort the muscle synergies in the same order for each subgroup, the *k*-means algorithm was applied to the W matrix [22]. Clustering was performed by means of the MATLAB® routine "*kmeans*" using the following input parameters: N as number of *k*-means clusters, 1000 as maximum number of iterations, 15 as number of replicates, and cosine as distance metric. The activation coefficients matrix C was ordered accordingly.

To explore different solutions of the NNMF algorithm, the factorization process was run many times on the same gait data, changing the number of muscle synergies (N) in the range [1, 8].

4. Optimal Number Selection: VAF-base Methods

Variance Accounted For (VAF) is widely used in literature to compute the reconstruction accuracy of a factorization algorithm [23,24,43–46,112,118,120,125,126] . VAF is defined as the uncentered Pearson's correlation coefficient expressed in percentage, as it follows:

$$VAF = \left(1 - \frac{\sum_{k=1}^{m}(M_k - M_k^R)^2}{\sum_{k=1}^{m} M_k^2}\right) \cdot 100 \qquad \textbf{(3.10)}$$

where m represents the number of muscles observed, $\sum_{k=1}^{m}(M_k - M_k^R)^2$ describes the sum of the squared errors between the original (M_k) and reconstructed (M_k^R) sEMG signals of the k-synergy, and $\sum_{k=1}^{m} M_k^2$ represents the total sum of squared M_k values with respect to zero. The optimal number of muscle synergies (N_{opt}) is often selected by applying different approaches on the plot of the VAF versus the number of muscle synergies (called VAF curve).

Figure 3.8 shows an example of VAF curves extracted from (**Figure 3.8A**) real and (**Figure 3.8B**) simulated sEMG signals.

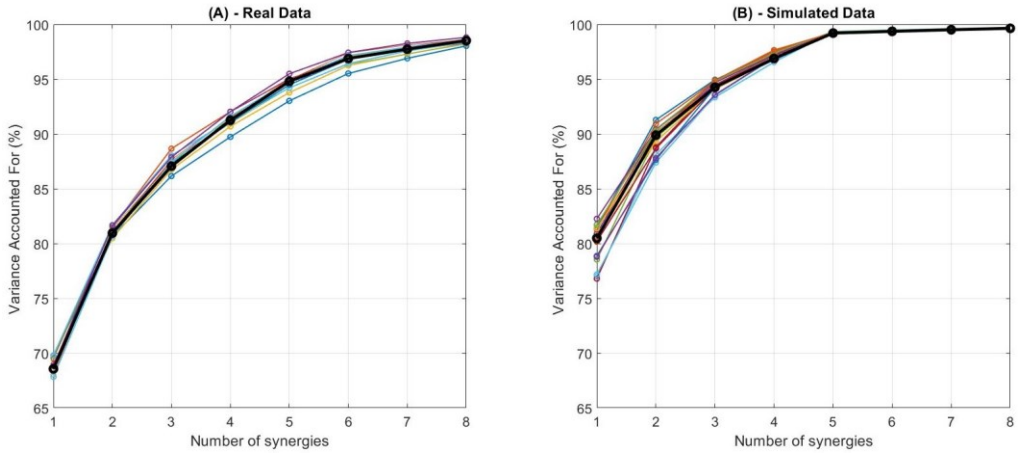

Figure 3.8 Example of ***VAF*** curves extracted from (A) real and (B) simulated sEMG signals. For each tested number of synergies, the Variance Accounted For (***VAF***) measures the correlation between the original and the reconstructed sEMG data. Each colored line represents a ***VAF*** curve extracted from a single 10-gait-cycle subgroup, while black lines represent the average ***VAF*** cuvrve computed over subgroups.

In this chapter, the performance of the MCDA-based approach is quantitatively compared with respect to three standard VAF-based approaches: (*i*) Threshold VAF (T_{VAF}), (*ii*) Elbow VAF (E_{VAF}), and (*iii*) Plateau VAF (P_{VAF}) methods.

i. *Threshold VAF* (T_{VAF}): this approach defines N_{opt} as the first number of synergies granting a VAF value above a heuristically defined cut-off threshold. This threshold is commonly set at 90% VAF [23,24,43,44,46,112,118,120,125,126] .

ii. *Elbow VAF (E_{VAF}):* this approach defines N_{opt} as the number of synergies at which the VAF curve achieves the highest curvature ("elbow") [32]. More specifically, slope changes are detected by computing the curvature for every three consecutive VAF curve points (i.e., the first curvature is computed considering N = 1, 2, and 3; the second curvature considering N = 2, 3, 4, etc.). Finally, the optimal number of muscle synergies is defined as the number of synergies in correspondence of the highest curvature among the computed ones.

iii. *Plateau VAF (P_{VAF})*: this approach defines N_{opt} as the number of synergies beyond which the VAF curve reaches a plateau. More specifically, the VAF curve is iteratively fitted by means of the least-squares linear regression, first considering all the VAF curve points, and then moving the fit window toward the right side of the VAF curve by excluding the smallest number of muscle synergies. The first fit iteration considers all the VAF curve points (e.g., N ranges from 1 to 8) for the linear regression, the second fit iteration considers only the last seven VAF curve points (N ranges from 2 to 8), and so on until only the last two VAF curve points are considered. For each fit, the Mean Squared Error (MSE) was computed and compared with respect to a heuristically defined threshold, that in this study was set equal to 10^{-5} [16,47]. Finally, the optimal number of muscle synergies is defined as the first number of synergies at which the linear fit produces a $MSE \leq 10^{-5}$.

5. Optimal Number Selection: MCDA-based Method

Multi-Criteria Decision Analysis (MCDA) was developed in the field of operational research and consists of a family of methods that aim at selecting the optimal solution (among all the possible alternatives) by explicitly taking into account multiple criteria. To find a reliable and systematic solution to the muscle synergy number problem, moving from single criterion approaches (e.g., VAF- or R^2-based approaches) to a multicriteria approach, an MCDA model is herein proposed to obtain a systematic and reliable approach to criteria modeling and alternatives evaluation.

To define the best MCDA model, the following four main steps were considered:

i. The definition of the alternatives set
ii. The definition of the evaluation criteria
iii. The choice and definition of the multicriteria aggregation procedure

Definition of the alternatives set

The alternatives considered in the MCDA model were defined as the different ranks of the factorization process (r), i.e., all the possible solutions explored by the NNMF algorithm. Since the factorization is usually repeated several times on the

same data, changing the factorization rank (i.e., the number of muscle synergies N) between 1 and 8, eight different alternatives were considered in the decision-making process. Thus, each alternative corresponds to a different number of muscle synergies.

Definition of the evaluation criteria

The main objective of the MCDA approach was to find a robust and repeatable approach for the selection for the optimal number of muscle synergies, moving from single criterion approaches, such as VAF- or R^2-base approaches, to a multicriteria approach. To define the evaluation criteria, this main objective was divided into four sub-objectives:

i. Maximize the reconstruction accuracy of the factorization algorithm
ii. Maximize the muscle synergy consistency
iii. Minimize the muscle synergy redundancy
iv. Maximize the factorization model robustness.

As shown in **Table 3.4**, these four sub-objectives were translated into six evaluation criteria to measure the degree to which an alternative attains each sub-objective.

TABLE 3.4
OBJECTIVE, SUB-OBJECTIVES, AND EVALUATION CRITERIA

SUB-OBJECTIVES	*EVALUATION CRITERIA (CRITERION WEIGHT)*
Maximize the reconstruction accuracy of the factorization algorithm	Evaluation of Variance Accounted For (10%)
Maximize the muscle synergy consistency	Evaluation of Weight Vector Intra-Cluster Consistency (18%)
	Evaluation of Activation Coefficient Intra-Cluster Consistency (18%)
Minimize the muscle synergy redundancy	Evaluation of Weight Vector Inter-Cluster Similarity (17%)
	Evaluation of Activation Coefficient Inter-Cluster Similarity (17%)
Maximize the factorization model robustness	Evaluation of Cross-Variance Accounted For (20%)

In the following, the six evaluation criteria are detailed:

i. *Evaluation of Variance Accounted For (VAF)*: this criterion quantifies the reconstruction accuracy of the factorization results and it is defined as the uncentered Pearson's correlation coefficient, expressed in percentage, as defined in **Equation** (**3.10**). A high value of VAF (high accuracy) is desired to obtain an accurate reconstruction accuracy.

ii. *Evaluation of the Weight Vector and Activation Coefficient Intra-Cluster Consistency (ICC)*: these criteria quantify the consistency of weight

vectors (ICC_W) and activation coefficients (ICC_C) over time (i.e., over the different 10-gait-cycle subgroups) by computing the cosine similarity (CS) [30]of the previously sorted weight vectors W_k (**3.11**) and activation coefficient vectors $C(t)_k$ (**3.12**), separately. More specifically, CS was computed between the weight vector (or activation coefficient) belonging to the *i-th* subgroup and the cluster centroid, defined as the average over all the 10-gait-cycle subgroups, of the *k*-synergy as described in (**3.4**) and (**3.12**):

$$CS_{W,k}^{i} = \left(\frac{W_k^i \cdot \bar{W}_k}{\|W_k^i\| \, \|\bar{W}_k\|}\right) \cdot 100 \qquad (\mathbf{3.11})$$

$$CS_{C,k}^{i} = \left(\frac{C_k^i \cdot \bar{C}_k}{\|C_k^i\| \, \|\bar{C}_k\|}\right) \cdot 100 \qquad (\mathbf{3.12})$$

where $CS_{W,k}^{i}$ and $CS_{C,k}^{i}$ represent the CS computed between the weight vectors W_k of the *i-th* subgroup and the cluster centroid of the *k*-synergy and between the activation coefficients $C(t)_k$ of the *i-th* subgroup and the cluster centroid of the *k*-synergy, respectively. The CS values range between 0 (meaning no similarity) and 100 (meaning complete similarity). Then, ICC was defined, separately for each *k*-synergy, as the average of the $CS_{W,k}$ and $CS_{C,k}$ values for the weight vectors and the activation coefficients, separately. Notice that the average operator is always applied across 10-gait-cycle subgroups. Finally, the "*min*" function is used to select the most variable muscle synergy ("worst" condition), obtaining a single ICC value for each number of muscle synergies N. The ICC value ranges from 0 (i.e., completely different muscle synergy across subgroups) to 100 (i.e., perfectly repeatable muscle synergy among the different subgroups). A high value of ICC (high consistency) is desired to be able to assess repeatable muscle synergies.

iii. *Evaluation of the Weight Vector and Activation Coefficient Inter-Cluster Similarity (ICS)*: these criteria quantify the level of similarity of weight vectors (ICC_W) and activation coefficients (ICC_C) belonging to different muscle synergies by computing the cosine similarity (CS) [30]. For each number of synergies (N>1), and for each synergy i (with i = 1, …, N), CS was computed between the cluster centroids (defined as the average over all the 10-gait-cycle subgroups) of different muscle synergies for the weight vectors and the activation coefficients, separately. Finally, the "*max*" function is used to select the most similar muscle synergy ("worst" condition), obtaining a single ICS-value for each number of muscle synergies N as detailed in (**3.13**) and (**3.14**):

$$ICS_W = \max\left(\frac{\bar{W}^i \cdot \bar{W}^k}{\|\bar{W}^i\| \, \|\bar{W}^k\|}\right) \qquad (\mathbf{3.13})$$

$$ICS_C = \max\left(\frac{\bar{C}^i \cdot \bar{C}^k}{\|C^i\| \, \|\bar{C}^k\|}\right) \quad \textbf{(3.14)}$$

where $\bar{W}^i$ and $\bar{W}^k$ represent the average weight vectors (cluster centroid) computed across subgroups for the *i*- and *k*-synergy, respectively. Instead, $\bar{C}^i$ and $\bar{C}^k$ represent the average activation coefficient vectors (cluster centroid) computed across subgroups for the *i*- and *k*-synergy, respectively. ICS values can range from 0 to 1: ICS = 0 indicates a complete dissimilarity, while ICS = 1 indicates a complete similarity between $\bar{W}^i$ and $\bar{W}^k$ or between $\bar{C}^i$ and $\bar{C}^k$. A small value of ICS (low similarity) is desired to avoid redundant information.

iv. *Evaluation of the Muscle Synergy Robustness*: this criterion quantifies the robustness of the factorization model over different 10-gait-cycle subgroup through the Cross-Variance Accounted For ($CrossVAF$) [111], defined as it follows:

$$CrossVAF^{i,j} = \left(1 - \frac{\sum_{k=1}^{m}(M_k^i - M_k^{R,j})^2}{\sum_{k=1}^{m}(M_k^i)^2}\right) \cdot 100 \quad \textbf{(3.15)}$$

where M_k^i and $M_k^{R,j}$ represent the original and the reconstructed sEMG signals of the *k*-muscle for the *i*- and *j-th* 10-gait-cycle subgroup, respectively. This parameter is used to assess how well the muscle synergies extracted for the *i-th* subgroup reconstruct the sEMG signals that belong to the *j-th* subgroup. The average $CrossVAF$ value was then computed over all the possible couples of 10-gait-cycle subgroups. The average $CrossVAF$ can assume values ranging from 0% (i.e., low correlation between the original and the reconstructed sEMG signals) to 100% (i.e., a high correlation between the original and the reconstructed sEMG signals). A high value of $CrossVAF$ (high robustness) is desired to assess a robust factorization model.

Selection and Definition of the Multicriteria Aggregation Procedure

Although the problem addressed in the present chapter can be described as a selection problem, herein it was addressed as a ranking problem, in which the alternatives are ranked from the best to the worst with the possibility of *ex-aequo* and/or incomparability between alternatives.

The multicriteria aggregation procedure ELECTRE III (ELimination Et Choix Traduisant la REalitè or ELimination and Choice Expressing the REality) [144–147] was used to rank the alternatives from the best to the worst based on their performance on the six evaluation criteria previously defined (**Table 3.4**). More specifically, ELECTRE-III [144–147] is a partially compensatory ordinal method specifically developed for ranking problems. Considering the decision-making process addressed in this chapter, it is desired to minimize the compensation effect

and penalize unbalanced alternatives, i.e., alternatives with a mix of very good and very bad evaluations. ELECTRE III is based on 4 basic outranking relations between alternatives [147]:

- *Indifference*: it represents a condition where there are clear and positive reasons that justify the equivalence between the two alternatives *A* and *B*
- *Strict preference*: it represents a condition where there are clear and positive reasons in favor of one of the two alternatives
- *Weak preference*: it represents a condition where there are clear and positive reasons in favor of one of the two alternatives, but they are insufficient to justify a *strict preference* relation
- *Incomparability*: it represents a condition where there are no clear and positive reasons that would justify any of the above-mentioned relations.

The outranking of an alternative *A* by an alternative *B* (defined by assigning to the pair of alternatives *A* and *B* one and only one of the four basic outranking relations above defined) is determined by concordance and discordance tests. In particular, for each pair of alternatives, the concordance and discordance indexes are computed on the basis of the evaluation matrix, i.e., the performance of each alternative on each criterion. **Table 3.5** represents an example of an evaluation matrix, used as input of the ELECTRE III model, computed from real sEMG signals of a PD subject of the sample population during a walking task.

TABLE 3.5
EVALUATION MATRIX OF A PD PATIENT OF THE SAMPLE POPULATION.

Alternatives	**Evaluation Criteria**					
	VAF **(%)**	ICC_W **(a.u.)**	ICC_C **(a.u.)**	ICS_W **(a.u.)**	ICS_C **(a.u.)**	$CrossVAF$ **(%)**
1 Synergy	76.37	1.00	1.00	NaN[1]	NaN[1]	72.14
2 Synergies	85.42	1.00	0.99	0.42	0.61	78.12
3 Synergies	89.95	0.99	0.99	0.38	0.69	79.16
4 Synergies	93.55	0.99	0.99	0.35	0.70	80.61
5 Synergies	95.62	0.98	0.99	0.38	0.78	80.83
6 Synergies	97.08	0.99	0.99	0.34	0.93	80.17
7 Synergies	98.00	0.75	0.89	0.36	0.92	80.02
8 Synergies	98.68	0.94	0.98	0.53	0.94	79.73

[1] Inter-cluster similarity cannot be computed for a number of synergy $N = 1$.

The concordance index of a pair of alternatives *A* and *B* is used to validate the assertion that *"A outranks B"* and to measure the credibility of this assertion. From a mathematical point of view, it is defined as the weighted sum of the criteria on which *A* is evaluated at least as good as *B*. In particular, the importance weight for each criterion were defined for each of the six criteria using the revised Simon's procedure [148] as shown in brackets in **Table 3.4**.

The discordance index for the alternatives *A* and *B* on criterion *j*, instead, is used to assess the degree to which criterion *j* goes against the assertion that *"A outranks B"*. Finally, a ranking of the alternatives from the best one to the worst

one was obtained from the strict and weak outranking relations. **Figure 3.9** shows an example of outranking graph obtained considering real sEMG signals of a PD subject of the sample population during walking.

In the outranking graph, when two alternatives are represented at the same rank, it means that they are incomparable (e.g., "6 Synergies" and "8 Synergies" alternatives in **Figure 3.9**) or equivalent.

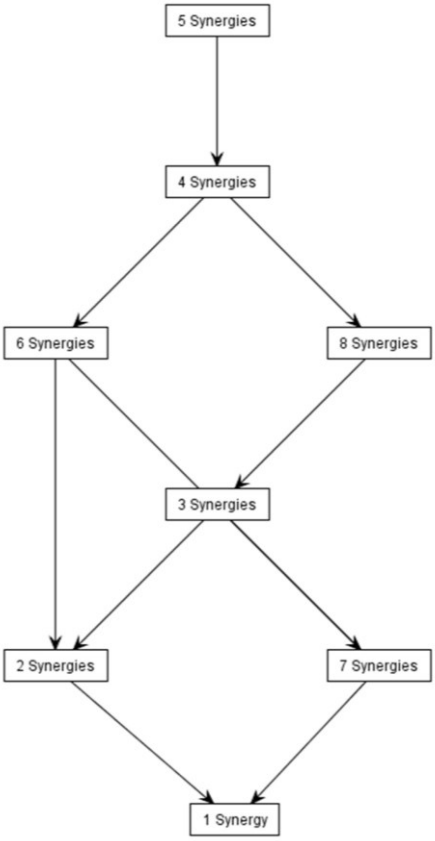

Figure 3.9 Outranking graph extracted through the ELECTRE III methods considering a PD subject of the sample population. Alternatives are ranked from the best one (top) to the worst (bottom) one. The "5 Synergies" alternative was selected as the best alternative. Therefore, the optimal number of muscle synergies was defined equal to 5.

ELECTRE-III model was implemented and validated using MATLAB® release 2020b (The MathWorks Inc., Natick, MA, USA), modifying the MCDA-ULaval open-source software developed by professor Irène Abi-Zeid of Laval University of Québec, Canada. The original MCDA-ULaval open-source software, developed in Java, can be freely found online at the following address: https://cersvr1.fsa.ulaval.ca/mcda-ulaval/?q=en.

6. Performance Evaluation

The optimal numbers of muscle synergies computed through the four different approaches (T_{VAF}, E_{VAF}, P_{VAF}, and ELECTRE III) were quantitatively compared in terms of (i) estimation bias and (ii) Mean Absolute Error (MAE), both for the

simulated and real datasets. The MAE was used to quantify how far a given approach deviates from the ground truth (i.e., the correct number of muscle synergies), while the estimation bias was used to know whether an approach goes wrong by defect or excess. More specifically, the indexes were defined as it follows:

$$bias = \frac{1}{n}\sum_{i=1}^{n}(\widehat{N}_\iota - N_{opt,i}) \quad \textbf{(3.16)}$$

$$MAE = \frac{1}{n}\sum_{i=1}^{n}(\left|\widehat{N}_\iota - N_{opt,i}\right|) \quad \textbf{(3.17)}$$

where $N_{opt,i}$ is the optimal number of muscle synergies for the i-th subject (ground truth) and $\widehat{N}_\iota$ is the estimated optimal number of muscle synergies identified by one of the tested approaches.

To be able to know which number of muscle synergies should be considered optimal (N_{opt}), ground truth was defined for both the simulated and real signals. Considering the simulated data, the ground truth was known *a-priori* based on the sEMG signal simulation process. Considering the real data, instead, the judgment of two expert operators (Mr. Marco Ghislieri and Prof. Valentina Agostini) was used to define the ground truth. Their judgment was performed blind to the details of the ELECTRE III algorithm as well as to the results of the various methods tested. For each real signal, they analyzed the muscle synergy plots considering different numbers of muscle synergies N (in the range between 1 and 8 muscle synergies) and they chose - separately - the number they considered as correct (N_{opt}), based on their knowledge of motor control strategies, muscle synergy analysis, and gait biomechanics. More specifically, the operators used basically the same criteria to identify the correct number of muscle synergies. They considered the consistency in time of the motor control strategies (muscle synergies are expected not to change too much over task duration) and the biomechanical task associated to each muscle synergy by assessing which number of synergies better represent a set of well-distinguished functions and avoiding the presence of redundant information (i.e., avoiding having two identical or "too similar" muscle synergies). However, expert judgment is subjective, at least to some extent. Cohen's kappa statistic [149] was used to compute the degree of agreement between raters. In case of disagreement, the two expert operators discussed the discordant cases to achieve a common ground truth.

7 Effect of SNR on Muscle Synergy Number Selection

To assess the effect of the SNR on the performance of the four approaches, the performance parameters described above were computed on the simulated dataset, separately for each of the eight SNR values (SNR = 6, 10, 13, 16, 20, 23, 26, 30 dB).

8 Statistical Analysis

One-way repeated-measures analysis of variance ($ANOVA$) followed by *post-hoc* analysis with Tukey's adjustment for multiple comparisons was performed to assess statistically significant differences in the performance of the four tested approaches for selecting the optimal number of muscle synergies, considering both simulated and real data. The effect size of the statistically significant differences was calculated through the Hedges' g including the correction for small sample sizes [113]. The significance level (α) was set equal to 0.05.

3.7 Results

First, the results supporting the applicability of the ELECTRE III approach for selecting the optimal number of muscle synergies are presented, considering simulated sEMG signals. Second the performance of the four approaches (T_{VAF}, E_{VAF}, P_{VAF}, and the newly introduced ELECTRE III) on simulated sEMG signals are compared, highlighting the effect of the SNR. Finally, ELECTRE III is validated on real data.

Simulated Data

The performance of the four different approaches were assessed and compared in terms of (i) estimation bias and (ii) Mean Absolute Error (MAE):

i. Estimation bias: On average, an estimation bias of -2.0 ± 1.6 muscle synergies, -0.4 ± 1.1 muscle synergies, 1.7 ± 0.7 muscle synergies, and -0.6 ± 0.9 muscle synergies was found on the simulated dataset, considering the T_{VAF}, the E_{VAF}, the P_{VAF}, and the MCDA approach, respectively. One-way ANOVA followed by *post-hoc* analysis revealed significant differences between each pair of approaches ($p < 0.001$)

ii. Mean Absolute Error: On average, a MAE of 2.0 ± 1.6 muscle synergies, 0.4 ± 1.1 muscle synergies, 1.7 ± 0.7 muscle synergies, and 0.8 ± 0.8 muscle synergies were found on the simulated dataset, considering the T_{VAF}, E_{VAF}, P_{VAF}, and the ELECTRE III approach, respectively. One-way ANOVA followed by *post-hoc* analysis revealed significant differences between each pair of approaches ($p < 0.001$)

Figure 3.10 compares the performance of the four approaches tested (T_{VAF}, E_{VAF}, P_{VAF}, and the newly introduced ELECTRE III), based on the two parameters introduced above. The average values and standard errors of the parameters were estimated on the simulated dataset.

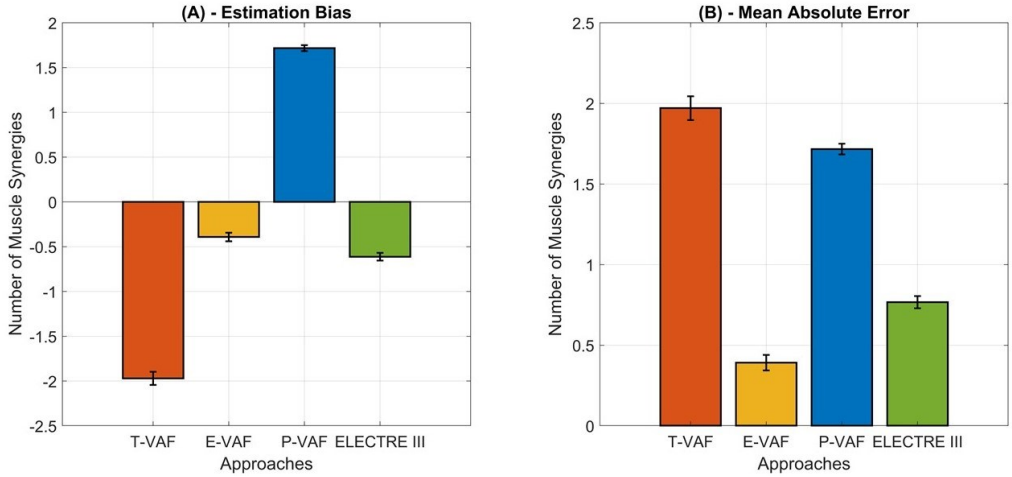

Figure 3.10 Comparison of the performance of the four tested approaches ($\boldsymbol{T_{VAF}}$, $\boldsymbol{E_{VAF}}$, $\boldsymbol{P_{VAF}}$, and the newly introduced ELECTRE III approach) estimated considering (A) the estimation bias and (B) the Mean Average Error ($\boldsymbol{MAE}$). Average values are represented with the indication of the standard errors. Considering both parameters, statistically significant differences were detected between each pair of approaches.

Effect of SNR on Muscle Synergy Number Selection

The effect of the SNR on the approaches' performance was assessed by computing the "performance" parameters (estimation bias and mean absolute error), separately for each simulated SNR-value.

Figure 3.11 represents, for each tested approach, the average values (and standard errors) of estimation bias (**Figure 3.11A**) and MAE (**Figure 3.11B**), for each simulated SNR-value.

For both parameters, threshold-independent approaches (E_{VAF} and ELECTRE III) revealed a higher performance across the different SNR values, suggesting a lower effect of SNR on the selection of the optimal number of muscle synergies with respect to the other two threshold-dependent approaches (T_{VAF} and P_{VAF}). Even if the E_{VAF} approach revealed the highest performance in terms of estimation bias and MAE, the approach less affected by the SNR was the ELECTRE III, revealing similar performance across the different values of SNR. The approach more affected by the SNR, instead, was the T_{VAF}, with an evident decrease in the performance for simulated sEMG signals with SNR-values lower than 16 dB. On average, a significant decrease in the performance of all the tested approaches was detected for simulated sEMG signals with SNR lower than 16 dB.

Real Data

The performance of the four different approaches on real sEMG signals were assessed with respect to the ground truth by considering the same two parameters described for the simulated dataset. The inter-rater agreement, computed by means of Cohen's kappa, was equal to 0.5, suggesting a moderate agreement between the

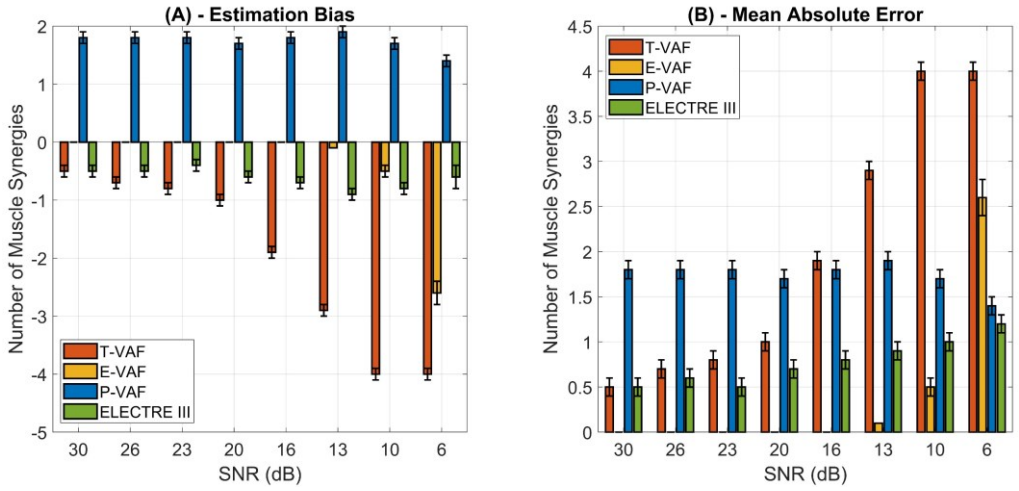

Figure 3.11 Comparison of the performance of the four tested approaches ($\boldsymbol{T_{VAF}}$, $\boldsymbol{E_{VAF}}$, $\boldsymbol{P_{VAF}}$, and the newly introduced ELECTRE III approach) estimated considering (A) the estimation bias and (B) the Mean Average Error ($\boldsymbol{MAE}$). Average values are represented with the indication of the standard errors.

two expert operators. In the following, the results obtained considering the two above-mentioned parameters are detailed:

i. *Estimation bias:* On average, an estimation bias of 0.9 ± 0.3 muscle synergies, -0.8 ± 0.2 muscle synergies, -0.8 ± 0.2 muscle synergies, and 0.0 ± 0.3 muscle synergies was found on the real dataset, considering the T_{VAF}, the E_{VAF}, the P_{VAF}, and the ELECTRE III approach, respectively. One-way ANOVA followed by *post-hoc* analysis revealed statistically significant differences between the T_{VAF} and E_{VAF} approaches ($p = 0.003$, $g = 5.88$) and between the T_{VAF} and P_{VAF} approaches ($p = 0.001$, $g = 6.25$), while no differences were found between the ELECTRE III approach and the VAF-based approaches.

ii. *Mean Absolute Error:* An average MEA of 1.1 ± 0.3 muscle synergies, 0.8 ± 0.2 muscle synergies, 0.8 ± 0.2 muscle synergies, and 0.5 ± 0.3 muscle synergies was computed from the real dataset, considering the T_{VAF}, the E_{VAF}, the P_{VAF}, and ELECTRE III approach, respectively. One-way ANOVA followed by *post-hoc* analysis revealed no statistically significant differences between the four tested approaches ($p > 0.05$).

Considering the real sEMG data, **Figure 3.12** compares the performance of the four approaches (T_{VAF}, E_{VAF}, P_{VAF}, and the newly introduced ELECTRE III approach), considering the estimation bias (**Figure 3.12A**) and MAE (**Figure 3.12B**) parameters previously defined. The average values and standard errors of the computed parameters are reported, as well as asterisks to highlight statistical differences ($p < 0.05$) between each pair of approaches.

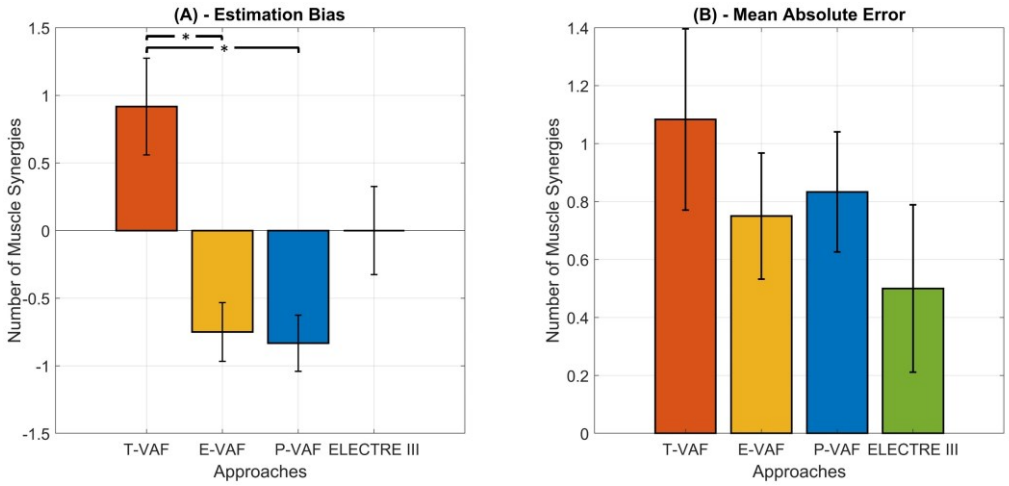

Figure 3.12 Comparison of the performance of the four tested approaches ($\boldsymbol{T_{VAF}}$, $\boldsymbol{E_{VAF}}$, $\boldsymbol{P_{VAF}}$, and the newly introduced ELECTRE III approach) estimated considering (A) the estimation bias and (B) the Mean Average Error ($\boldsymbol{MAE}$). Average values are represented with the indication of the standard errors. Statistically significant differences ($p < 0.05$) are highlighted by means of asterisks (*).

3.8 Discussion and Conclusions

In literature, the muscle synergy theory has been proposed to assess the modular organization of the CNS during different movement tasks, such as walking and running, in both physiological and pathological populations. In the last years, several studies demonstrated that the optimal number of muscle synergies can be a meaningful feature for the assessment of the motor control complexity in patients affected by neuromuscular or neurodegenerative diseases, such as brain injury [124] and Parkinson's disease [45]. According to these studies, the number of muscle synergies and their composition could be correlated with the motor control capacity and its reduction in pathological conditions [33]. Despite the growing interest in the assessment of the optimal number of muscle synergies, there is a lack of standardized methods for the precise identification of the number of synergies, making comparisons between studies and cohorts difficult. The number of muscle synergies characterizing a given movement, indeed, significantly varies within and across studies, even for healthy individuals. Hence, as muscle synergy analysis is growing in popularity in motor control neuroscience and rehabilitation engineering, how to improve and, hopefully, to standardize the selection of the optimal number of muscle synergies are timely and important questions.

The approach currently accepted and most widely used by researchers for the identification of the optimal number of muscle synergies is based on the application of an arbitrary cut-off threshold based on the Variance Accounted For (VAF) [23,24,43–46,112,118,120,125,126], defined as the uncentered Pearson's correlation between the original and the reconstructed sEMG signals. More specifically, the optimal number of muscle synergies is defined as the first number of synergies that produces a VAF value equal to or higher than an arbitrary cut-off threshold. This cut-off threshold is usually set at 90% [23,24,43,44,46,112,118,120,125,126], but several other studies considered

threshold values that range from 80% to 95% [45]. Several are the disadvantages of this VAF-based approach. First, the discordance over the VAF threshold values significantly intensifies the confusion over the selection of the optimal number of muscle synergies and reduces results comparability between studies. Second, even small variations in the cut-off threshold value could significantly change the final results in terms of number of muscle synergies. Third, there is no evidence why the same cut-off threshold value should be applied for all individuals and cohorts. Finally, since the VAF is defined as the uncentered Pearson's correlation, different values of mean activity computed from different muscles may strongly affect the selection of the optimal number of muscle synergies.

To the best of the author's knowledge, few other studies have proposed alternatives to the VAF threshold approach. In the study by Kim *et al.*[130], a novel approach was proposed to enhance precision and reliability in synergy number identification based on k-means clustering and intra-cluster correlation analysis. However, this approach was tested considering sEMG data acquired only from eight leg muscles of a small sample population (9 healthy subjects) during treadmill walking. Delis *et al.*[131], instead, developed a more "physiological" approach, introducing a task decoding-based metric during an arm pointing task.

In this chapter, a novel approach for choosing the optimal number of muscle synergies is proposed and validated on both simulated and real sEMG data. The novel ELECTRE III approach has potential advantages with respect to the commonly used VAF-based threshold methods, such as the use of minimization and maximization approaches rather than an arbitrary threshold and the applicability to a variety of different motor tasks. It relies on six parameters directly computed from muscle synergy results: the reconstruction accuracy, weight vector and activation coefficient intra-cluster consistency, weight vector and activation coefficient inter-cluster similarity, and muscle synergy robustness. The applicability of the proposed approach was first checked considering simulated sEMG data. Then, its performance was quantitatively compared against three widely used VAF-based approaches (T_{VAF}, E_{VAF}, and P_{VAF}), in terms of estimation bias ($Bias$) and Mean Absolute Error (MAE). Finally, ELECTRE III is validated on real data.

Considering the simulated sEMG signals, the two threshold-independent approaches (E_{VAF} and ELECTRE III) outperform the other two threshold-dependent methods (T_{VAF} and P_{VAF}) in terms of both estimation bias and mean absolute error. In particular, E_{VAF} outperform all the other approaches, revealing high performance considering both the estimation bias and the mean absolute error. These results confirm the hypothesis that the threshold-dependent approaches could be more affected by even small changes in the sEMG characteristics that could modify the VAF curve, such as the SNR, compared to the threshold-independent approaches. Indeed, considering the effect of the SNR on the approaches' performance, the most affected ones were, as expected, the threshold-dependent approaches (i.e., T_{VAF} and P_{VAF}), revealing a significant decrease in the performance for simulated sEMG signals with SNR-values lower than 16 dB. ELECTRE III approach, instead, revealed similar performance across the tested

VAF values, suggesting to be less affected by the SNR with respect to the other three approaches.

Considering real sEMG signals, results similar to those of the other three methods were achieved, applying the ELECTRE III approach, in terms of estimation bias and mean absolute error. However, it could be noticed that there are some clear differences in the performance of the threshold-dependent approaches between the simulated and the real sEMG signals. In particular, when considering the simulated data, T_{VAF} and P_{VAF} approaches underestimate and overestimate the number of muscle synergies, respectively, while a complementary behavior is assessed considering the real data. This is probably due to the nature of the simulated dataset: the simulated signals may be less complex to factorize and, then, the VAF assumes higher values already at small numbers of synergies. Indeed, the estimation bias values show that the T_{VAF} always goes wrong by defect.

Therefore, the results presented in this chapter demonstrated the applicability of the proposed $MCDA$-based approach for the selection of the optimal number of muscle synergies, showing equal or higher performance with respect to the other three single-criterion methods. However, even if the ELECTRE III revealed lower performance with respect to the E_{VAF} approach, the former can represent a valid alternative for the selection of the muscle synergy number, moving from single criterion approaches, such as VAF- or R^2-base approaches, to a multicriteria approach.

The MCDA-based approach has several advantages with respect to the commonly used VAF-based methods, such as the use of maximization and minimization approaches rather than arbitrary thresholds and its applicability to sEMG signals acquired from different sets of muscles and during different motor tasks (contrary to the study by Delis *et al.* [131]). Instead, one of the limitations of the proposed approach is that it requires several 10-gait-cycle subgroups to extract the evaluation matrix. This requirement does not limit the feasibility and applicability of the proposed methodology to pathological populations. Indeed, gait analysis is commonly used to quantitatively assess patients' locomotion performance only in those patients able to independently walk, for some minutes, without walking aids or external supports. In the past, several studies demonstrated the feasibility of gait data acquisition, during recording sessions lasting 3 minutes, in patients suffering from different neurological conditions, e.g., normal pressure hydrocephalus[89], mild ataxia[116], and cerebral palsy[117].

The author is aware that the number of muscle synergies can be also strongly influenced by other steps in the muscle synergy extraction process [23,36,38,39,44,49–53], such as the sEMG collection and pre-processing (e.g., low-pass filtering techniques) [49–51,53], the number and choice of muscles acquired [23], and sEMG data preparation before factorization (e.g., averaging or concatenating sEMG epochs) [38]. However, the focus of this chapter is on developing an approach that can be applied subsequent to a factorization algorithm to select the optimal number of muscle synergies and not on evaluating the effect of different pre-processing techniques on the identification of the synergy number.

Future developments of the proposed approach will include the assessment of the MCDA-based approach on larger and different cohorts (for age or pathological condition) and during different motor tasks, the optimization of the approach by tuning the importance weights of each evaluation criterion, the evaluation of different sets of evaluation criteria, and the evaluation of the effect of the number of 10-gait-cycle subgroup per subject on the ELECTRE III performance.

In conclusion, a multicriteria approach for the identification of the optimal number of muscle synergies was proposed and validated on simulated and real sEMG signals. The proposed approach outperforms the other threshold-dependent VAF-based approaches in terms of estimation bias and mean absolute error and overcomes their limitations, being independent of arbitrary cut-off thresholds. Moreover, it may help the standardization of motor control studies based on muscle synergies among different research laboratories.

Chapter 4

Motor Control Strategies during Non-Cyclic Movements

In the following chapter, the methodological issues in the assessment of motor control strategies during single-leg stance tasks are discussed. First, a novel pre-processing approach for the selection of sEMG epochs corresponding to *"well-balanced"* and *"unbalanced"* single-leg stance is assessed and validated (**Methodological Issue – Muscle Synergy Assessment during Single-Leg Stance**). Second, differences in terms of balance control strategies between *"well-balanced"* and *"unbalanced"* single-leg stance epochs are analyzed by using the muscle synergy theory (**Methodological Issue – Muscle Synergy Assessment during Single-Leg Stance**). Then, to investigate muscle synergies in lower limb and back muscles during a single-leg stance task with and without visual information, the proposed approach is assessed considering a sample population of healthy young individuals (**Application - Influence of Visual Feedback on Muscle Synergies**).

Methodological Issue – Muscle Synergy Assessment during Single-Leg Stance

Some of the results presented in this paragraph are reproduced and modified from an article published in *IEEE Transactions on Neural Systems and Rehabilitation Engineering* (Volume: 28, Issue: 12, Dec. 2020) by Ghislieri *et al*. The final authenticated version of the manuscript is available online at http://dx.doi.org/10.1109/TNSRE.2020.3030847.

4.1 Introduction

The upright stance is a useful test condition to assess motor skills and evaluate proprioception and coordination with applications both in clinics and sport. Several

balance conditions can be studied to assess postural sway, such as Double-Leg Stance (DLS), tandem, semi-tandem, and Single-Leg Stance (SLS) [150]. Each of these balance tasks is characterized by different motor control strategies and levels of difficulty in carrying out the task. In particular, SLS or unipedal stance requires the maintenance of the upright stance using a single limb, and it may be challenging in patients affected by Chronic Ankle Instability (CAI) [151–153]. Moreover, considering a specific balance task, different conditions of visual and somatosensory integrations can be tested [154]. Typically, along with the eyes open (EO) condition, in which the subject exploits the visual feedback to maintain balance, a condition with eyes closed (EC) is also studied to evaluate the effect of visual deprivation on postural balance control [155–157].

The study of muscle synergies is facing new challenges in the field of postural balance analysis. To the best of the author's knowledge, the analysis of muscle synergies during balance tasks is mainly focused on the evaluation of balance recovery after a "controlled" perturbation [26,158–161]. More specifically, a few studies have demonstrated that muscle synergies are highly consistent across different balance tasks and levels of difficulty [26,28,162]. This suggests that, increasing the task complexity, there should be only slight modifications to the basic motor control strategies involved in postural balance control. However, no studies have assessed the motor control strategies adopted to maintain balance during SLS. One possible reason may be the difficulty to select epochs of sEMG signals when the subject firmly maintains unipedal stance. Indeed, it is important to separate sEMG epochs in which balance is properly maintained from those in which a slight disequilibrium occurs. Therefore, this chapter aims at defining a robust approach for the segmentation of the sEMG time-instants relative to a "*well-balanced*" (WB) SLS or an "*unbalanced*" (UB) SLS to be used as inputs of the muscle synergy extraction algorithm. The proposed approach might help the interpretation of muscle synergies in the SLS task.

4.2 Materials and Methods

1. Sample Population

A sample population of twenty-two healthy subjects (11 females and 11 males; age: 24 ± 3 years; height: 175.7 ± 9.6 cm; weight: 65.9 ± 12.2 kg) was enrolled in the study. None of the volunteers reported lower limb injuries or had neurological/musculoskeletal disorders that could compromise the execution of the balance task. All the subjects were right-limb dominant, according to the preferred lower limb to start walking. This study was reviewed and approved by the Ethics Committee of the Area Vasta Emilia Centro della Regione Emilia Romagna (CE AVEC 193/2019/Sper/IOR approved on October 4, 2019). All participants signed written informed consent for the protocol before each experimental session, and all the acquisitions were performed in accordance with the Declaration of Helsinki.

2. Experimental Protocol

The subjects were asked to perform a SLS task twice in two different conditions: eyes open (EO) and eyes closed (EC). The order condition was randomized for each subject by tossing a coin. In particular, for each condition, subjects were asked to perform a transition from double-leg stance (DLS) to single-leg stance (SLS), to maintain SLS for at least 30 seconds, and then to return back to double-leg stance. If the subject failed to maintain the SLS balance for at least 30 s and required to land on both feet during the task, the test was stopped and repeated until the minimum time duration was reached. The test was performed on a firm surface (force plate), with the subject keeping the arms straight at the sides. **Figure 4.1** shows a schematic representation of the experimental protocol.

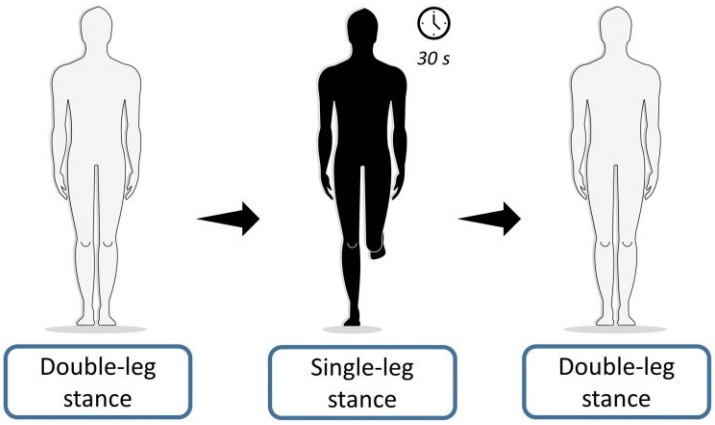

Figure 4.1 Schematic representation of the experimental protocol. Subjects were asked to perform a transition from double-leg stance (DLS) to single-leg stance (SLS), maintaining SLS for at least 30 seconds, and the returning back to DLS to end the task. Reprinted from "*Muscle Synergy Assessment During Single-Leg Stance*" by Ghislieri *et al.* (2020).

3. Data Acquisitions

During each experimental session, sEMG, foot-switch, and ground reaction force signals were simultaneously acquired. sEMG signals were recorded through active probes (FREEEMG 1000, BTS Bioengineering, Milan, Italy) placed over the main muscles of the lower limb and the trunk. Foot-switch signals (FREEEMG 1000 – Footswitch Kit, BTS Bioengineering, Milan, Italy) were acquired to detect the onset/offset timing of the SLS task, while ground reaction forces were detected through a force plate (Dynamic Walkway P6000, BTS Bioengineering, Milan, Italy) to assess body sway.

More specifically, sEMG active probes were placed over the following 13 muscles of the dominant lower limb (the one sustaining the SLS) and the trunk bilaterally: right Longissimus Dorsii (LD_R), left Longissimus Dorsii (LD_L), Gluteus Medius (GMD), Rectus Femoris (RF), Lateral Hamstring (LH), Medial Hamstring (MH), Vastus Medialis (VM), Vastus Lateralis (VL), Lateral Gastrocnemius (LGS), Peroneus Longus (PL), Peroneus Brevis (PB), Soleus (SOL), and Tibialis Anterior (TA). These signals were acquired at a sampling frequency of 1 kHz.

The foot-switch sensor was placed under the first metatarsal head of the non-dominant foot (corresponding to the left foot, for each subject of the sample population).

All the acquired signals were then imported into MATLAB® release R2019b (The MathWorks Inc., Natick, MA, USA) to be offline processed through custom routines.

Figure 4.2 shows a schematic representation of the acquisition system composed of the sEMG active probes placed over the main muscles of the dominant lower limb and the trunk, the foot-switch sensor mounted on the contralateral side to detect the SLS timing, and the force plate used to assess body sway.

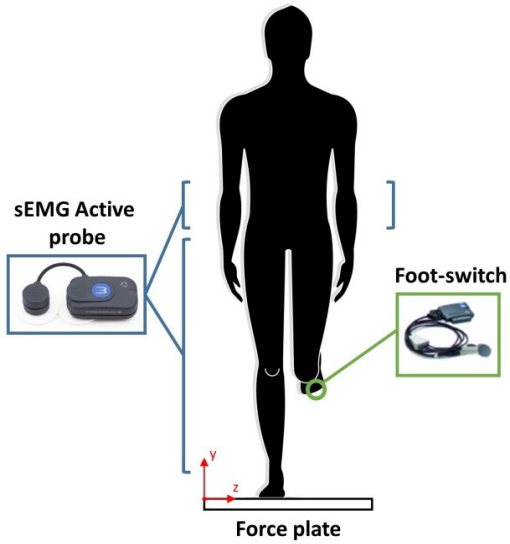

Figure 4.2 Schematic representation of the acquisition system. sEMG active probes were placed over the main muscles of the dominant lower limb (sustaining the SLS) and the trunk. A foot-switch was placed beneath the first metatarsal head of the contralateral foot (left side for all the subjects of the sample population) to detect the SLS timing. A force plate was used to assess body sway during SLS. Reprinted from "*Muscle Synergy Assessment During Single-Leg Stance*" by Ghislieri *et al.* (2020).

4. Segmentation of WB and UB SLS

The signals acquired from the foot-switch sensor placed beneath the contralateral foot (left) and the ground reaction force acquired from the force plate were used to segment the sEMG time-instants relative to WB or UB SLS.

In particular, the foot-switch signal was used to detect the time-instants when the subjects performed the transition from DLS to SLS and vice versa. First, the foot-switch signal was normalized in amplitude between 0 (open foot-switch, foot raised from the floor) and 1 (closed foot-switch, foot on the floor). Second, the onset of the SLS task was established 5 seconds after the 1-to-0 transition, while the offset was established 5 seconds before the 0-to-1 transition, discarding from the analysis DLS-to-SLS and SLS-to-DLS transitions.

To distinguish between WB and UB sEMG epochs during SLS, the ground reaction force acquired through the force plate was used. The *x*-axis of the ground reaction force is aligned to the antero-posterior (AP) direction, the *y*-axis is aligned to the down-top vertical direction, and the *z*-axis is aligned to the medio-lateral (ML) direction. Due to the high correlation between the planar components (AP

and ML) and the vertical component of the ground reaction force, only AP and ML were considered to segment WB and UB sEMG epochs, discarding the vertical component of the force [150].

Both the ground reaction force components (AP and ML) were first low-pass filtered through a 5th order Butterworth digital filter with a cut-off frequency of 10 Hz [163,164]. Then, the resultant force ($Fres$) was computed as described in (**4.1**):

$$Fres = \sqrt{F_{AP}^2 + F_{ML}^2} \quad \textbf{(4.1)}$$

where F_{AP} and F_{ML} represent the AP and ML components of the low-pass filtered ground-reaction force, respectively.

The Root-Mean-Square (RMS) of the resultant reaction force ($Fres_{RMS}$) was computed by windowing the signal into 1s-epochs without overlap to ensure a sufficient number of samples to be used as input of the muscle synergy extraction algorithm. Finally, an adaptive threshold (Th_c) was applied to the $Fres_{RMS}$ signal to detect the sEMG time-instants relative to a WB or UB SLS, defined as in (**4.2**):

$$Th_c = mean(Fres_{RMS}) + c \cdot std(Fres_{RMS}) \quad \textbf{(4.2)}$$

where c is a multiplicative constant.

Due to the high inter-subject variability of the $Fres_{RMS}$ signals and strong correlation between the ground reaction forces and several anthropometric parameters (e.g., body weight, body height, and leg length), an adaptive threshold was preferable to a fixed threshold to properly detect well-balanced and unbalanced SLS epochs according to the distribution of the ground reaction forces of each subject.

Figure 4.3 represents the segmentation masks used to select the "*well-balanced*" and "*unbalanced*" SLS epochs from a healthy subject of the sample population, considering three different values of the multiplicative constant c (c = 0.5, c = 1.0, c = 1.5). These c-values have been chosen to achieve a sufficient number of sEMG time-instants for muscle synergy extraction (for both WB and UB epochs).

More specifically, each Segmentation Mask (SM) was a binary mask defined as it follows:

- SM = 1, if $Fres_{RMS} \leq Th_c$ (WB epochs)
- SM = 0, if $Fres_{RMS} > Th_c$ (UB epochs).

where Th_c represents the adaptive threshold value given the value of the multiplicative constant c.

The sEMG epochs relative to a "*well-balanced*" and "*unbalanced*" SLS were then segmented using the above defined SM.

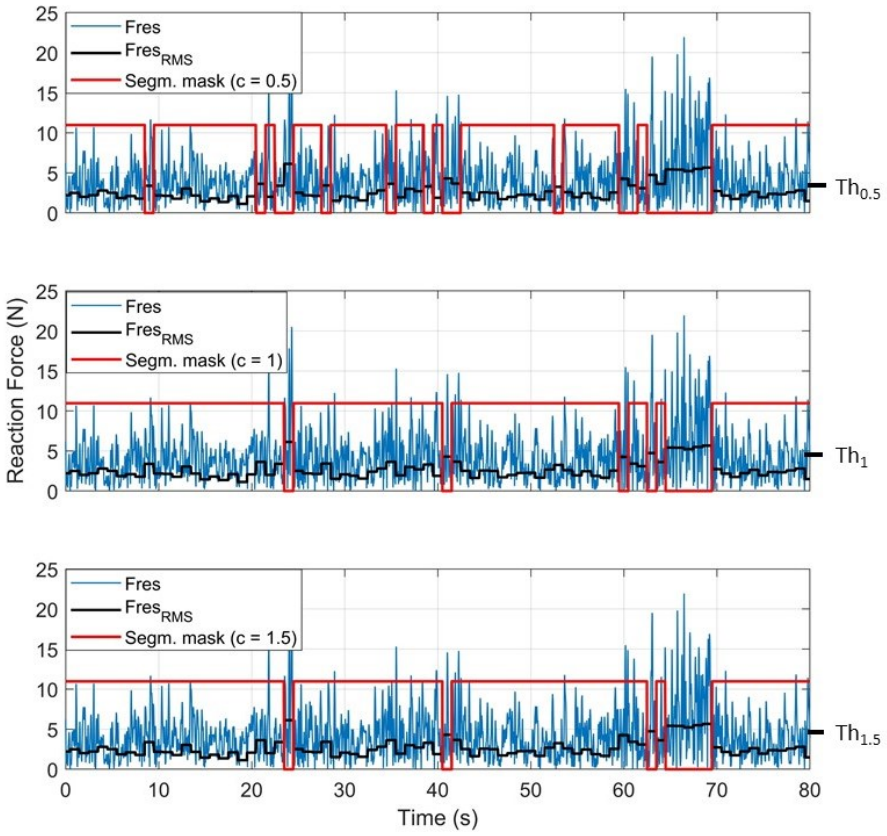

Figure 4.3 Segmentation masks used to select the "*well-balanced*" and "*unbalanced*" SLS epochs for a representative subject of the sample population, considering three different values of the multiplicative constant *c*. In blue it is represented the resultant reaction force (***Fres***) during SLS task, in black the RMS of the resultant reaction force (***Fres$_{RMS}$***), and in red the segmentation mask computed considering each of the three different values of *c*. Each segmentation mask assumes values equal to 1 in correspondence of "*well-balanced*" SLS epochs and to 0 otherwise ("*unbalanced*" SLS epochs). Reprinted from "*Muscle Synergy Assessment During Single-Leg Stance*" by Ghislieri *et al.* (2020).

5. Muscle Synergy Extraction and Number Selection

After sEMG segmentation, muscle synergies were extracted and properly sorted for the WB and UB SLS epochs, separately. First, the segmented sEMG signals were high-pass filtered at 35 Hz through an 8th order Butterworth digital filter to attenuate motion artifacts. Second, signals were demeaned and full-wave rectified to obtain non-negative signals. Third, rectified sEMG signals were low-pass filtered at 12 Hz through a 5th order low-pass Butterworth digital filter [165]. Fourth, each envelope was normalized in amplitude with respect to its global maximum to ensure equally weighted contributions of all the acquired muscles in the muscle synergy extraction process [165].

Afterward, muscle synergies were extracted from the amplitude-normalized sEMG envelopes by means of the NNMF algorithm [28,41]. The NNMF decomposes the original sEMG envelope matrix ($M(t)$) as the linear combination of two different components: the time-dependent activation coefficients ($C(t)$) and the time-independent weight vectors (W) [34] as described in **(3.2)**

The activation coefficient vector $C(t)_k$ describes the modulation over time of the muscles enrolled in the *k*-synergy (the temporal component of the motor

control), while the weight vector W_k represents the contribution of each muscle to the *k*-synergy (the spatial component of the motor control).

The MATLAB® function "*nnmf*" was used to factorize the original sEMG envelope matrix, setting the routine's input parameters as detailed in **TABLE 4.1**. The input parameters used in this study were optimized in previous works focused on muscle synergy extraction during gait [46,66]. To explore different solutions of the NNMF algorithm, the "*nnmf*" function was run several times on the same sEMG data, changing the number of muscle synergies (N) from 1 to 8.

TABLE 4.1
INPUT PARAMETERS OF THE MATLAB® ROUTINE "*NNMF*" USED FOR MUSCLE SYNERGY EXTRACTION

Parameters	Values
Algorithm	multiplicative update
Function tolerance	$1e^{-6}$
Number of replicates	50
Number of iterations	1000

Reprinted from "*Muscle Synergy Assessment During Single-Leg Stance*" by *Ghislieri et al*. (2020).

The reconstruction accuracy of the original sEMG envelope matrix ($M(t)$) was assessed for each number of muscle synergies (N) by computing the total Variance Accounted For ($tVAF$), defined as the uncentered Pearson's correlation coefficient expressed in percentage **(3.3)**.

The optimal number of muscle synergies (N_{opt}) was first selected by choosing the least number of muscle synergies ensuring $tVAF \geq 90\%$ (global criterion) [55]. Second, considering the number of muscle synergies selected according to the global criterion, the Variance Accounted For (VAF) was also computed for each of the acquired muscles. If $VAF \geq 75\%$ for each of the 13 muscles (local criterion), it was concluded that no additional muscle synergies were needed to reconstruct the original sEMG envelopes. Otherwise ($VAF < 75\%$), the number of muscle synergies (N) was incremented until all the muscles achieved a VAF value equal to or greater than 75% [28,166].

To graphically represent the muscle synergies, the weight vectors (W) were normalized in amplitude in the range [0, 1] with respect to their global maximum. Then, the activation coefficient vectors ($C(t)$) were multiplied by the correspondent normalized values.

Since the factorization algorithm may return W and $C(t)$ in a different order for each subject or test condition, proper sorting was required. For this purpose, a *k*-means clustering algorithm was applied to the weight vectors (W) [22]. The clustering algorithm was set considering N_{opt} as number of *k*-means clusters, 1000 as maximum number of iterations, 15 as number of replicates, and cosine similarity as distance metric. Activation coefficients were then sorted accordingly.

6. Robustness Assessment

To assess the robustness of the proposed approach with respect to the segmentation threshold Th_c, muscle synergies were extracted from sEMG envelopes relative to WB or UB SLS epochs, considering 3 different values of the multiplicative constant c: c = 0.5, c = 1.0, and c = 1.5.

Afterward, the muscle synergies extracted considering the three different thresholds $Th_{0.5}$, $Th_{1.0}$, and $Th_{1.5}$ were quantitatively compared in terms of (i) the consistency of the optimal number of muscle synergies (N_{opt}), and (ii) the similarity of weight vectors estimated through Pearson's correlation coefficient (R).

7. Muscle Synergy Analysis

To prove the necessity to segment WB or UB SLS epochs, the correspondent muscle synergies were extracted (setting c = 1.0) and compared one to each other in terms of (i) the optimal number of muscle synergies (N_{opt}), (ii) the average recruitment level of the activation coefficient vectors ($Recr$), and (iii) the balance control strategies (S).

i. Optimal Number of Muscle Synergies (N_{opt})

The optimal number of muscle synergies (N_{opt}) necessary to accurately model the original sEMG signals was selected by choosing the smallest number of synergies which guarantees $tVAF \geq 90\%$ (global criterion) and $VAF \geq 75\%$ (local criterion) for each of the acquired muscles [28,55,166].

ii. Average Recruitment Level ($Recr$)

Since no typical cyclostationary processes can be assessed during the SLS task, any direct or morphological interpretation of the activation coefficient vectors $C(t)_k$ is difficult. Hence, the average recruitment level ($Recr_k$) was considered to quantitatively compare muscle synergy activation coefficient vectors ($C(t)$) [28]. The $Recr_k$ was computed as the average (over time) of the activation coefficient vector $C(t)_k$ of the k-synergy.

iii. Balance Control Strategy (S)

Starting from the balance task performed and the recorded muscles, three different balance control strategies can be identified: (a) ankle control, (b) knee control, and (c) hip/trunk control [26]:

a. The ankle control strategy (S_{ankle}) is mainly characterized by the activation of PL, PB, TA, LGS, and SOL muscles.
b. The knee control strategy (S_{knee}) is mainly characterized by the activation of VM, VL, and RF muscles.
c. The hip/trunk control strategy (S_{hip}) is mainly characterized by the activation of LH, MH, GMD, LD_R, and LD_L muscles.

The average weight vector (W_k) across those muscles belonging to the same balance control strategy was computed to quantitatively assess each balance control strategy, as detailed in (**4.3**):

$$S_{j,k} = \frac{\sum_{i=1}^{m} W_{k,i}}{m} \quad \textbf{(4.3)}$$

where $S_{j,k}$ represents the *j-th* balance control strategy (*j*=1: ankle control; 2: knee control; 3: hip/trunk control) for the *k*-synergy, and m represents the number of muscles enrolled in the *j-th* balance control strategy.

Finally, only a single balance control strategy (S_k) was associated with each muscle synergy by calculating the highest $S_{j,k}$ among those computed for the same *k*-synergy, as detailed in (**4.4**):

$$S_k = \max(S_{1k}, S_{2k}, S_{3k}) \quad (\mathbf{4.4})$$

where *k* can assume value from 1 to 3 ($S_1 = S_{ankle}$, $S_2 = S_{knee}$, $S_3 = S_{hip}$).

8. Statistical Analysis

To assess the robustness of the proposed approach with respect to the segmentation threshold, a two-way analysis of variance (ANOVA) followed by *post-hoc* analysis with Bonferroni adjustment for multiple comparisons was performed.

First, the Lilliefors test was used to test the hypothesis of normality of the distribution, setting the significance level (α) equals to 0.05. Second, according to the results of the Lilliefors test, the Wilcoxon signed-rank test (α = 0.05) or the two-tailed paired Student's *t*-test (α = 0.05) was performed to assess significant changes in the optimal number of muscle synergies, in the average recruitment levels, and in the balance control strategies considering different sEMG epochs (WB and UB).

The effect size of the statistically significant differences was calculated by means of the Hedges' *g* including the correction for small sample sizes [113].

4.3 Results

Results revealed, on average, a similar number of WB and UB SLS epochs (8 ± 3 WB/UB epochs), but different epoch durations were measured. Considering the EO condition, the average WB and UB epoch durations were equal to 70.5 ± 9.8 s and 10.3 ± 2.9 s, respectively, while considering the EC condition, they were equal to 42.8 ± 27.3 s and 5.8 ± 3.8 s.

First, the results related to the robustness assessment of the segmentation threshold were presented. Second, the muscle synergies obtained considering the WB and UB SLS epochs are quantitatively compared to justify the separation into WB and UB epochs of SLS.

1. Robustness of the Segmentation Threshold

All the tested segmentation thresholds ($Th_{0.5}$, $Th_{1.0}$, and $Th_{1.5}$) required the same number of muscle synergies (N_{opt}) to accurately model the original sEMG signals with a $tVAF \geq 90\%$ and a $VAF \geq 75\%$ for each of the acquired muscles. In particular, considering WB SLS epochs, 4 muscle synergies were needed to reconstruct the sEMG signals for all the tested thresholds, both in EO and EC conditions. The same results were obtained considering UB epochs.

Moreover, results revealed high values of the Pearson's correlation coefficients between each pair of thresholds. Considering the WB SLS epochs, no statistically significant differences in terms of weight-vector correlation among the 3 thresholds ($p = 0.17$) and the 2 tested conditions ($p = 0.87$) were detected. Considering the UB SLS epochs, no statistically significant differences among thresholds ($p = 0.28$) were detected, while a significant decrease ($p = 0.01$, $g = 0.47$) in the weight correlation was detected in the EO condition with respect to the EC condition.

TABLE 4.2 represents the average Pearson's correlation coefficients (R) between each pair of thresholds, separately for WB and UB SLS epochs. Results reveal a very high similarity among the muscle synergy weight vectors extracted considering the 3 thresholds, both in WB and UB epochs.

Considering the high similarity of the weight vectors and the high consistency of the optimal number of muscle synergies obtained from the 3 thresholds, the multiplicative constant c of the segmentation threshold was set equal to 1.0.

2. "Well-balanced" and "Unbalanced" Single-Leg Stance

No statistically significant differences were found in terms of the number of muscle synergies between WB and UB SLS epochs. Considering the EO condition, 4 muscle synergies were necessary to reconstruct the original sEMG signals with an average $tVAF$ value of 93.0% ± 1.2% for WB, and 93.1% ± 1.3% for UB, respectively. For the EC condition, similar results were obtained. More specifically, 4 muscle synergies were extracted with an average $tVAF$ value of 92.6% ± 1.5% for WB, and 92.8% ± 1.3%, for UB, respectively.

TABLE 4.2
WEIGHT VECTOR CORRELATION (R) AVERAGED ON THE SAMPLE POPULATION

SLS epochs		Pearson's Correlation Coefficient (R) (mean ± standard deviation)		
		$Th_{0.5}$ vs Th_1	$Th_{0.5}$ vs $Th_{1.5}$	Th_1 vs $Th_{1.5}$
Well-balanced	**EO**	0.91 ± 0.16	0.92 ± 0.14	0.95 ± 0.11
	EC	0.91 ± 0.15	0.89 ± 0.17	0.97 ± 0.08
Unbalanced	**EO**	0.84 ± 0.19	0.75 ± 0.20	0.80 ± 0.20
	EC	0.88 ± 0.17	0.86 ± 0.17	0.90 ± 0.18

$Th_{0.5}$: first threshold with c=0.5; $Th_{1.0}$: second threshold with c=1.0; $Th_{1.5}$: third threshold with c=1.5. EO: Eyes Open; EC: Eyes Closed.

Reprinted from "*Muscle Synergy Assessment During Single-Leg Stance*" by Ghislieri *et al.* (2020).

Figure 4.4 shows muscle synergy results, averaged over the sample population, extracted considering the EO condition (**Figure 4.4A)** and the EC condition (**Figure 4.4B)**, respectively. Moreover, for each balance condition, the muscle synergies extracted considering WB and UB SLS epochs are compared. More specifically, **Figure 4.4** represents, for each k-synergy, both the average recruitment level ($Recr_k$) and the weight vector (W_k).

Wilcoxon signed-rank test revealed a statistically significant increase in the average recruitment levels of three out of four muscle synergies extracted considering UB epochs with respect to those extracted considering WB epochs, during both EO and EC conditions. **TABLE 4.4** details the average recruitment levels

of each muscle synergy with the indication of the statistically significant differences between WB and UB SLS epochs (indicated by asterisks).

In **Figure 4.4A** and **Figure 4.4B,** statistically significant changes ($p < 0.05$) of the average recruitment levels and the muscles' contribution to each muscle synergy are indicated by asterisks during the EO and EC conditions, respectively.

TABLE 4.4
RECRUITMENT LEVELS ($Recr$) AVERAGED ON THE SAMPLE POPULATION

Recruitment Levels		**Average Recruitment Levels ($Recr$) (mean ± standard deviation)**	
		Well-balanced (WB)	***Unbalanced (UB)***
EO	$Recr_1$	$0.20 \pm 0.06^{*}$	$0.24 \pm 0.05^{*}$
	$Recr_2$	$0.19 \pm 0.05^{**}$	$0.24 \pm 0.05^{**}$
	$Recr_3$	0.22 ± 0.06	0.24 ± 0.06
	$Recr_4$	$0.15 \pm 0.04^{*\dagger}$	$0.17 \pm 0.05^{*\ddagger}$
EC	$Recr_1$	$0.17 \pm 0.05^{***}$	$0.25 \pm 0.05^{***}$
	$Recr_2$	0.19 ± 0.07	0.22 ± 0.06
	$Recr_3$	$0.19 \pm 0.06^{*}$	$0.22 \pm 0.07^{*}$
	$Recr_4$	$0.19 \pm 0.05^{***\dagger}$	$0.23 \pm 0.05^{***\ddagger}$

$Recr_k$ represents the average recruitment level of the k-synergy (k = 1,2,3,4). The asterisk (*) indicates a statistically significant difference ($p < 0.05$) between well-balanced (WB) and unbalanced (UB) epochs of single-leg stance (SLS), while the dagger (†) between eyes open (EO) and eyes closed (EC) conditions. Single, double, and triple asterisks (or daggers) represent p-values lower than 0.05, 0.01, and 0.001, respectively. Reprinted from "*Muscle Synergy Assessment During Single-Leg Stance*" by Ghislieri *et al.* (2020).

TABLE 4.3
BALANCE CONTROL STRATEGIES (S) AVERAGED ON THE SAMPLE POPULATION

Balance Control Strategies		**Average Balance Control Strategies (S) (mean ± standard deviation)**	
		Well-balanced (WB)	***Unbalanced (UB)***
EO	Ankle	$0.37 \pm 0.11^{*\dagger}$	$0.43 \pm 0.11^{*}$
	Knee	$0.63 \pm 0.24^{\dagger}$	0.73 ± 0.22
	Hip/Trunk	0.51 ± 0.14	0.56 ± 0.16
EC	Ankle	$0.43 \pm 0.12^{\dagger}$	0.40 ± 0.12
	Knee	$0.76 \pm 0.20^{\dagger}$	0.79 ± 0.24
	Hip/Trunk	0.50 ± 0.20	0.49 ± 0.08

Average balance controls of each of the three identified strategies. The asterisk (*) indicates a statistically significant difference ($p < 0.05$) between well-balanced (WB) and unbalanced (UB) epochs of single-leg stance (SLS), while the dagger (†) between eyes open (EO) and eyes closed (EC) conditions. Single, double, and triple asterisks (or daggers) represent p-values lower than 0.05, 0.01, and 0.001, respectively. Reprinted from "*Muscle Synergy Assessment During Single-Leg Stance*" by Ghislieri *et al.* (2020).

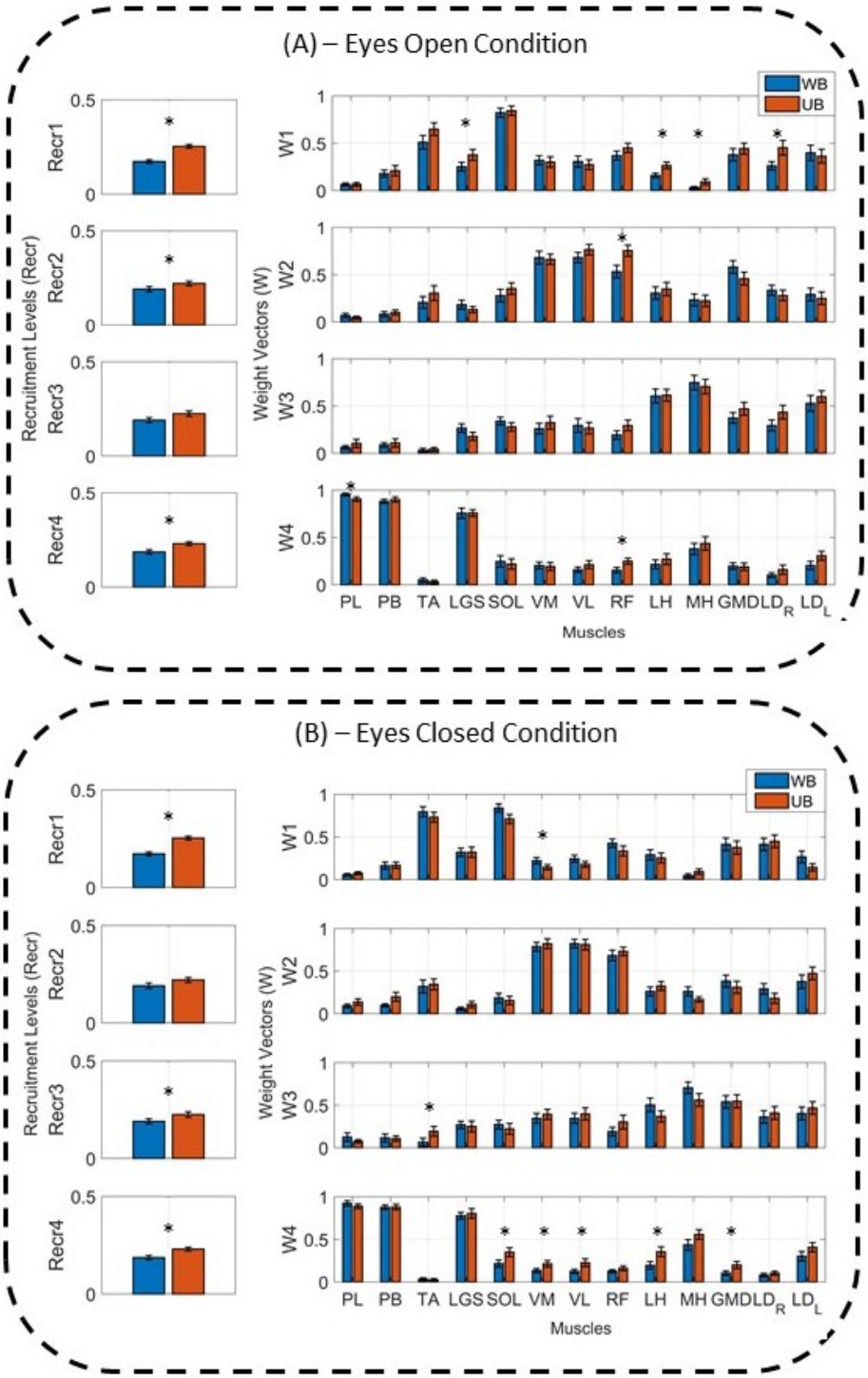

Figure 4.4 Comparison of the muscle synergies extracted during *"well-balanced"* (WB) and *"unbalanced"* (UB) epochs of single-leg stance (SLS), for both the eyes open (EO) and eyes closed (EC) conditions. In both panel (A) and (B), the colored vertical bars represent the average recruitment levels $Recr_k$ (on the left) and weight vectors W_k (on the right) of the *k*-synergy, over the sample population, with the superimposition of the standard error (black lines). The asterisk (*) indicates a statistically significant difference ($p < 0.05$). Reprinted from "*Muscle Synergy Assessment During Single-Leg Stance*" by Ghislieri *et al.* (2020).

According to equation (**4.4**), the ankle control strategy (S_{ankle}) can be mainly associated to the first and the fourth muscle synergies, the knee control strategy (S_{knee}) to the second muscle synergy, and the hip/trunk control strategy (S_{hip}) to the third muscle synergy. Considering the EO condition, results revealed a statistically significant increase ($p = 0.05$, $g = 0.13$) of the ankle control strategy

recruitment during the UB SLS epochs with respect to the WB ones. No statistically significant differences between WB and UB SLS epochs were found considering the knee and hip/trunk balance control strategies, mainly associated with the third and fourth muscle synergies. No statistically significant differences in terms of balance control strategies were detected between WB and UB SLS epochs. **TABLE 4.3** shows the values of the balance control strategies, averaged over the sample population, with the indication of the statistically significant changes between WB and UB epochs of SLS (indicated by asterisks).

Results presented in this chapter reveal differences both in terms of average recruitment levels and balance control strategies between muscle synergies extracted from WB and UB SLS epochs, justifying the proposed segmentation approach as a necessary pre-processing procedure to properly assess the motor control strategies and to help the interpretation of the muscle synergies during SLS.

4.4 Discussion and Conclusions

The muscle synergy theory was widely used in literature to assess human motor control strategies during different motor tasks, such as gait and balance exercise. In the last years, muscle synergy assessment during different balance conditions was mainly focused on the evaluation of balance recovery after a "controlled" perturbation [26,158–161], rather than on the maintenance of the balance condition itself. The segmentation approach proposed in this chapter can be a useful tool for the assessment of the motor control strategies adopted to maintain single-leg stance, distinguishing between "*well-balanced"* (WB) and "*unbalanced"* (UB) SLS epochs.

The robustness of the segmentation approach with respect to the threshold selection was verified obtaining high consistency of the optimal number of muscle synergies and high similarity of the weight vectors (Pearson's correlation coefficient R ranges from 0.75 to 0.97) across the three different values of the adaptive segmentation threshold. Muscle synergies extracted from WB and UB SLS epochs are consistent with previous studies [26,28] both in terms of activation coefficients and weight vectors. However, due to the reduced complexity of the balance exercise analyzed in this chapter, a fewer number of muscle synergies was needed to properly reconstruct the original sEMG signals with respect to the previous studies, in which SLS was assessed after the application of multidirectional perturbations.

The number and the composition of the muscle synergies revealed no statistically significant differences between the WB and UB SLS epochs. However, differences in terms of average recruitment levels and balance control strategies were detected, suggesting a slightly different motor control strategy between WB and UB SLS epochs. More specifically, UB SLS epochs require on average higher recruitment levels with respect to the WB SLS epoch, considering both the EO and EC conditions, and an increased ankle control strategy, in the EO condition. These differences justify the necessity to distinguish between WB and UB single-leg stance epochs before muscle synergy extraction. Results presented in this chapter

are in line with those of previous studies in which the effect of the task complexity, postural configuration, and loading conditions on motor control strategies were assessed [26,30,31]. According to these studies, our central nervous system recruits similar muscle synergies rather than generating a completely new set of muscle synergies for each balance condition. Indeed, only slight modifications to the basic motor control strategies (number and composition of the muscle synergies) involved in SLS were detected, while differences in terms of average recruitment levels and balance control strategies were assessed between EO and EC conditions. Considering the WB and UB SLS epochs, the EC condition requires a higher average recruitment level of the fourth muscle synergy (mainly associated with the ankle control strategy), and an increased level of ankle and knee control strategies, suggesting higher recruitment of the muscle synergies controlling the distal muscles.

This study was conducted on a sample population of young healthy subjects that are able to maintain the upright stance on one foot, even with their eyes closed, for at least 30 s. This may represent a first limitation of the study, since it may be difficult to apply the same experimental protocol also to elderly or pathological populations affected by severe balance impairments. Moreover, muscle synergy results obtained (similarity between motor control strategies adopted during WB and UB SLS epochs), can be biased by the specific population considered. Different results might be obtained in populations with diminished equilibrium skills or severe balance impairments. Another limitation of this study is that it focused only on balance strategies during SLS maintenance, without analyzing transition tasks. The analyzed signals started 5 seconds after the first (DLS-to-SLS) transition and stopped 5 seconds before the second (SLS-to-DLS) transition. Therefore, our findings on motor control strategies adopted during SLS (excluding the transitions) cannot be extended to task transitions.

In conclusion, results demonstrate that the proposed segmentation approach is robust with respect to the selection of the segmentation threshold and can be successfully used as a pre-processing step before muscle synergy extraction, allowing for a better assessment of the modular organization of the central nervous system during the maintenance of the single-leg stance. Further studies will focus on the application of this approach to sEMG signals acquired from subjects affected by chronic ankle instability (CAI) during SLS, to assess its applicability in pathological conditions.

Application - Influence of Visual Feedback on Muscle Synergies

4.5 Introduction

The ability to maintain single-leg stance is essential during daily living activities, as a single task as well as a component of other more complex tasks, such as walking and running. It is a simple but challenging condition for balance control and for this reason it is widely used for training and rehabilitation [167,168]. In research and clinical practice, it is widely used as a testing task as it allows quantifying balance alterations and deficits of the single lower limb otherwise concealed during the performance of double leg tasks [169–174].

From a physiological point of view, the single-leg stance can be considered as a high demanding postural task for neuromuscular and central nervous systems requiring an efficient integration of somatosensory, visual, and vestibular information with the aim to orchestrate a continuous and effective motor response to manage a reduced base of support [175]. The effectiveness of postural control has been usually expressed by means of mechanical parameters such as the center of pressure (COP), joints, or body segment displacement [176–178]. Previous literature studies have reported the essential role of the ankle joint for postural stabilization in particular when tasks show an increase in instability, as in the transition from double- to single-limb stance [179] or from stable to unstable surfaces [170]. When the ankle movements are not sufficient to guarantee balance, the involvement of more proximal joints and body segments has been reported [170,180]. Further, an increase in the instability during stance tasks has been also reported in case of a number of pathological conditions [172,181,182] and in case of abnormal sensitive information [172,183,184]. Above all, it has been shown that vision has a key role in posture control and that the lack of visual feedback or abnormal visual feedback leads to peculiar adaptations in mechanical parameters featuring postural tasks [155,185].

Even if mechanical parameters, such as COP or joint displacement, are useful to quantify instability during postural tasks, they do not give adequate information on motor control. Essential information for motor control assessment comes from the analysis of muscle activations, which mediates CNS control and mechanical expression of movement.

While a wide number of studies investigated multi-muscles activations during double limb stance, in the transition from double to single stance, or during various stance tasks in response to sudden perturbations [26,158,159,186,187], less is known about quiet single-limb stance. Few studies focused on ankle/foot muscle activations, given their important role as previously described [188,189].

However, the investigation of muscle activations around a single joint is reductive, since it is well known that CNS organizes motor response to a given task in terms of muscle synergies [28,190]. This means that CNS coordinates the

activation of a set of muscles that are synergistic for a given task, or a number of similar tasks [26].

To the best of the author's knowledge, the muscle synergies used for balance control during the maintenance of single-leg stance (SLS) conditions are not known. Since this task is largely used, discovering the muscle synergies adopted by healthy individuals is essential to address future research, such as training, rehabilitation, and functional assessment both in healthy and pathological individuals. The aim of this chapter is to investigate muscle synergies in lower limb and back muscles during a single-leg stance task, with and without visual information, in healthy young individuals.

4.6 Materials and Methods

1 Participants

Eleven male participants (age: 23.9 years ± 2.2 years; height: 182 cm ± 8.4 cm; body mass: 74.5 kg ± 10.8 kg) and eleven female participants (age: 24.5 years ± 2.9 years; height: 169 cm ± 5.8 cm; body mass: 57.2 kg ± 6.5 kg) were recruited to participate in the study. Inclusion criteria were *a*) age between 20 and 35 years, *b*) physical activity level of 2 and 3 according to the Saltin and Grimby scale [191], thus excluding sedentary individuals and competitive athletes, and *c*) absence of known neurological diseases. Exclusion criteria were *a*) previous injuries or surgery, and *b*) abnormalities in lower limb and foot joints.

Each participant signed informed consent before participating in the study. The study was conducted in accordance with the Declaration of Helsinki and received ethical approval from the Ethics Committee of the Area Vasta Emilia Centro della Regione Emilia Romagna (CE AVEC 193/2019/Sper/IOR approved on October 4, 2019).

2 Experimental Protocol and Data Analysis

Participants were asked to stand barefoot on a force platform (Dynamic Walkway P6000, BTS Bioengineering, Milan, Italy) with the dominant limb and to maintain the contralateral knee joint flexed at approximately 90°. They were asked to look forward, to maintain upper limbs aligned to the trunk, and to remain as still as possible for at least 30 seconds (see **Figure 4.5**). Minimal arms movements were allowed, however, participants were asked to minimize them as much as possible. They performed the task in both eyes open (EO) and eyes closed (EC) conditions. These two conditions were performed in a random order for each subject (by tossing a coin) and with two minutes of rest between trials. Muscle activations were recorded from 13 muscles of the lower limb and trunk by means of electromyography wireless probes (BTS FreeEMG 1000, BTS Bioengineering, Milan, Italy) fixed on sEMG electrodes (Ag/AgCl) applied over Tibialis Anterior (TA), Peroneus Longus (PL), Peroneus Brevis (PB), Soleus (SOL), Lateral Gastrocnemius (LGS), Vastus Medialis (VM), Vastus Lateralis (VL), Rectus Femoris (RF), Lateral Hamstring (LH), Medial Hamstring (MH), Gluteus Medius

(GMD), right Longissimus Dorsii (LD_R) and left Longissimus Dorsii (LD_L) in accordance with SENIAM recommendations [192]. To reduce the skin impedance, before electrode application, the skin area was shaved and cleaned with ethyl alcohol. A footswitch (FSW) was placed under the first metatarsal head of the non-dominant foot. Force platform, sEMG, and FSW signals were part of the same integrated system and were recorded with a 1000 Hz sampling rate.

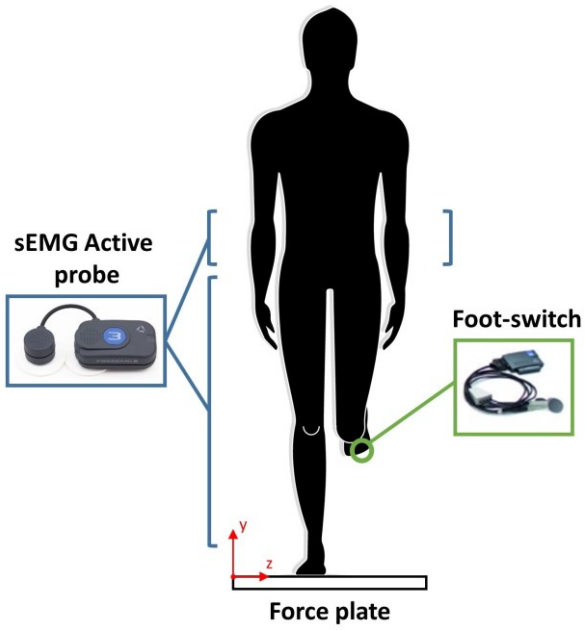

Figure 4.5 Schematic representation of the acquisition system. sEMG probes are positioned over the main muscles of the dominant lower limb (sustaining the single-leg stance) and the trunk. A foot-switch is placed under the first metatarsal head of the contralateral foot to detect the onset/offset timing of SLS. A force plate is used to assess body sway during SLS. Reprinted from "*Muscle Synergy Assessment During Single-Leg Stance*" by Ghislieri *et al.* (2020).

3 Muscle Synergy Analysis

Muscle synergies extracted from the segmented sEMG signals during the two different task conditions (EO and EC) were quantitatively compared in terms of (*i*) the optimal number of muscle synergies (N_{opt}), (*ii*) the average recruitment levels ($Recr$), and (*iii*) balance control strategies (S).

i. Optimal number of muscle synergies (N_{opt}): the optimal number of muscle synergies (N_{opt}) was selected for each subject and task condition by choosing the smallest number of muscle synergies (N) which guarantees $tVAF \geq 90\%$ (global criterion) and $VAF \geq 75\%$ (local criterion) for each of the acquired muscles.

ii. Average recruitment levels ($Recr$): since no typical cyclostationary processes can be assessed during single-leg stance, it is difficult to compute average activation coefficients over the sample population. Thus, the activation coefficients ($C(t)$) were compared in terms of average recruitment level ($Recr_k$), defined as the average (over time) of each activation coefficient vector $C(t)_k$ [27,28]. The average recruitment level values range between 0 (no

recruitment) and 1 (maximum recruitment) and quantify how much a specific muscle synergy is activated in the execution of the task.

iii. Balance control strategies (S): considering the task performed and the acquired muscles, three different balance control strategies were identified: (a) ankle control, (b) knee control, and (c) hip/trunk control. The ankle control strategy (S_{ankle}) was mainly related to the activation of 5 muscles of the leg (PL, PB, LGS, TA, and SOL), the knee control strategy (S_{knee}) to the activation of 3 muscles of the shank (VM, VL, and RF), and the hip/trunk control strategy (S_{hip}) to the activation of 5 muscles of the proximal lower limb and the trunk (LH, MH, GMD, LD_L, and LD_R). Balance control strategies were quantified for each k-synergy by computing the average weight vector (W_k) over the muscles belonging to the same balance control strategy, obtaining three balance control strategy values for each muscle synergy. A single balance control strategy was finally associated with each muscle synergy by selecting the highest balance control strategy among the three computed.

4 Statistical Analysis

To assess statistically significant changes in the optimal number of muscle synergies considering the two different task conditions (EO and EC), the hypothesis of normality of the distribution was firstly tested through the Lilliefors test. If the normality hypothesis was rejected, the Wilcoxon signed-rank test was performed, otherwise, a two-tailed paired Student's t-test was performed. Two-way ANOVA for repeated measures followed by post-hoc analysis with Tukey adjustment for multiple comparisons was performed to evaluate the differences between conditions (OE and CE) and muscle synergies (factors: condition and synergies), for both the average recruitment levels ($Recr$) and balance control strategies (S). For the weight vectors (W), an analogous two-way ANOVA was applied to evaluate the differences between conditions and muscles. The effect size of the statistically significant differences was calculated by means of the Hedges' g including the correction for small sample sizes [113].

All the levels of significance (α) were set equal to 0.05. The statistical analysis was carried out using the Statistical and Machine Learning Toolbox of MATLAB®.

4.7 Results

In the following, the muscle synergy results are computed considering the two different single-leg stance conditions (EO and EC). More specifically, muscle synergies were compared in terms of (i) the optimal number of muscle synergies, (ii) average recruitment levels, and (iii) balance control strategies.

i. Optimal number of muscle synergies (N_{opt})

The application of the Wilcoxon signed-rank test revealed no statistically significant differences (p = 0.52) in the optimal number of muscle synergies (N_{opt}) between the EO and EC conditions. In particular, 4 muscle synergies

were needed to accurately model the motor control strategies during both the EO and EC conditions.

Figure 4.6 shows the muscle synergies, averaged over the sample population, extracted from the two different task conditions: EO represented in blue and EC in red. More specifically, for each muscle synergy, the recruitment levels $Recr_k$ (on the left) and the weight vectors W_k (on the right) are represented. The asterisk (*) indicates statistically significant differences between conditions (repeated measures ANOVA, $p < 0.05$), both for the average recruitment levels and weight vectors.

ii. Average recruitment levels (Recr)

A statistically significant decrease ($p = 0.02$, $g = 3.35$) in the average recruitment level of the third muscle synergy extracted during the EC condition (0.17 ± 0.01) with respect to the EO condition (0.21 ± 0.01) was assessed. No statistically significant differences were detected considering the remaining three muscle synergies between EO and EC conditions, suggesting no changes in the recruitment levels of those synergies due to the loss of visual feedback.

Figure 4.6 shows the average recruitment levels (on the left), over the sample population, extracted during EO and EC single-leg stance conditions.

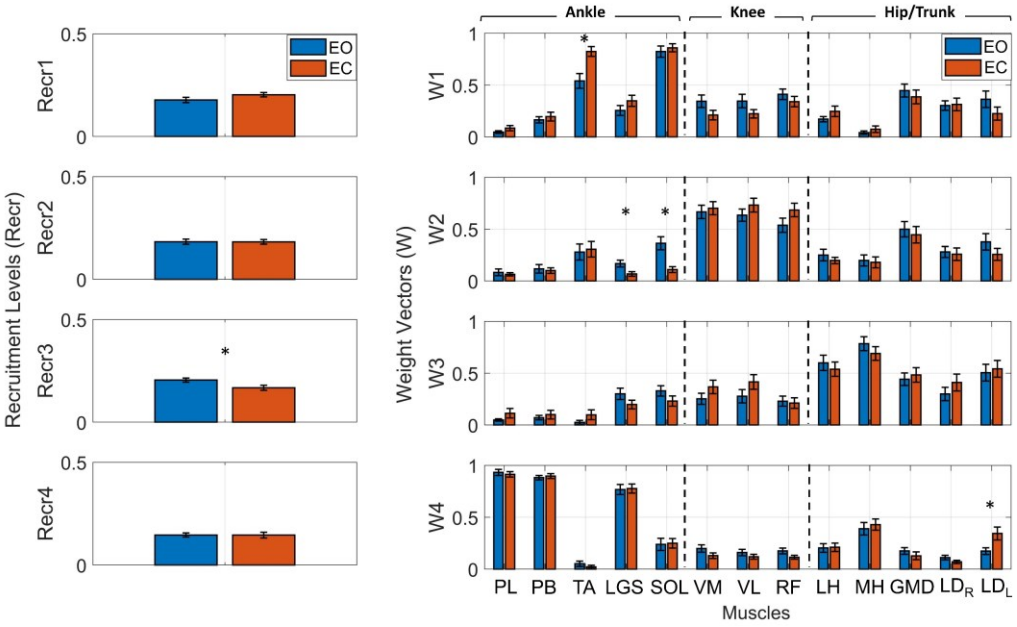

Figure 4.6 Comparison of muscle synergies extracted during eyes open (EO) and eyes closed (EC) single-leg stance conditions. Color vertical bars represent average recruitment levels $\boldsymbol{Recr_k}$ (on the left) and weight vectors $\boldsymbol{W_k}$ (on the right) of the *k*-synergy, over the sample population, with the superimposition of the standard error (black lines). The asterisk (*) represents a statistically significant difference between conditions, in the weight vectors and average recruitment levels.

iii. Balance control strategies (S)

As shown in **Figure 4.6**, the first and the fourth muscle synergies can be mainly associated with an ankle control strategy, since the muscles mainly enrolled are those belonging to the leg (PL, PB, LGS, and SOL), the second muscle synergy to a knee control strategy and the third muscle synergy to a

hip/trunk control strategy. ANOVA for repeated measures revealed a statistically significant increase (p = 0.03, g = 0.78) of the ankle control strategies (S_{ankle}) during the EC condition (0.52 ± 0.06) with respect to the EO condition (0.47 ± 0.06). No additional statistically significant differences were detected considering the remaining two balance control strategies (S_{knee} and S_{hip}) between conditions.

TABLE 4.5 represents the values of the balance control strategies, averaged over the sample population, with the indication of the statistically significant changes between EO and EC conditions.

TABLE 4.5
BALANCE CONTROL STRATEGIES (S) AVERAGED ON THE SAMPLE POPULATION

BALANCE CONTROL STRATEGIES	AVERAGE BALANCE CONTROL STRATEGIES (S) (MEAN ± STANDARD DEVIATION)		
	EO	*EC*	*ANOVA (P-VALUE)*
S_{ankle}	0.47 ± 0.06	0.52 ± 0.06	**0.03**
S_{knee}	0.61 ± 0.24	0.71 ± 0.25	0.22
S_{hip}	0.53 ± 0.15	0.53 ± 0.17	0.89

S_{ankle}: ankle control strategy, S_{knee}: knee control strategy, and S_{hip}: hip/trunk contorl strategy.

4.8 Discussion and Conclusions

Since the work by Horak and Nashner (1986), it is widely recognized the essential role of the ankle joint in the control of upright stance and for the maintenance of posture when balance is challenged by perturbations of the supporting surface. In these circumstances, muscles around the ankle joint provide the first activation strategy for balance maintenance [180]. In this chapter, no perturbations were applied to the supporting surface, and participants were required to maintain a quiet single-leg stance (SLS). The key role of the ankle joint for posture control in a quiet stance is confirmed by the observation of two ankle-dominant muscle synergies adopted by the participants in this study. The first ankle-dominant synergy (W_1) is mainly featured by the Tibialis Anterior (TA) and the Soleus (SOL) muscle activation. The second ankle dominant muscle synergy (W_4) is mainly featured by Peroneus Longus (PL), Peroneus Brevis (PB), and Gastrocnemius Lateralis (LGS) muscle activations. These two synergies may reflect the activations related to antero-posterior sway and medio-lateral sway, respectively, which may occur during a SLS task. In particular the co-activation of antagonist muscles (TA and SOL) might represent a strategy to cope with reduced base of support, with the aim to reduce movement variability and maintaining stability. Previous studies found an increase in TA and SOL activations in particular in older adults to compensate for reduced vision [193] or decreased tendon stiffness [194], and both in children and elderly which showed a diminished postural steadiness when compared with young adults [195].

Literature reports that as more difficult the task becomes as higher is the involvement of more proximal joints for the maintenance of balance, in particular

the hip [170,180]. In experimental settings, the difficulty of the task is usually increased by increasing the magnitude of a perturbation, by decreasing the supporting surface, or by changing the features of the supporting surface [28,159,170,187]. For example, it has been reported that by moving from a stable to an unstable surface, the angular displacement of the ankle was stable across all the testing conditions, with the knee and hip displacement arising when the difficulty of the task was higher [170,196].

In this chapter, the difficulty of the task was not modified throughout the experiment and the support surface was not unstable. However, standing on a single limb might be considered a *per se* difficult task because of the reduced base of support in comparison to the common double-leg stance (DLS) condition. Usually, when the support base is reduced, a precaution strategy consisting of moving forward the center of mass is adopted to avoid falling backward. This condition may justify the existence of the hip/trunk balance control strategy (characterized by the activation of the LH, MH, GMD, LD_L, and LD_R muscles) adopted by all the volunteers during the SLS condition. It is reasonable to think that the participants of the present study used the hip/trunk control strategy (W_3) to compensate for the ankle dorsiflexion used to move forward the center of mass to manage the reduced base of support. It should be also mentioned that in a condition of quiet stance the co-existence of the hip control strategy (W_2) and the ankle control strategy (W_1 and W_4) has been reported [196], highlighting that the two strategies are not different entities, but one predominates depending upon the task and conditions of the environment.

Previous literature has reported an increase in the knee joint displacement during SLS conditions when the difficulty of the task increased, i.e., the surface became less stable [170]. Thus, in this study, the knee synergy was probably used when the ankle synergy was not effective for the maintenance of balance, but the condition did not require yet the involvement of the hip or the back synergies. These results highlight the fine coordination between ankle muscles and quadriceps muscle. This was especially observed in the closed-eyes condition when the lack of visual information led to an increase in the difficulty of the task. In fact, it was observed a significantly lower activation of the SOL and LGS muscles when the knee-dominant synergy was used.

The results presented in this chapter show that 4 muscle synergies are needed during single-leg stance during eyes open (EO) as well as eyes closed (EC) conditions. In addition, there is no difference in the average recruitment levels between the EO and EC conditions, except for the hip/trunk muscle synergy, which showed a decrease in activation during the EC condition compared to the EO condition. At the same time, an increase in the ankle balance control strategy was found in the EC condition compared to the EO condition. However, despite some differences in the EC condition compared to the EO condition, the number of synergies used is the same between the conditions, as well as the average recruitment levels. This is in accordance with previous literature reporting the stability of muscle synergies adopted between tasks with different visual feedback conditions [187,197]. It has been shown that the lack of visual feedback does not

affect muscle synergies, since standing postural control mostly relies on proprioceptive feedback [187,197]. Furthermore, the results of previous investigations show that proprioceptive disturbance, but not visual disturbances, affected muscle synergies [187] and increases body sway [197]. Regarding the results of the present chapter, it can be thus speculated that the lack of visual information affects the modulation of muscle activations without altering the number and composition of the muscle synergies adopted.

Moreover, the results of this chapter suggest that muscle synergies could be not exclusively managed throughout a feedforward control, but can be modulated with a feedback control based on the signals arising from sensory receptors, with the aim to correct movement errors which may occur in some circumstances. It is likely to think that the maintenance of the single-limb stance in this study was controlled with pre-programmed muscles synergies. However, the difficulty of the task leading to continuous losses and recovery of balance, probably need a continuous movement correction based on a feedback control relying on information arising from sensory receptors. Animal studies have reported organized patterns of muscles activations in response to focal stimulation of the spinal cord [11], thus suggesting that a feedback control may be launched at spinal level in response to specific sensory stimuli to modulate the centrally organized synergy recruitment. It is likely to think that similar patterns may regulate muscle synergies also in humans.

To the best of the author's knowledge, this is the first study investigating muscle synergies deputed to the maintenance of posture during a single-leg stance task, in an EO and EC condition. Due to the large use of this kind of task in clinical practice, both for rehabilitation and functional assessment, as well as in sport practice for training and testing, the results of the present study give important information on motor control of this kind of task in healthy individuals. Future studies should investigate muscle synergies also in other populations to investigate the effects of orthopedic and neurologic pathologies on muscle synergies, as well as the effect of rehabilitation and training.

The main limitation of this study is that only healthy young individuals were recruited, and thus the results cannot be generalized to all healthy individuals. Future studies should identify muscle synergies used for single-leg stance also in other age groups. A second limitation of the study is that muscle synergies for the transition between double- and single-limb stance (and vice versa) were not analyzed, thus the results of the present study have to be considered exclusively for steady single-limb stance tasks.

In conclusion, the single-leg stance is featured by four major muscle synergies, two ankle-dominant, one knee-dominant, and one hip/trunk-dominant. The lack of visual feedback did not affect the number of synergies used. In general, an increase of activation of the ankle muscles and a decrease in the recruitment of the hip/trunk synergy was observed in the absence of visual information in comparison to the normal vision condition. Future studies should investigate muscle synergies during single-leg stance also in other age groups, and it seems of high clinical relevance to investigate synergies on orthopedic and neurologic patients to address clinical practice and rehabilitation interventions.

Chapter 5

Conclusions and Perspectives

With this doctoral thesis, the author endeavored to provide a deeper insight into the neuromuscular control of human movements, focusing on two essential daily life activities: human locomotion and balance control.

In the first part of the thesis, it was assessed the modular organization of the CNS during cyclical movements (i.e., human locomotion), using the widely used muscle synergy theory. The first step was to develop a reliable and accurate method for extracting muscle activation intervals during cyclical movements to be used as a pre-processing step before muscle synergy extraction (**A Deep Learning Approach for Muscle Activity Detection**). First, the applicability of the proposed approach was assessed considering simulated sEMG data and, then, its performance was compared against other standard muscle activity detectors using real sEMG signals both in physiological and pathological conditions. The second step was to methodologically assess two of the main weaknesses of the muscle synergy theory: the sEMG pre-processing steps before factorization and the selection of the optimal number of muscle synergies (i.e., the factorization rank). Considering the sEMG pre-processing weakness, a novel pre-processing approach based on the extraction of the principal activations before muscle synergy extraction was proposed and validated on real sEMG data, allowing a more interpretable assessment of the modular organization of the CNS during a walking task without any loss of information (**Methodological Issue - Muscle Synergies Extracted Using Principal Activations**). Considering the synergy number selection weakness, a novel method, based on multi-criteria decision analysis, for the selection of the optimal number of muscle synergies was proposed to overcome the limitations of the standard VAF-based approaches. Following an approach similar to the one proposed for the muscle activity detector, the applicability of the approach was first assessed considering simulated sEMG data and, then, its performance was compared against other standard VAF-based approaches using real sEMG signals both in physiological and pathological conditions (**Methodological Issue – Multi-**

Criteria Decision Analysis for Selecting the Optimal Number of Muscle Synergies).

In the second part of the thesis, instead, it was assessed the modular organization of the CNS during non-cyclical movements (i.e., single-leg stance) through the muscle synergy theory. As in the first part of the thesis, the first step was to develop a reliable and accurate method for the segmentation of the sEMG time-instants relative to a "*well-balanced*" single-leg stance or an "*unbalanced*" single-leg stance to be used as inputs of the muscle synergy extraction algorithm (**Methodological Issue – Muscle Synergy Assessment during Single-Leg Stance**). Subsequently, the consolidated method was applied to the analysis of the modular organization of single-leg stance with and without visual feedback considering a healthy sample population (**Application - Influence of Visual Feedback on Muscle Synergies**).

In the following paragraphs, the practical implications of the studies presented in this doctoral thesis will be discussed, also addressing their limitations and the scientific perspectives that emerged from this work.

Muscle Activity Detection

Determining the onset and offset time-instants of muscle activations during human movements is of great interest in different research fields including gait analysis, motor rehabilitation, sport science, myoelectric control of prostheses, human-machine interaction, design of biofeedback systems, and pre-processing of muscle synergy extraction. More specifically, the accurate temporal analysis of muscle activation in terms of burst onset, duration of the activation interval, and burst offset, can be useful in the assessment of the altered locomotion patterns of orthopedic and neurological patients.

The LSTM-based muscle activity detector presented in the first study of this thesis can be considered a valuable tool in all the applications requiring an accurate and effective recognition/distinction of muscle activity from background noise. In particular, it significantly outperforms previous detectors (such as the statistical double threshold detector and Teager-Kaiser Energy Operator detector) in terms of detection accuracy, it directly works on "raw" sEMG signals (does not require any additional input parameters), and it is robust even when applied to signals with low to medium signal-to-noise ratio.

Future works will be focused on testing the proposed approach also on sEMG signals acquired from subjects with musculoskeletal or neurodegenerative disorders other than Parkinson's disease and on developing a novel formulation of this approach for real-time muscle activity detection.

This novel muscle activity detector is currently being applied in a number of projects investigating muscle activity during walking. First, thanks to the collaboration with the Stereotactic and Functional Neurosurgery Unit of the University of Turin (Italy), it is being applied to assess the effect of Deep Brain Stimulation (DBS) neurosurgery on the muscle activity of patients affected by Parkinson's disease during walking by analyzing the onset, the offset, and the

duration of each muscle activation within a gait cycle. Second, the detector is currently being used as a pre-processing step before the application of the CIMAP (Clustering for Identification of Muscle Activation Patterns) algorithm, allowing the extraction of principal and secondary muscle activation intervals from sEMG signals during cyclic movements. Finally, thanks to the collaboration with the Department of Control and Computer Engineering (DAUIN) of Politecnico di Torino, the proposed muscle activity detector is being used to control a haptic exoskeleton for postural rehabilitation of patients with locomotor impairments. More specifically, the muscle activation intervals extracted through the LSTM-MAD from sEMG signals are currently being used to predict the angular positions of leg joints and control the exoskeleton.

Muscle Synergies during Walking

Human locomotion is one of the most widely studied and complex motor tasks, due to the multiple degrees of freedom of the skeletal muscle system, the several biomechanical functions carried out during each gait cycle, and the high cycle-by-cycle variability of muscle activation intervals. Several studies already demonstrated that human locomotion can be modeled by a small set of muscle synergies characterized by specific biomechanical functions. Despite the growing interest in the assessment of the modular organization of the CNS during walking through the muscle synergy theory, there is a lack of standards and common procedures for the sEMG pre-processing steps and the extraction of muscle synergies (e.g., selection of the optimal number of muscle synergies).

In the present doctoral thesis, these two weaknesses of the muscle synergy theory were assessed by presenting two novel methodological approaches that could provide a deeper insight into human motor control.

Considering the former, an innovative pre-processing technique for muscle synergy extraction was proposed combining Statistical Gait Analysis (SGA) and CIMAP algorithm, allowing for obtaining the principal and secondary activations. Results presented in this thesis demonstrated that the extraction of the principal activations only can be successfully used as a pre-processing step before muscle synergy extraction, allowing a more interpretable assessment of the modular organization of the CNS during a walking task in both physiological and pathological populations without any loss of information. Even if long-lasting signal recordings (at least 2-3 minutes are required to obtain a sufficient number of typical gait cycles) are needed to be able to properly compute the principal activations, this requirement does not limit the feasibility and applicability of the proposed approach to pathological populations. Indeed, gait analysis is commonly used to quantitatively assess patients' locomotion performance only in those patients able to independently walk, for some minutes, without walking aids or external supports. One possible limitation of the present approach is that only principal activation intervals were used to extract muscle synergies, since the assessment of the variability expressed by the muscle synergy analysis could be particularly significant when analyzing sEMG data acquired from subjects affected

by movement disorders. To overcome this limitation, future studies will focus on muscle synergies extracted from the secondary activations (SAs), i.e., those muscle activations that occur only in some gait cycles and could have an auxiliary function in motor control, such as to provide corrections to motion and body segment posture.

Considering the latter weakness of the muscle synergy theory, a novel ELECTRE III approach for choosing the optimal number of muscle synergies was proposed and validated on both simulated and real sEMG data. Even if this approach does not outperform the other tested threshold-independent method (i.e., elbow VAF method), several are the potential advantages of the ELECTRE III approach compared to the commonly used VAF-based threshold methods, such as the use of minimization and maximization approaches rather than an arbitrary threshold, the use of a multi-criteria decision-making approach based on different parameters computed from the muscle synergy results (not only VAF values), and the applicability to a variety of different motor tasks. Future works will be focused on optimizing the proposed approach by considering additional evaluation criteria or changing their importance weights and on applying the ELECTRE III approach to the studies described in Chapter 3 to assess the robustness of the proposed results with respect to the approach for selecting the optimal number of muscle synergies.

Both these approaches are currently being applied in two different projects investigating motor control strategies of pathological populations during walking. First, thanks to the collaboration with the Stereotactic and Functional Neurosurgery Unit of the University of Turin (Italy), they are being applied to assess the changes in motor control strategies of patients affected by Parkinson's Disease (PD) due to Deep Brain Stimulation (DBS) neurosurgery. More specifically, this study aims at assessing differences in the number and composition of the muscle synergies extracted from 30 PD patients during a 5-minutes lasting walking task at a self-selected speed before and after the DBS neurosurgery. Second, the effect of cognitive dual-task (i.e., verbal fluency and music-based dual tasks) while walking on PD motor control strategies is currently being studied through the muscle synergy theory considering the same sample population above-mentioned.

Muscle Synergies during Single-Leg Stance

The ability to maintain the single-leg stance is essential during daily living activities, as a single task as well as a component of other more complex tasks, such as walking and running. It is a simple but challenging condition for balance control and for this reason it is widely used for training and rehabilitation. In research and clinical practice, it is widely used as a testing task as it allows to quantify balance alterations and deficits of the single lower limb otherwise concealed during the performance of double leg tasks. In the last years, muscle synergy assessment during different balance conditions (e.g., single-leg stance) was mainly focused on the evaluation of balance recovery after a "controlled" perturbation, rather than on the maintenance of the balance condition itself. Thus, the segmentation approach proposed in this thesis aims at providing a useful tool for the assessment of the

motor control strategies adopted to maintain the single-leg stance, distinguishing between "*well-balanced"* and "*unbalanced"* single-leg stance epochs.

Results demonstrated that the proposed segmentation approach is robust concerning the selection of the segmentation threshold and can be successfully used as a pre-processing step before muscle synergy extraction, allowing a better assessment of the modular organization of the central nervous system during the maintenance of the single-leg stance. Moreover, it was applied for the assessment of the effect of visual feedback on muscle synergies extracted from healthy subjects during unipedal stance, revealing a high consistency of motor controls strategies adopted by healthy subjects with and without visual feedback.

One of the advantages of the proposed approach is the possibility to assess motor control strategies used by subjects to maintain the balance condition, instead of evaluating balance recovery after a "controlled" perturbation. Instead, the fact that the proposed method was validated on a sample population of young healthy subjects that can maintain the single-leg stance for at least 30 s may represent a first limitation of the study, since it may be difficult to obtain similar task durations considering elderly or pathological populations affected by severe balance impairments. Moreover, different muscle synergy results might be obtained in populations with diminished equilibrium skills or severe balance impairments.

Currently, the proposed muscle synergy extraction approach is being applied in a project that aims at assessing the modular organization of CNS during single-leg stance in pathological conditions. More specifically, thanks to the collaboration with the Rizzoli Orthopedic Institute of Bologna (Italy), it is being applied to assess muscle synergies extracted during single-leg stance tasks from patients affected by Chronic Ankle Instability (CAI).

Appendix A

Extraction of Principal and Secondary Activations through CIMAP

A.1 Introduction

Instrumented gait analysis is a widely used approach to quantitatively and non-invasively assessed the physiological and pathological motor functions during human locomotion [198]. In particular, the analysis of muscle activation patterns is of great interest, in research as well as in clinical practice, to study the altered locomotion patterns of orthopaedic and neurological patients or to assess the efficacy of rehabilitation programs. Muscle activation patterns are computed from muscles' electrical activity acquired by means of surface electromyography (sEMG) during cyclic movements. Then, for each movement cycle (e.g., each gait cycle), muscle activation patterns are computed determining the timing of muscle activations (burst onset, duration, and end). However, the high cycle-to-cycle variability of sEMG activations intervals makes it difficult to obtain a synthetic and clear representation of the patient's motor functions [98,101]. **Figure A.1** represents an example of sEMG signals acquired from an 11-years-old child during three different gait cycles from the Lateral Hamstring (LH) muscle.

To overcome this limitation, Statistical Gait Analysis (SGA) [60] and Clustering for Identification of Muscle Activation Patterns (CIMAP) [103,104,199] algorithms were recently introduced. Statistical Gait Analysis allows an easier interpretation and comparison of muscle activation intervals through the acquisition and processing of a large number of gait cycles. CIMAP algorithm, indeed, enables the grouping into clusters of gait cycles characterized by similar muscle activation patterns. By combining SGA and CIMAP algorithms, principal activations (PAs) and secondary activations (SAs) can be computed from the sEMG signals [24,65,106]. Principal activations are defined as those muscle activations that are

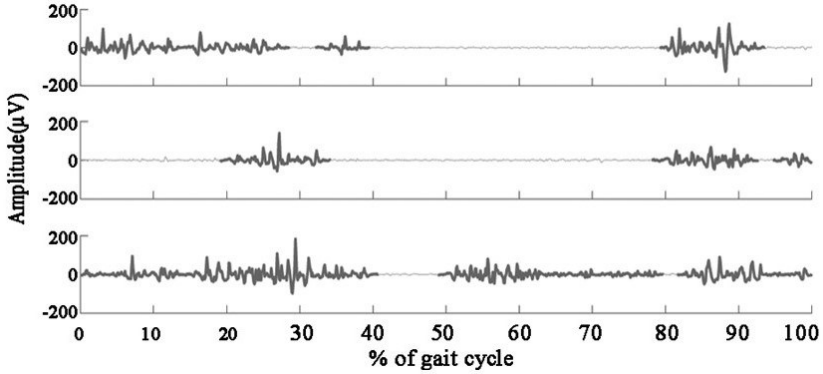

Figure A.1 Example of sEMG signals acquired from an 11-years-old healthy child during gait from Lateral Hamstring (LH) muscle.

necessary for the execution of a specific motor task and they describe the essential contribution of a specific muscle to the movement. The concept of PAs is complementary to the one of secondary activation, which are muscle activations that occur only in some gait cycles and could have an auxiliary function in motor control (e.g., to provide corrections to motion and body segment posture).

The extraction of principal and secondary muscle activations as a pre-processing step may significantly improve the analysis of sEMG signals, reducing the cycle-to-cycle variability and simplifying the understanding of muscle activation patterns both in physiological and pathological conditions.

This chapter aims at briefly describing the processing steps needed to compute the PAs and SAs from sEMG signals.

A.2 Extraction of Principal and Secondary Activations

Before computing principal and secondary activations, sEMG signals were pre-processed as it follows:

i. Muscle activation intervals were detected through the LSTM-MAD algorithm described in **0**. The detector's output is computed as a binary mask that was set equal to 1 in correspondence of the sEMG time-instants classified as muscle activity and to 0 otherwise (background noise)
ii. Time-segmentation of muscle activation intervals into gait cycles using foot-switch signal [108]
iii. Time-normalization of each gait cycle into 1000 time points.

Principal and secondary activations were computed from the muscle activation intervals, separately for each muscle, applying the optimized version of the CIMAP algorithm [104]. **Figure A.2** shows an example of the application of the CIMAP algorithm to sEMG signals acquired from a healthy subject during gait from Peroneus Longus (PL) and Gluteus Medius (GMD) muscles.

The CIMAP algorithm, based on agglomerative hierarchical clustering, groups together the gait cycles sharing similar muscle activation intervals. Each significant cluster is characterized by an element (called prototype) that is representative of all

the elements (gait cycles) belonging to the same cluster. Prototypes are computed as the median value of the elements belonging to the same cluster. **Figure A.2A** represents in blue the time-normalized activation intervals for each gait cycle, grouped in significant clusters sharing similar activation intervals. Each orange interval represents the prototype of a significant cluster.

Starting from a number of clusters equals to the number of gait cycles analyzed (each cluster contains a single element), the CIMAP algorithm iteratively merges the two "closest" clusters until a single cluster, containing all the gait cycles, is obtained. The complete linkage method is used to select the two "closest" clusters to be merged. The implemented linkage method uses the farthest distance between every pair of elements in the two considered clusters as merging criterion. During the linkage process, the distance between each couple of elements is assessed using the Manhattan distance. Hence, the dendrogram is constructed.

The final number of clusters (cutoff rule) was selected to achieve:

i. Clusters characterized by a comparable number of elements (C) within a significant cluster
ii. Small intra-cluster variability (ICV), computed as the Euclidian distance between each element of the cluster and the corresponding cluster's prototype.

More specifically, the optimized version of CIMAP algorithm defines a cutoff rule based on three different criteria. First, the differences of inter-cluster Euclidian distances ($Diff_k$) between two consecutive dendrogram iterations (k) are computed. Second, three cutoff points are computed based on the following three criteria:

i. First dendrogram iteration k in which $Diff_k \geq mean(Diff_k)$, where $mean(Diff_k)$ is the average of $Diff_k$ computed over all the iterations
ii. First dendrogram iteration k in which $Diff_k \geq mean(Diff_k) + 1 \cdot std(Diff_k)$, where $mean(Diff_k)$ and $std(Diff_k)$ are the average and the standard deviation of $Diff_k$ computed over all the iterations, respectively
iii. Starting from the last dendrogram iteration and stepping backwards, the first iteration in which $Diff_k$ series stop decreasing monotonically (after a moving average filtering step).

Finally, since the three cutoff criteria may result in different numbers of final clusters, the best cutoff was automatically identified using an index that takes into account both the intra-cluster variability (ICV) and the number of elements within each significant cluster (C_i), as described in (**A.1**):

$$Cutoff = \frac{\sum_{i=1}^{n} ICV_i / n}{\sum_{i=1}^{n} |C_i|} \quad \textbf{(A.1)}$$

where n represents the number of significant clusters, $|C_i|$ is the number of cycles belonging to the i-th cluster, and ICV_i represents the intra-cluster variability of the

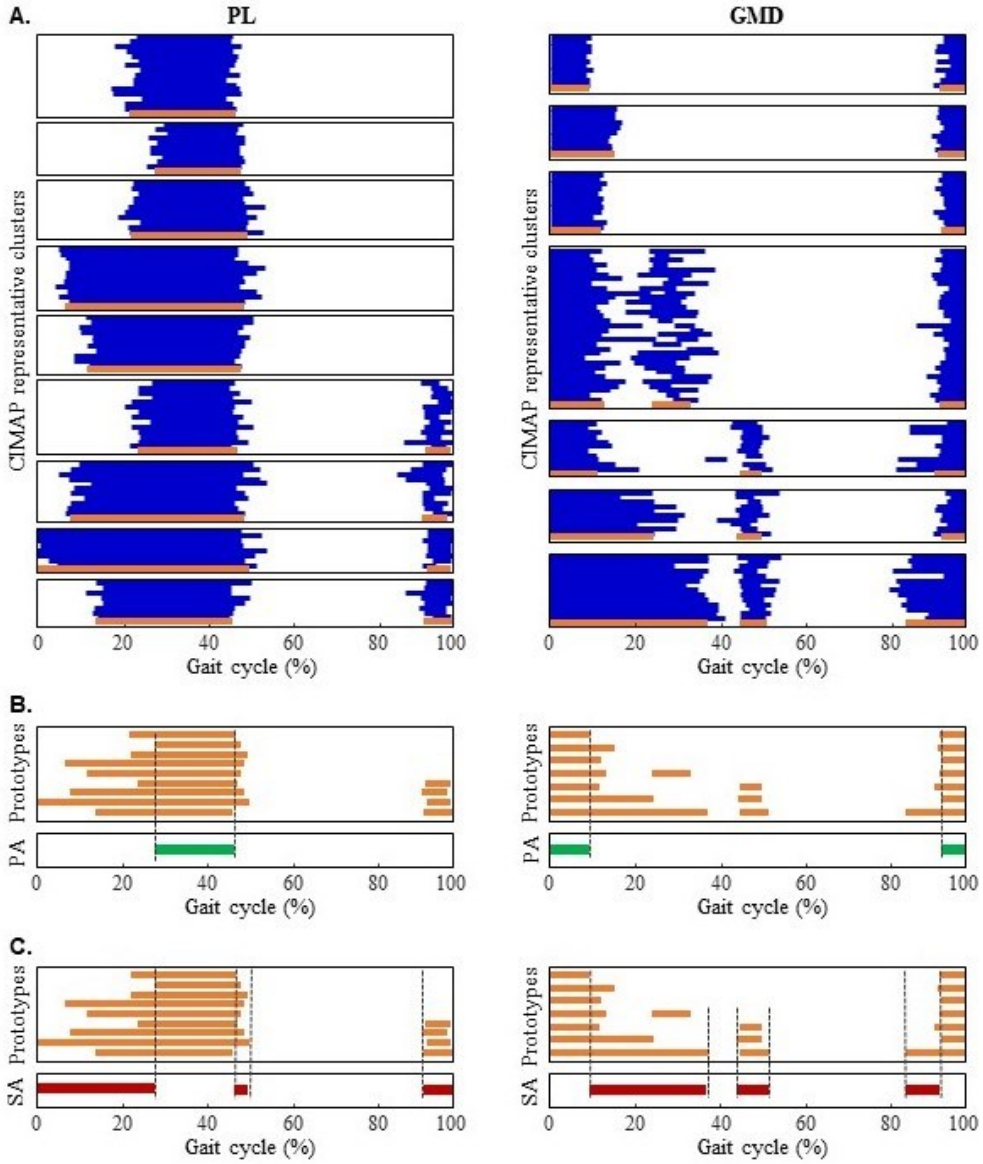

Figure A.2 Example of application of the CIMAP algorithm to sEMG signals acquired from a healthy subject during gait from PL (left) and GMD (right) muscles. (A) Blue intervals represent the cluster elements (muscle activation intervals computed through LSTM-MAD algorithm) normalized into 1000 time points with respect to the gait cycle duration, while orange intervals represent the prototypes of each cluster (computed as median of the elements that belong to the same cluster). (B) Principal activation (PA) is represented in green and is defined as the intersection of all the cluster's prototypes. (C) Secondary activation (SA) is represented in red and is defined as all the time-instants that are classified as muscle activity and are not PAs. Reprinted from "*How to Improve Robustness in Muscle Synergy Extraction*" by *Ghislieri et al.*

i-th cluster. Low values of the $Cutoff$ index correspond to clusters with a small intra-cluster variability and a high number of elements belonging to each significant cluster.

After the definition of the final number of clusters, the principal and secondary activations are computed, separately for each muscle, from the prototypes of the significant clusters. More specifically, the PAs are defined as the intersection of all the significant clusters' prototypes, while SAs are defined as all the time-instants classified as muscle activations, but excluded from the PAs, since they occur only

in some gait cycles. For each observed muscle, a single principal (or secondary) activation interval was obtained and defined as a 1000-samples binary mask.

Figure A.2B and **Figure A.2C** depict how the PAs and the SAs are obtained from the significant clusters' prototypes, respectively.

For each gait cycle, the extraction of the PAs (or SAs) from the original sEMG signals of a specific muscle was performed by time-windowing all the time-normalized gait cycles through the corresponding binary mask that was set equals to 1 in correspondence of the time-instants defined as PAs (or SAs) and to 0 otherwise (no PAs or SAs computed).

Figure A.3 shows an example of principal and secondary activation extraction performed on PL and GMD muscles acquired from a healthy subject during a single gait cycle.

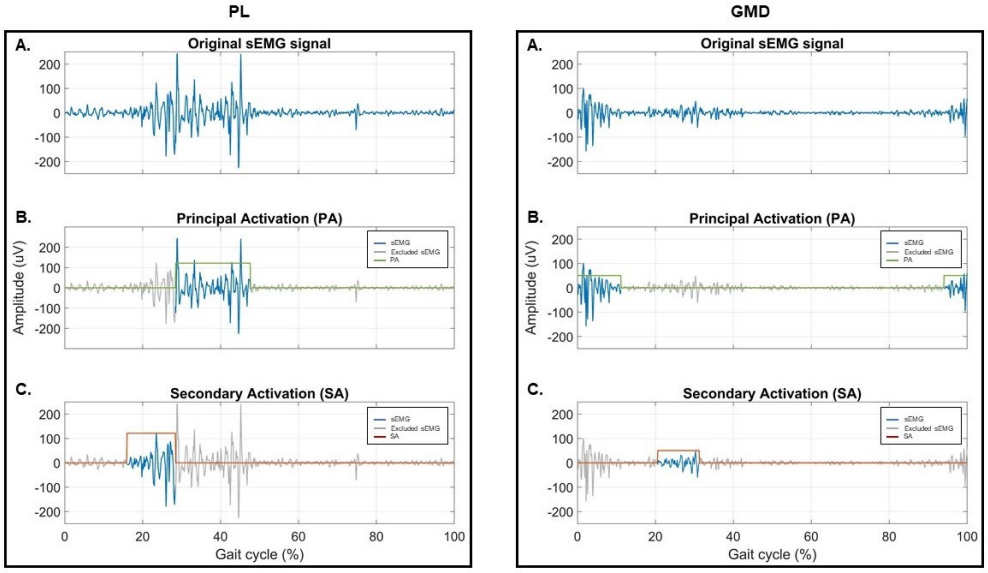

Figure A.3 Extraction of principal and secondary activations from PL (left) and GMD (right) muscles of a healthy subject during a walking task. (A) Original sEMG signals time-normalized with respect to the duration of the gait cycle. (B) Extraction of the principal activation (in green) from the original sEMG signal with the indication of the excluded sEMG time-instants in gray. (C) Extraction of the secondary activation (in red) from the original sEMG signals with the indication of the excluded sEMG time-instants in gray.

Appendix B

List of Abbreviations

The following abbreviations are used in the manuscript:

ANOVA	Analysis of Variance
CAI	Chronic Ankle Instability
CBA	Cost-Benefit Analysis
CIMAP	Clustering for Identification of Muscle Activation Pattern
CNS	Central Nervous System
DBS	Deep Brain Stimulation
ELECTRE	ELimination Et Choix Traduisant la REalitè
GMD	Gluteus Medius
ICV	Intra-Cluster Variability
LD_L	Left Longissimus Dorsii
LD_R	Right Longissimus Dorsii
LGS	Lateral Gastrocnemius
LH	Lateral Hamstring
LSTM	Long-Short Term Memory neural network
LSTM-MAD	Long-Short Term Memory for Muscle Activity Detection
MAE	Mean Absolute Error
MCDA	Multi Criteria Decision Analysis
MCDM	Multi Criteria Decision-Making
MH	Medial Hamstring
PAs	Principal Activations
PB	Peroneus Brevis
PL	Peroneus Longus
RF	Rectus Femoris
RMS	Root Mean Squared
RNN	Recurrent Neural Network
SAs	Secondary Activations
sEMG	Surface Electromyography signals
SGA	Statistical Gait Analysis
SNR	Signal-to-Noise Ratio

1	SOL	Soleus
2	TA	Tibialis Anterior
3	TKEO	Teager-Kaiser Energy Operator
4	UPDRS	Unified Parkison’s Disease Rating Score
5	VAF	Variance Accounted For
6	VL	Vastus Lateralis
7	VM	Vastus Medialis

References

[1] N.A. Bernstein, The co-ordination and regulation of movements, first edit, Pergamon Press Ltd., Pergamon Press, Oxford, 1967. http://ci.nii.ac.jp/naid/10008376164/ (accessed October 11, 2017).

[2] E. Bizzi, Computations underlying the execution of movement, in: J. Cogn. Neurosci., 2000: p. 13.

[3] J. Roh, V.C.K.K. Cheung, E. Bizzi, Modules in the brain stem and spinal cord underlying motor behaviors., J Neurophysiol. 106 (2011) 1363–1378. https://doi.org/10.1152/jn.00842.2010.

[4] A. d'Avella, Modularity for motor control and motor learning, in: Adv. Exp. Med. Biol., Springer New York LLC, 2016: pp. 3–19. https://doi.org/10.1007/978-3-319-47313-0_1.

[5] W.A. Lee, Neuromotor synergies as a basis for coordinated intentional action, J. Mot. Behav. 16 (1984) 135–170. https://doi.org/10.1080/00222895.1984.10735316.

[6] M.C. Tresch, P. Saltiel, E. Bizzi, The construction of movement by the spinal cord, Nat. Neurosci. 2 (1999) 162–167. https://doi.org/10.1038/5721.

[7] E. Bizzi, V.C.K. Cheung, The neural origin of muscle synergies, Front Comput Neurosci. 7 (2013) 51. https://doi.org/10.3389/fncom.2013.00051.

[8] A. D'Avella, M.C. Tresch, Modularity in the motor system: decomposition of muscle patterns as combinations of time-varying synergies, Adv. Neural Inf. Process. Syst. 14. 1 (2002) 141–148. https://doi.org/10.1.1.19.8895.

[9] C. Alessandro, I. Delis, F. Nori, S. Panzeri, B. Berret, Muscle synergies in neuroscience and robotics: from input-space to task-space perspectives, Front Comput Neurosci. 7 (2013) 1–16. https://doi.org/10.3389/fncom.2013.00043.

[10] J.J. Kutch, F.J. Valero-Cuevas, Challenges and new approaches to proving the existence of muscle synergies of neural origin, PLoS Comput Biol. 8 (2012). https://doi.org/10.1371/journal.pcbi.1002434.

[11] M.C. Tresch, E. Bizzi, Responses to spinal microstimulation in the chronically spinalized rat and their relationship to spinal systems activated by low threshold cutaneous stimulation, Exp. Brain Res. 129 (1999) 401–416. https://doi.org/10.1007/s002210050908.

[12] M.A. Lemay, W.M. Grill, Modularity of Motor Output Evoked by Intraspinal Microstimulation in Cats, J. Neurophysiol. 91 (2004) 502–514. https://doi.org/10.1152/jn.00235.2003.

[13] P. Saltiel, K. Wyler-Duda, A. D'Avella, M.C. Tresch, E. Bizzi, Muscle synergies encoded within the spinal cord: evidence from focal intraspinal NMDA iontophoresis in the frog., J Neurophysiol. 85 (2001) 605–619.

[14] T. Flash, B. Hochner, Motor primitives in vertebrates and invertebrates, Curr. Opin. Neurobiol. 15 (2005) 660–666. https://doi.org/10.1016/j.conb.2005.10.011.

[15] P.A. Guertin, Central pattern generator for locomotion: Anatomical, physiological, and pathophysiological considerations, Front. Neurol. 3 FEB (2013) 183. https://doi.org/10.3389/fneur.2012.00183.

[16] V.C.K. Cheung, L. Piron, M. Agostini, S. Silvoni, A. Turolla, E. Bizzi, Stability of muscle synergies for voluntary actions after cortical stroke in humans., Proc. Natl. Acad. Sci. U. S. A. 106 (2009) 19563–19568. https://doi.org/10.1073/pnas.0910114106.

[17] J. Taborri, V. Agostini, P.K.P.K. Artemiadis, M. Ghislieri, D.A.D.A. Jacobs, J. Roh, S. Rossi, Feasibility of Muscle Synergy Outcomes in Clinics, Robotics, and Sports: A Systematic Review, Appl. Bionics Biomech. 2018 (2018) 1–19. https://doi.org/10.1155/2018/3934698.

[18] I. Mileti, A. Zampogna, A. Santuz, F. Asci, Z. Del Prete, A. Arampatzis, E. Palermo, A. Suppa, Muscle synergies in parkinson's disease, Sensors (Switzerland). 20 (2020) 1–21. https://doi.org/10.3390/s20113209.

[19] Y.P. Ivanenko, R.E. Poppele, F. Lacquaniti, Five basic muscle activation patterns account for muscle activity during human locomotion, 556 (2004) 267–282. https://doi.org/10.1113/jphysiol.2003.057174.
[20] V. Monaco, A. Ghionzoli, S. Micera, Age-related modifications of muscle synergies and spinal cord activity during locomotion., J Neurophysiol. 104 (2010) 2092–2102. https://doi.org/10.1152/jn.00525.2009.
[21] S.A. Chvatal, L.H. Ting, T. Wallace, G. Tech, Voluntary and Reactive Recruitment of Locomotor Muscle Synergies during Perturbed Walking, J Neurosci. 32 (2012) 12237–12250. https://doi.org/10.1523/JNEUROSCI.6344-11.2012.
[22] K.M. Steele, M.C. Tresch, E.J. Perreault, Consequences of biomechanically constrained tasks in the design and interpretation of synergy analyses., J. Neurophysiol. 113 (2015) jn.00769.2013. https://doi.org/10.1152/jn.00769.2013.
[23] K.M. Steele, M.C. Tresch, E.J. Perreault, The number and choice of muscles impact the results of muscle synergy analyses, Front Comput Neurosci. 7 (2013) 1–9. https://doi.org/10.3389/fncom.2013.00105.
[24] D. Rimini, V. Agostini, M. Knaflitz, Intra-Subject Consistency during Locomotion : Similarity in Shared and Subject-Specific Muscle Synergies, Front. Hum. Neurosci. 11 (2017) 1–10. https://doi.org/10.3389/fnhum.2017.00586.
[25] L.H. Ting, J.M. Macpherson, A limited set of muscle synergies for force control during a postural task., J Neurophysiol. 93 (2005) 609–613. https://doi.org/10.1152/jn.00681.2004.
[26] G. Torres-Oviedo, L.H. Ting, Subject-Specific Muscle Synergies in Human Balance Control Are Consistent Across Different Biomechanical Contexts, J Neurophysiol. 103 (2010) 3084–3098. https://doi.org/10.1152/jn.00960.2009.
[27] S.A. Chvatal, L.H. Ting, Common muscle synergies for balance and walking, Front Comput Neurosci. 7 (2013) 48. https://doi.org/10.3389/fncom.2013.00048.
[28] G. Torres-Oviedo, L.H. Ting, Muscle synergies characterizing human postural responses, J Neurophysiol. 98 (2007) 2144–2156. https://doi.org/10.1152/jn.01360.2006.
[29] M. Ghislieri, M. Knaflitz, L. Labanca, G. Barone, L. Bragonzoni, M.G.G. Benedetti, V. Agostini, Muscle Synergy Assessment during Single-Leg Stance, IEEE Trans. Neural Syst. Rehabil. Eng. 28 (2020) 1. https://doi.org/10.1109/TNSRE.2020.3030847.
[30] A. D'Avella, E. Bizzi, Shared and specific muscle synergies in natural motor behaviors., Proc. Natl. Acad. Sci. U. S. A. 102 (2005) 3076–3081. https://doi.org/10.1073/pnas.0500199102.
[31] V.C.K.K. Cheung, A. D'Avella, E. Bizzi, Adjustments of motor pattern for load compensation via modulated activations of muscle synergies during natural behaviors., J Neurophysiol. 101 (2009) 1235–1257. https://doi.org/10.1152/jn.01387.2007.
[32] M.C. Tresch, V.C.K.K. Cheung, A. d'Avella, Matrix factorization algorithms for the identification of muscle synergies: evaluation on simulated and experimental data sets., J Neurophysiol. 95 (2006) 2199–2212. https://doi.org/10.1152/jn.00222.2005.
[33] L.H. Ting, H.J. Chiel, R.D. Trumbower, J.L. Allen, J.L. McKay, M.E. Hackney, T.M. Kesar, Neuromechanical principles underlying movement modularity and their implications for rehabilitation, Neuron. 86 (2015) 38–54. https://doi.org/10.1016/j.neuron.2015.02.042.
[34] K.E. Zelik, V. La Scaleia, Y.P. Ivanenko, F. Lacquaniti, Can modular strategies simplify neural control of multidirectional human locomotion?, J Neurophysiol. 111 (2014) 1686–1702. https://doi.org/10.1152/jn.00776.2013.
[35] F.M. Ramos, A. D'Avella, M. Hayashibe, Identification of time-varying and time-scalable synergies from continuous electromyographic patterns, IEEE Robot. Autom. Lett. 4 (2019) 3053–3058. https://doi.org/10.1109/LRA.2019.2924854.
[36] A. Santuz, A. Ekizos, L. Janshen, V. Baltzopoulos, A. Arampatzis, On the Methodological Implications of Extracting Muscle Synergies from Human Locomotion, Int. J. Neural Syst. 27 (2017) 1–15. https://doi.org/10.1142/S0129065717500071.
[37] M.H. Soomro, S. Conforto, G. Giunta, S. Ranaldi, C. De Marchis, Comparison of initialization techniques for the accurate extraction of muscle synergies from myoelectric signals via nonnegative matrix factorization, Appl. Bionics Biomech. 2018 (2018). https://doi.org/10.1155/2018/3629347.
[38] A.S. Oliveira, L. Gizzi, D. Farina, U.G. Kersting, D.J. Clark, M.R. Va, Motor modules of human locomotion: influence of EMG averaging, concatenation, and number of step cycles., Front Hum Neurosci. 8 (2014) 335. https://doi.org/10.3389/fnhum.2014.00335.
[39] J. Taborri, E. Palermo, Z. Del Prete, S. Rossi, On the reliability and repeatability of surface electromyography factorization by muscle synergies in daily life activities, Appl. Bionics Biomech. 2018 (2018). https://doi.org/10.1155/2018/5852307.
[40] V.C.K. Cheung, K. Devarajan, G. Severini, A. Turolla, P. Bonato, Decomposing time series

data by a non-negative matrix factorization algorithm with temporally constrained coefficients, in: Proc. Annu. Int. Conf. IEEE Eng. Med. Biol. Soc. EMBS, Institute of Electrical and Electronics Engineers Inc., 2015: pp. 3496–3499. https://doi.org/10.1109/EMBC.2015.7319146.

[41] H.S. Seung, D.D. Lee, H.S. Seung, Learning the parts of objects by non-negative matrix factorization., Nature. 401 (1999) 788–791. https://doi.org/10.1038/44565.

[42] D.D. Lee, H.S. Seung, Algorithms for nonnegative matrix factorization. Volume 13. NIPS, (2001).

[43] F.O. Barroso, D. Torricelli, F. Molina-Rueda, I.M. Alguacil-Diego, R. Cano-de-la-Cuerda, C. Santos, J.C. Moreno, J.C. Miangolarra-Page, J.L. Pons, Combining muscle synergies and biomechanical analysis to assess gait in stroke patients, J. Biomech. 63 (2017) 98–103. https://doi.org/10.1016/j.jbiomech.2017.08.006.

[44] M. Sartori, L. Gizzi, V.C.K. Cheung, C. Patten, C.L. Banks, M.M. Pai, T.E. Mcguirk, B.J. Fregly, Methodological Choices in Muscle Synergy Analysis Impact Differentiation of Physiological Characteristics Following Stroke, Front. Comput. Neurosci. | Www.Frontiersin.Org 1. 11 (2017) 1–12. https://doi.org/10.3389/fncom.2017.00078.

[45] K.L. Rodriguez, R.T. Roemmich, B. Cam, B.J. Fregly, C.J. Hass, Persons with Parkinson's disease exhibit decreased neuromuscular complexity during gait, Clin. Neurophysiol. 124 (2013) 1390–1397. https://doi.org/10.1016/j.clinph.2013.02.006.

[46] M. Ghislieri, V. Agostini, M. Knaflitz, Muscle Synergies Extracted Using Principal Activations: Improvement of Robustness and Interpretability, 28 (2020). https://doi.org/10.1109/TNSRE.2020.2965179.

[47] V.C.K. Cheung, A. d'Avella, M.C. Tresch, E. Bizzi, Central and sensory contributions to the activation and organization of muscle synergies during natural motor behaviors., J Neurosci. 25 (2005) 6419–6434. https://doi.org/10.1523/JNEUROSCI.4904-04.2005.

[48] H. Kim, H. Park, Nonnegative matrix factorization based on alternating nonnegativity constrained least squares and active set method, SIAM J. Matrix Anal. Appl. 30 (2008) 713–730. https://doi.org/10.1137/07069239X.

[49] P. Kieliba, P. Tropea, E. Pirondini, M. Coscia, S. Micera, F. Artoni, How are Muscle Synergies Affected by Electromyography Pre-Processing?, IEEE Trans. Neural Syst. Rehabil. Eng. 26 (2018) 882–893. https://doi.org/10.1109/TNSRE.2018.2810859.

[50] B.R. Shuman, M.H. Schwartz, K.M. Steele, Electromyography Data Processing Impacts Muscle Synergies during Gait for Unimpaired Children and Children with Cerebral Palsy, Front Comput Neurosci. 11 (2017) 1–9. https://doi.org/10.3389/fncom.2017.00050.

[51] F. Hug, N. a. Turpin, S. Dorel, A. Guével, Smoothing of electromyographic signals can influence the number of extracted muscle synergies, Clin. Neurophysiol. 123 (2012) 1895–1896. https://doi.org/10.1016/j.clinph.2012.01.015.

[52] J. Taborri, E. Palermo, D. Masiello, S. Rossi, Factorization of EMG via muscle synergies in walking task : evaluation of intra-subject and inter-subject variability, in: I2MTC IEEE Conf., IEEE, 2017: pp. 708–713. https://doi.org/10.1109/I2MTC.2017.7969775.

[53] E. Scalona, J. Taborri, Z. Del Prete, E. Palermo, S. Rossi, EMG factorization during walking: Does digital filtering influence the accuracy in the evaluation of the muscle synergy number?, in: MeMeA 2018 - 2018 IEEE Int. Symp. Med. Meas. Appl. Proc., Institute of Electrical and Electronics Engineers Inc., 2018. https://doi.org/10.1109/MeMeA.2018.8438760.

[54] A. D'Avella, A. Portone, L. Fernandez, F. Lacquaniti, Control of Fast-Reaching Movements by Muscle Synergy Combinations, J Neurosci. 26 (2006) 7791–7810. https://doi.org/10.1523/JNEUROSCI.0830-06.2006.

[55] D.J. Clark, L.H. Ting, F.E. Zajac, R.R. Neptune, S.A. Kautz, Merging of healthy motor modules predicts reduced locomotor performance and muscle coordination complexity post-stroke., J Neurophysiol. 103 (2010) 844–857. https://doi.org/10.1152/jn.00825.2009.

[56] S.A. Kautz, Mark G. Bowden, D.J. Clark, R.R. Neptune, Comparison of Motor Control Deficits During Treadmill and Overground Walking Poststroke, Neurorehabil Neural Repair. 25 (2017) 1–23. https://doi.org/10.1007/s00210-015-1172-8.The.

[57] M. Coscia, V. Monaco, C. Martelloni, B. Rossi, C. Chisari, S. Micera, Muscle synergies and spinal maps are sensitive to the asymmetry induced by a unilateral stroke, J. Neuroeng. Rehabil. 12 (2015) 1–16. https://doi.org/10.1186/s12984-015-0031-7.

[58] K.M. Steele, A. Rozumalski, M.H. Schwartz, Muscle synergies and complexity of neuromuscular control during gait in cerebral palsy, Dev. Med. Child Neurol. 57 (2015) 1176–1182. https://doi.org/10.1111/dmcn.12826.

[59] J. Roh, W.Z. Rymer, R.F. Beer, Robustness of muscle synergies underlying three-dimensional force generation at the hand in healthy humans, J. Neurophysiol. 107 (2012)

2123–2142.
[60] V. Agostini, A. Nascimbeni, A. Gaffuri, P. Imazio, M.G. Benedetti, M. Knaflitz, Agostini V., Nascimbeni A., Gaffuri A., Imazio P., Benedetti M.G., Knaflitz M., V. Agostini, A. Nascimbeni, A. Gaffuri, P. Imazio, M.G. Benedetti, M. Knaflitz, Normative EMG activation patterns of school-age children during gait, Gait Posture. 32 (2010) 285–289. https://doi.org/https://doi.org/10.1016/j.gaitpost.2010.06.024.
[61] A.D. Vigotsky, I. Halperin, G.J. Lehman, G.S. Trajano, T.M. Vieira, Interpreting signal amplitudes in surface electromyography studies in sport and rehabilitation sciences, Front. Physiol. (2018). https://doi.org/10.3389/fphys.2017.00985.
[62] S. Micera, J. Carpaneto, S. Raspopovic, Control of hand prostheses using peripheral information, IEEE Rev. Biomed. Eng. (2010). https://doi.org/10.1109/RBME.2010.2085429.
[63] M. Simao, N. Mendes, O. Gibaru, P. Neto, A Review on Electromyography Decoding and Pattern Recognition for Human-Machine Interaction, IEEE Access. (2019). https://doi.org/10.1109/ACCESS.2019.2906584.
[64] S. Ma, M. Varley, L.K. Shark, J. Richards, EMG biofeedback based VR system for hand rotation and grasping rehabilitation, in: Proc. Int. Conf. Inf. Vis., IEEE, 2010: pp. 479–484. https://doi.org/10.1109/IV.2010.73.
[65] D. Rimini, V. Agostini, S. Rosati, C. Castagneri, G. Balestra, M. Knaflitz, Influence of pre-processing in the extraction of muscle synergies during human locomotion, Proc. Annu. Int. Conf. IEEE Eng. Med. Biol. Soc. EMBS. (2017) 2502–2505. https://doi.org/10.1109/EMBC.2017.8037365.
[66] M. Ghislieri, V. Agostini, M. Knaflitz, How to Improve Robustness in Muscle Synergy Extraction, in: IEEE, 2019: pp. 1525–1528. https://doi.org/10.1109/EMBC.2019.8856438.
[67] C. Castagneri, V. Agostini, S. Rosati, G. Balestra, M. Knaflitz, Asymmetry Index in Muscle Activations, IEEE Trans. Neural Syst. Rehabil. Eng. 27 (2019) 772–779. https://doi.org/10.1109/TNSRE.2019.2903687.
[68] P. Bonato, T. D'Alessio, M. Knaflitz, A statistical method for the measurement of muscle activation intervals from surface myoelectric signal during gait, IEEE Trans. Biomed. Eng. 45 (1998) 287–299. https://doi.org/10.1109/10.661154.
[69] V. Agostini, M. Knaflitz, An algorithm for the estimation of the signal-to-noise ratio in surface myoelectric signals generated during cyclic movements, IEEE Trans. Biomed. Eng. 59 (2012) 219–225. https://doi.org/10.1109/TBME.2011.2170687.
[70] A. Phinyomark, E. Scheme, EMG Pattern Recognition in the Era of Big Data and Deep Learning, Big Data Cogn. Comput. 2 (2018) 21. https://doi.org/10.3390/bdcc2030021.
[71] J. Yousefi, A. Hamilton-Wright, Characterizing EMG data using machine-learning tools, Comput. Biol. Med. 51 (2014) 1–13. https://doi.org/10.1016/j.compbiomed.2014.04.018.
[72] F. Alnajjar, T. Wojtara, H. Kimura, S. Shimoda, Muscle synergy space: learning model to create an optimal muscle synergy, Front Comput Neurosci. 7 (2013) 1–10. https://doi.org/10.3389/fncom.2013.00136.
[73] M. Ortiz-Catalan, R. Brånemark, B. Håkansson, R. Branemark, B. Hakansson, Real-time classification of simultaneous hand and wrist motions using Artificial Neural Networks with variable threshold outputs, Conf. Proc. IEEE Eng. Med. Biol. Soc. 2013 (2013) 6651–4. https://doi.org/10.1109/EMBC.2013.6611081.
[74] H.M. Shim, H. An, S. Lee, E.H. Lee, H.K. Min, S. Lee, EMG pattern classification by split and merge deep belief network, Symmetry (Basel). 8 (2016). https://doi.org/10.3390/sym8120148.
[75] H. min Shim, S. Lee, Multi-channel electromyography pattern classification using deep belief networks for enhanced user experience, J. Cent. South Univ. 22 (2015) 1801–1808. https://doi.org/10.1007/s11771-015-2698-0.
[76] U. Côté-Allard, C.L. Fall, A. Campeau-Lecoursy, C. Gosseliny, F. Laviolettez, B. Gosselin, Transfer learning for sEMG hand gestures recognition using convolutional neural networks, 2017 IEEE Int. Conf. Syst. Man, Cybern. SMC 2017. 2017-Janua (2017) 1663–1668. https://doi.org/10.1109/SMC.2017.8122854.
[77] M. Atzori, M. Cognolato, H. Müller, Deep learning with convolutional neural networks applied to electromyography data: A resource for the classification of movements for prosthetic hands, Front. Neurorobot. 10 (2016) 1–10. https://doi.org/10.3389/fnbot.2016.00009.
[78] T. Varrecchia, C. D'Anna, M. Schmid, S. Conforto, Generalization of a wavelet-based algorithm to adaptively detect activation intervals in weak and noisy myoelectric signals, Biomed. Signal Process. Control. 58 (2020). https://doi.org/10.1016/j.bspc.2019.101838.
[79] C. D'Anna, T. Varrecchia, M. Schmid, S. Conforto, Using the frequency signature to detect

muscular activity in weak and noisy myoelectric signals, Biomed. Signal Process. Control. 52 (2019) 69–76. https://doi.org/10.1016/j.bspc.2019.02.026.
[80] I.. Basheer, M. Hajmeer, Artificial neural networks: fundamentals, computing, design, and application, J. Microbiol. Methods. 43 (2000) 3–31. https://doi.org/10.1016/S0167-7012(00)00201-3.
[81] A. Graves, Generating Sequences With Recurrent Neural Networks, (2013) 1–43. http://arxiv.org/abs/1308.0850.
[82] S. Hochreiter, J. Schmidhuber, Long Short-Term Memory, Neural Comput. 9 (1997) 1735–1780. https://doi.org/10.1162/neco.1997.9.8.1735.
[83] Y. Goldberg, Neural Network Methods for Natural Language Processing, Synth. Lect. Hum. Lang. Technol. 10 (2017) 1–309. https://doi.org/10.2200/S00762ED1V01Y201703HLT037.
[84] X. Li, P. Zhou, A.S. Aruin, Teager-kaiser energy operation of surface EMG improves muscle activity onset detection, Ann. Biomed. Eng. 35 (2007) 1532–1538. https://doi.org/10.1007/s10439-007-9320-z.
[85] S. Solnik, P. DeVita, P. Rider, B. Long, T. Hortobágyi, Teager-Kaiser operator improves the accuracy of EMG onset detection independent of signal-to-noise ratio, Acta Bioeng. Biomech. 10 (2008) 65–68.
[86] W.A. Gardner, A. Napolitano, L. Paura, Cyclostationarity: Half a century of research, Signal Processing. 86 (2006) 639–697. https://doi.org/10.1016/J.SIGPRO.2005.06.016.
[87] C.J. De Luca, L. Donald Gilmore, M. Kuznetsov, S.H. Roy, Filtering the surface EMG signal: Movement artifact and baseline noise contamination, J. Biomech. 43 (2010) 1573–1579. https://doi.org/10.1016/j.jbiomech.2010.01.027.
[88] V. Agostini, D. Ganio, K. Facchin, L. Cane, S. Moreira Carneiro, M. Knaflitz, Gait parameters and muscle activation patterns at 3, 6 and 12 months after total hip arthroplasty., J. Arthroplasty. 29 (2014) 1265–72. https://doi.org/10.1016/j.arth.2013.12.018.
[89] V. Agostini, M. Lanotte, M. Carlone, M. Campagnoli, I. Azzolin, R. Scarafia, G. Massazza, M. Knaflitz, Instrumented Gait Analysis for an Objective Pre-/Postassessment of Tap Test in Normal Pressure Hydrocephalus, Arch. Phys. Med. Rehabil. 96 (2015) 1235–1241. https://doi.org/10.1016/j.apmr.2015.02.014.
[90] V. Agostini, M. Knaflitz, Statistical Gait Analysis, Distrib. Diagnosis Home Healthc. Stevenson (2012) 99–121.
[91] V. Agostini, M. Ghislieri, S. Rosati, G. Balestra, M. Knaflitz, Surface Electromyography Applied to Gait Analysis: How to Improve Its Impact in Clinics?, Front. Neurol. 11 (2020) 1–13. https://doi.org/10.3389/fneur.2020.00994.
[92] F. Lacquaniti, Y.P. Ivanenko, A. D'Avella, K.E. Zelik, M. Zago, Evolutionary and developmental modules, Front Comput Neurosci. 7 (2013) 61. https://doi.org/10.3389/fncom.2013.00061.
[93] D.P. Kingma, J.L. Ba, Adam: A method for stochastic optimization, in: 3rd Int. Conf. Learn. Represent. ICLR 2015 - Conf. Track Proc., International Conference on Learning Representations, ICLR, 2015. https://arxiv.org/abs/1412.6980v9 (accessed May 4, 2021).
[94] R. a Bogey, L. a Barnes, J. Perry, Computer algorithms to characterize individual subject EMG profiles during gait., Arch. Phys. Med. Rehabil. 73 (1992) 835–841. https://doi.org/0003-9993(92)90155-P [pii].
[95] C. De Marchis, S. Ranaldi, M. Serrao, A. Ranavolo, F. Draicchio, F. Lacquaniti, S. Conforto, Modular motor control of the sound limb in gait of people with trans-femoral amputation, J. Neuroeng. Rehabil. 16 (2019). https://doi.org/10.1186/s12984-019-0616-7.
[96] E. Ambrosini, C. De Marchis, A. Pedrocchi, G. Ferrigno, M. Monticone, M. Schmid, T. D'Alessio, S. Conforto, S. Ferrante, Neuro-Mechanics of Recumbent Leg Cycling in Post-Acute Stroke Patients, Ann. Biomed. Eng. 44 (2016) 3238–3251. https://doi.org/10.1007/s10439-016-1660-0.
[97] J. Perry, Gait Analysis: Normal and Pathological Function, J. Pediatr. Orthop. 12 (1992) 815. https://doi.org/10.1001.
[98] D.A. Winter, H.J. Yack, EMG profiles during normal human walking: stride-to-stride and inter-subject variability, Electroencephalogr. Clin. Neurophysiol. 67 (1987) 402–411. https://doi.org/10.1016/0013-4694(87)90003-4.
[99] S. Hagio, M. Fukuda, M. Kouzaki, Identification of muscle synergies associated with gait transition in humans, Front Hum Neurosci. 9 (2015) 1–12. https://doi.org/10.3389/fnhum.2015.00048.
[100] F. Di Nardo, A. Mengarelli, A. Strazza, V. Agostini, M. Knaflitz, L. Burattini, S. Fioretti, A new parameter for quantifying the variability of surface electromyographic signals during gait: The occurrence frequency, J. Electromyogr. Kinesiol. 36 (2017) 25–33.

https://doi.org/10.1016/j.jelekin.2017.06.006.
[101] F. Di Nardo, E. Maranesi, A. Mengarelli, G. Ghetti, L. Burattini, S. Fioretti, Assessment of the variability of vastii myoelectric activity in young healthy females during walking: A statistical gait analysis, J. Electromyogr. Kinesiol. 25 (2015) 800–807. https://doi.org/10.1016/j.jelekin.2015.07.004.
[102] A. Strazza, A. Mengarelli, S. Fioretti, L. Burattini, V. Agostini, M. Knaflitz, F. Di Nardo, Surface-EMG analysis for the quantification of thigh muscle dynamic co-contractions during normal gait, Gait Posture. 51 (2017) 228–233. https://doi.org/10.1016/j.gaitpost.2016.11.003.
[103] S. Rosati, V. Agostini, M. Knaflitz, G. Balestra, Muscle activation patterns during gait: A hierarchical clustering analysis, Biomed. Signal Process. Control. 31 (2017) 463–469. https://doi.org/10.1016/j.bspc.2016.09.017.
[104] S. Rosati, C. Castagneri, V. Agostini, M. Knaflitz, G. Balestra, Muscle contractions in cyclic movements: Optimization of CIMAP algorithm, Proc. Annu. Int. Conf. IEEE Eng. Med. Biol. Soc. EMBS. (2017) 58–61. https://doi.org/10.1109/EMBC.2017.8036762.
[105] C. Castagneri, V. Agostini, G. Balestra, M. Knaflitz, M. Carlone, G. Massazza, EMG Asymmetry Index in Cyclic Movements, in: 2018 IEEE Life Sci. Conf., 2018: pp. 223–226. https://doi.org/10.1109/LSC.2018.8572041.
[106] C. Castagneri, V. Agostini, S. Rosati, G. Balestra, M. Knaflitz, Longitudinal assessment of muscle function after Total Hip Arthroplasty : Use of clustering to extract principal activations from EMG signals, in: 2018 IEEE Int. Symp. Med. Meas. Appl., 2018: pp. 1–5. https://doi.org/10.1109/MeMeA.2018.8438802.
[107] C.G. Goetz, B.C. Tilley, S.R. Shaftman, G.T. Stebbins, S. Fahn, P. Martinez-Martin, W. Poewe, C. Sampaio, M.B. Stern, R. Dodel, B. Dubois, R. Holloway, J. Jankovic, J. Kulisevsky, A.E. Lang, A. Lees, S. Leurgans, P.A. LeWitt, D. Nyenhuis, C.W. Olanow, O. Rascol, A. Schrag, J.A. Teresi, J.J. van Hilten, N. LaPelle, P. Agarwal, S. Athar, Y. Bordelan, H.M. Bronte-Stewart, R. Camicioli, K. Chou, W. Cole, A. Dalvi, H. Delgado, A. Diamond, J.P. Dick, J. Duda, R.J. Elble, C. Evans, V.G. Evidente, H.H. Fernandez, S. Fox, J.H. Friedman, R.D. Fross, D. Gallagher, C.G. Goetz, D. Hall, N. Hermanowicz, V. Hinson, S. Horn, H. Hurtig, U.J. Kang, G. Kleiner-Fisman, O. Klepitskaya, K. Kompoliti, E.C. Lai, M.L. Leehey, I. Leroi, K.E. Lyons, T. McClain, S.W. Metzer, J. Miyasaki, J.C. Morgan, M. Nance, J. Nemeth, R. Pahwa, S.A. Parashos, J.S.J.S. Schneider, A. Schrag, K. Sethi, L.M. Shulman, A. Siderowf, M. Silverdale, T. Simuni, M. Stacy, M.B. Stern, R.M. Stewart, K. Sullivan, D.M. Swope, P.M. Wadia, R.W. Walker, R. Walker, W.J. Weiner, J. Wiener, J. Wilkinson, J.M. Wojcieszek, S. Wolfrath, F. Wooten, A. Wu, T.A. Zesiewicz, R.M. Zweig, Movement Disorder Society-Sponsored Revision of the Unified Parkinson's Disease Rating Scale (MDS-UPDRS): Scale presentation and clinimetric testing results, Mov. Disord. 23 (2008) 2129–2170. https://doi.org/10.1002/mds.22340.
[108] V. Agostini, G. Balestra, M. Knaflitz, Agostini V., Balestra G., Knaflitz M., V. Agostini, G. Balestra, M. Knaflitz, Segmentation and classification of gait cycles, IEEE Trans. Neural Syst. Rehabil. Eng. 22 (2014) 946–952. https://doi.org/10.1109/TNSRE.2013.2291907.
[109] B.P.F. O'Callaghan, E.P. Doheny, C. Goulding, E. Fortune, M.M. Lowery, Adaptive gait segmentation algorithm for walking bout detection using tri-axial accelerometers, in: Proc. Annu. Int. Conf. IEEE Eng. Med. Biol. Soc. EMBS, Institute of Electrical and Electronics Engineers Inc., 2020: pp. 4592–4595. https://doi.org/10.1109/EMBC44109.2020.9176460.
[110] M.W. Flood, B.P.F. O'Callaghan, M.M. Lowery, Gait Event Detection from Accelerometry Using the Teager-Kaiser Energy Operator, IEEE Trans. Biomed. Eng. 67 (2020) 658–666. https://doi.org/10.1109/TBME.2019.2919394.
[111] L. Gizzi, S. Muceli, F. Petzke, D. Falla, Experimental Muscle Pain Impairs the Synergistic Modular Control of Neck Muscles., PLoS One. 10 (2015) e0137844. https://doi.org/10.1371/journal.pone.0137844.
[112] D. Rimini, V. Agostini, M. Knaflitz, Evaluation of muscle synergies stability in human locomotion: A comparison between normal and fast walking speed, I2MTC 2017 - 2017 IEEE Int. Instrum. Meas. Technol. Conf. Proc. (2017). https://doi.org/10.1109/I2MTC.2017.7969722.
[113] L. V. Hedges, Distribution Theory for Glass's Estimator of Effect size and Related Estimators, J. Educ. Stat. 6 (1981) 107–128. https://doi.org/10.3102/10769986006002107.
[114] V. Monaco, A. Ghionzoli, P. Dario, S. Micera, Muscle synergies during walking: comparison between young and elderly people. Preliminary results, in: 2008 30th Annu. Int. IEEE EMBS Conf., 2008: pp. 5370–5373.
[115] J.L. Allen, J.L. McKay, A. Sawers, M.E. Hackney, L.H. Ting, Increased neuromuscular consistency in gait and balance after partnered, dance-based rehabilitation in Parkinson's

disease, J. Neurophysiol. 118 (2017) 363–373. https://doi.org/10.1152/jn.00813.2016.
[116] M.G. Benedetti, V. Agostini, M. Knaflitz, V. Gasparroni, M. Boschi, R. Piperno, Self-reported gait unsteadiness in mildly impaired neurological patients: an objective assessment through statistical gait analysis., J. Neuroeng. Rehabil. 9 (2012) 64. https://doi.org/10.1186/1743-0003-9-64.
[117] V. Agostini, A. Nascimbeni, A. Gaffuri, M. Knaflitz, Agostini Valentina, Nascimbeni Alberto, Gaffuri Andrea, Knaflitz Marco, V. Agostini, A. Nascimbeni, A. Gaffuri, M. Knaflitz, Multiple gait patterns within the same Winters class in children with hemiplegic cerebral palsy, Clin. Biomech. 30 (2015) 908–914. https://doi.org/10.1016/j.clinbiomech.2015.07.010.
[118] D.F. Feeney, R.A. Capobianco, J.R. Montgomery, J. Morreale, A.M. Grabowski, R.M. Enoka, Individuals with sacroiliac joint dysfunction display asymmetrical gait and a depressed synergy between muscles providing sacroiliac joint force closure when walking, J. Electromyogr. Kinesiol. 43 (2018) 95–103. https://doi.org/10.1016/j.jelekin.2018.09.009.
[119] I. Mileti, A. Zampogna, J. Taborri, F. Martelli, S. Rossi, Z. Del Prete, M. Paoloni, A. Suppa, E. Palermo, Parkinson's disease and Levodopa effects on muscle synergies in postural perturbation, in: Med. Meas. Appl. MeMeA 2019 - Symp. Proc., Institute of Electrical and Electronics Engineers Inc., 2019. https://doi.org/10.1109/MeMeA.2019.8802229.
[120] S. Grazioso, T. Caporaso, A. Palomba, S. Nardella, B. Ostuni, D. Panariello, G. Di Gironimo, A. Lanzotti, Assessment of upper limb muscle synergies for industrial overhead tasks: A preliminary study, in: 2019 IEEE Int. Work. Metrol. Ind. 4.0 IoT, MetroInd 4.0 IoT 2019 - Proc., Institute of Electrical and Electronics Engineers Inc., 2019: pp. 89–92. https://doi.org/10.1109/METROI4.2019.8792842.
[121] A. D'Avella, P. Saltiel, E. Bizzi, Combinations of muscle synergies in the construction of a natural motor behavior., Nat. Neurosci. 6 (2003) 300–308. https://doi.org/10.1038/nn1010.
[122] M.C. Tresch, V.C.K. Cheung, Matrix Factorization Algorithms for the Identification of Muscle Synergies : Evaluation on Simulated and Experimental Data Sets Matrix Factorization Algorithms for the Identification of Muscle Synergies : Evaluation on Simulated and Experimental Data Sets, J Neurophysiol. 95 (2006) 2199–2212. https://doi.org/10.1152/jn.00222.2005.
[123] K. Devarajan, V.C.K. Cheung, On nonnegative matrix factorization algorithms for signal-dependent noise with application to electromyography data, Neural Comput. 26 (2014) 1128–1168.
[124] J.L. Allen, S.A. Kautz, R.R. Neptune, The influence of merged muscle excitation modules on post-stroke hemiparetic walking performance, Clin. Biomech. 28 (2013) 697–704. https://doi.org/10.1016/j.clinbiomech.2013.06.003.
[125] M. Ghislieri, V. Agostini, M. Knaflitz, The effect of signal-to-noise ratio on muscle synergy extraction, in: 2018 IEEE Life Sci. Conf. LSC 2018, Institute of Electrical and Electronics Engineers Inc., 2018: pp. 227–230. https://doi.org/10.1109/LSC.2018.8572075.
[126] U. Pale, M. Atzori, H. Müller, A. Scano, Variability of muscle synergies in hand grasps: Analysis of intra-and inter-session data, Sensors (Switzerland). 20 (2020) 1–27. https://doi.org/10.3390/s20154297.
[127] M. Hirashima, T. Oya, How does the brain solve muscle redundancy? Filling the gap between optimization and muscle synergy hypotheses, Neurosci. Res. 104 (2016) 80–87. https://doi.org/10.1016/j.neures.2015.12.008.
[128] H. Yokoyama, N. Kaneko, T. Ogawa, N. Kawashima, K. Watanabe, K. Nakazawa, Cortical Correlates of Locomotor Muscle Synergy Activation in Humans: An Electroencephalographic Decoding Study, IScience. 15 (2019) 623–639. https://doi.org/10.1016/j.isci.2019.04.008.
[129] A. Sawers, J.L. Allen, L.H. Ting, Long-term training modifies the modular structure and organization of walking balance control, J Neurophysiol. 114 (2015) 3359–3373. https://doi.org/10.1152/jn.00758.2015.
[130] Y. Kim, T.C. Bulea, D.L. Damiano, Novel Methods to Enhance Precision and Reliability in Muscle Synergy Identification during Walking, Front Hum Neurosci. 10 (2016) 1–12. https://doi.org/10.3389/fnhum.2016.00455.
[131] I. Delis, B. Berret, T. Pozzo, S. Panzeri, Quantitative evaluation of muscle synergy models: a single-trial task decoding approach., Front Comput Neurosci. 7 (2013) 8. https://doi.org/10.3389/fncom.2013.00008.
[132] H. Akaike, Factor analysis and AIC, in: Sel. Pap. Hirotugu Akaike, Springer, 1987: pp. 371–386.
[133] A.T. Basilevsky, Statistical factor analysis and related methods: theory and applications, John Wiley & Sons, 2009.

[134] T. Minka, Automatic choice of dimensionality for PCA, Adv. Neural Inf. Process. Syst. 13 (2000) 598–604.
[135] W. Zucchini, An introduction to model selection, J. Math. Psychol. 44 (2000) 41–61.
[136] V. Diaby, K. Campbell, R. Goeree, Multi-criteria decision analysis (MCDA) in health care: A bibliometric analysis, Oper. Res. Heal. Care. 2 (2013) 20–24. https://doi.org/10.1016/j.orhc.2013.03.001.
[137] A. Angelis, P. Kanavos, Multiple Criteria Decision Analysis (MCDA) for evaluating new medicines in Health Technology Assessment and beyond: The Advance Value Framework, Soc. Sci. Med. 188 (2017) 137–156. https://doi.org/10.1016/j.socscimed.2017.06.024.
[138] T.D.C. Frazão, D.G.G. Camilo, E.L.S. Cabral, R.P. Souza, Multicriteria decision analysis (MCDA) in health care: A systematic review of the main characteristics and methodological steps, BMC Med. Inform. Decis. Mak. 18 (2018) 1–16. https://doi.org/10.1186/s12911-018-0663-1.
[139] F. Marleau Donais, I. Abi-Zeid, E.O.D. Waygood, R. Lavoie, A review of cost–benefit analysis and multicriteria decision analysis from the perspective of sustainable transport in project evaluation, EURO J. Decis. Process. 7 (2019) 327–358. https://doi.org/10.1007/s40070-019-00098-1.
[140] F. Marleau Donais, I. Abi-Zeid, E.O.D. Waygood, R. Lavoie, Assessing and ranking the potential of a street to be redesigned as a Complete Street: A multi-criteria decision aiding approach, Transp. Res. Part A Policy Pract. 124 (2019) 1–19. https://doi.org/10.1016/j.tra.2019.02.006.
[141] H.E. Mutikanga, S.K. Sharma, K. Vairavamoorthy, Multi-criteria Decision Analysis: A Strategic Planning Tool for Water Loss Management, Water Resour. Manag. 25 (2011) 3947–3969. https://doi.org/10.1007/s11269-011-9896-9.
[142] C. Bouchard, N. Beauchamp, I. Abi-Zeid, L. Lamontagne, J. Desrosiers, M. Rodriguez, Multicriteria decision analysis for the selection of a small drinking water treatment system, J. Water Supply Res. Technol. - AQUA. 59 (2010) 230–242. https://doi.org/10.2166/aqua.2010.071.
[143] S. Ranaldi, C. De Marchis, M. Rinaldi, S. Conforto, The effect of Non-Negative Matrix Factorization initialization on the accurate identification of muscle synergies with correlated activation signals, MeMeA 2018 - 2018 IEEE Int. Symp. Med. Meas. Appl. Proc. (2018) 1–5. https://doi.org/10.1109/MeMeA.2018.8438602.
[144] J.R. Figueira, S. Greco, B. Roy, R. Słowiński, An Overview of ELECTRE Methods and their Recent Extensions, J. Multi-Criteria Decis. Anal. 20 (2013) 61–85. https://doi.org/10.1002/mcda.1482.
[145] J.R. Figueira, V. Mousseau, B. Roy, ELECTRE methods, Int. Ser. Oper. Res. Manag. Sci. 233 (2016) 155–185. https://doi.org/10.1007/978-1-4939-3094-4_5.
[146] J.R. Figueira, S. Greco, B. Roy, R. Słowiński, ELECTRE Methods: Main Features and Recent Developments, in: Springer, Berlin, Heidelberg, 2010: pp. 51–89. https://doi.org/10.1007/978-3-540-92828-7_3.
[147] B. Roy, The Outranking Approach and the Foundations of Electre Methods, in: Readings Mult. Criteria Decis. Aid, Springer Berlin Heidelberg, 1990: pp. 155–183. https://doi.org/10.1007/978-3-642-75935-2_8.
[148] J. E E Figueira, B. Roy, Decision Aiding Determining the weights of criteria in the ELECTRE type methods with a revised Simos' procedure, n.d. www.elsevier.com/locate/dsw (accessed March 18, 2021).
[149] J. Cohen, A Coefficient of Agreement for Nominal Scales, Educ. Psychol. Meas. 20 (1960) 37–46. https://doi.org/10.1177/001316446002000104.
[150] M. Ghislieri, L. Gastaldi, S. Pastorelli, S. Tadano, V. Agostini, Wearable Inertial Sensors to Assess Standing Balance: A Systematic Review, Sensors. 19 (2019) 4075. https://doi.org/10.3390/s19194075.
[151] M.J. dos Santos, A.L. Gorges, J.L. Rios, Individuals with chronic ankle instability exhibit decreased postural sway while kicking in a single-leg stance, Gait Posture. 40 (2014) 231–236. https://doi.org/10.1016/j.gaitpost.2014.04.002.
[152] S. Van Deun, F.F. Staes, K.H. Stappaerts, L. Janssens, O. Levin, K.K.H. Peers, Relationship of chronic ankle instability to muscle activation patterns during the transition from double-leg to single-leg stance, Am. J. Sports Med. 35 (2007) 274–281. https://doi.org/10.1177/0363546506294470.
[153] M. Pope, L. Chinn, D. Mullineaux, P.O. McKeon, L. Drewes, J. Hertel, Spatial postural control alterations with chronic ankle instability, Gait Posture. 34 (2011) 154–158. https://doi.org/https://doi.org/10.1016/j.gaitpost.2011.04.012.
[154] V. Agostini, E. Chiaramello, C. Bredariol, C. Cavallini, M. Knaflitz, Postural control after

traumatic brain injury in patients with neuro-ophthalmic deficits., Gait Posture. 34 (2011) 248–253. https://doi.org/10.1016/j.gaitpost.2011.05.008.
[155] V. Agostini, A. Sbrollini, C. Cavallini, A. Busso, G. Pignata, M. Knaflitz, The role of central vision in posture: Postural sway adaptations in Stargardt patients, Gait Posture. 43 (2016) 233–238. https://doi.org/https://doi.org/10.1016/j.gaitpost.2015.10.003.
[156] D. Barbado Murillo, R. Sabido Solana, F.J. Vera-Garcia, N. Gusi Fuertes, F.J. Moreno, Effect of increasing difficulty in standing balance tasks with visual feedback on postural sway and EMG: Complexity and performance, Hum. Mov. Sci. 31 (2012) 1224–1237. https://doi.org/https://doi.org/10.1016/j.humov.2012.01.002.
[157] P. Balestrucci, E. Daprati, F. Lacquaniti, V. Maffei, Effects of visual motion consistent or inconsistent with gravity on postural sway, Exp. Brain Res. 235 (2017) 1999–2010. https://doi.org/10.1007/s00221-017-4942-3.
[158] V. Munoz-Martel, A. Santuz, A. Ekizos, A. Arampatzis, Neuromuscular organisation and robustness of postural control in the presence of perturbations, Sci. Rep. 9 (2019) 12273. https://doi.org/10.1038/s41598-019-47613-7.
[159] M. Yamagata, A. Falaki, M.L.M.L. Latash, Stability of vertical posture explored with unexpected mechanical perturbations: synergy indices and motor equivalence, Exp. Brain Res. 236 (2018) 1501–1517. https://doi.org/10.1007/s00221-018-5239-x.
[160] T. Wojtara, F. Alnajjar, S. Shimoda, H. Kimura, Muscle synergy stability and human balance maintenance, J Neuroeng Rehabil. 11 (2014) 129. https://doi.org/10.1186/1743-0003-11-129.
[161] P.A. Burtner, C. Qualls, M.H. Woollacott, Muscle activation characteristics of stance balance control in children with spastic cerebral palsy, Gait Posture. 8 (1998) 163–174. https://doi.org/https://doi.org/10.1016/S0966-6362(98)00032-0.
[162] G. Torres-Oviedo, J.M. Macpherson, L.H. Ting, Muscle Synergy Organization Is Robust Across a Variety of Postural Perturbations, J Neurophysiol. 96 (2006) 1530–1546. https://doi.org/10.1152/jn.00810.2005.
[163] K.L. Hsieh, K.L. Roach, D.A. Wajda, J.J. Sosnoff, Smartphone technology can measure postural stability and discriminate fall risk in older adults., Gait Posture. 67 (2019) 160–165. https://doi.org/10.1016/j.gaitpost.2018.10.005.
[164] M. Mancini, F.B. Horak, C. Zampieri, P. Carlson-Kuhta, J.G. Nutt, L. Chiari, Trunk accelerometry reveals postural instability in untreated Parkinson's disease, Parkinsonism Relat. Disord. 17 (2011) 557–562. https://doi.org/10.1016/J.PARKRELDIS.2011.05.010.
[165] D. Torricelli, F. Barroso, M. Coscia, C. Alessandro, F. Lunardini, E.B. Esteban, A. Avella, Muscle Synergies in Clinical Practice: Theoretical and Practical Implications, 10 (2016) 251–272. https://doi.org/10.1007/978-3-319-24901-8.
[166] L.H. Ting, S.A. Chvatal, Motor control: theories, experiments, and applications, (2010) 102–138.
[167] I. Makhlouf, A. Chaouachi, M. Chaouachi, A. Ben Othman, U. Granacher, D.G. Behm, Combination of Agility and Plyometric Training Provides Similar Training Benefits as Combined Balance and Plyometric Training in Young Soccer Players, Front. Physiol. 9 (2018) 1611. https://doi.org/10.3389/fphys.2018.01611.
[168] N.M. Youssef, A.M. Abdelmohsen, A.A. Ashour, N.M. Elhafez, S.M. Elhafez, Effect of different balance training programs on postural control in chronic ankle instability: A randomized controlled trial, Acta Bioeng. Biomech. 20 (2018) 159–169. https://doi.org/10.5277/ABB-01101-2018-02.
[169] J. Hertel, M.R. Gay, C.R. Denegar, Differences in Postural Control During Single-Leg Stance Among Healthy Individuals With Different Foot Types., J. Athl. Train. 37 (2002) 129–132. http://www.ncbi.nlm.nih.gov/pubmed/12937424 (accessed November 19, 2020).
[170] B.L. Riemann, J.B. Myers, S.M. Lephart, Comparison of the ankle, knee, hip, and trunk corrective action shown during single-leg stance on firm, foam, and multiaxial surfaces, Arch. Phys. Med. Rehabil. 84 (2003) 90–95. https://doi.org/10.1053/apmr.2003.50004.
[171] T. Zumbrunn, B.A. MacWilliams, B.A. Johnson, Evaluation of a single leg stance balance test in children, Gait Posture. 34 (2011) 174–177. https://doi.org/10.1016/j.gaitpost.2011.04.005.
[172] A.K. Stensdotter, J. Bjerke, M. Djupsjöbacka, Postural sway in single-limb and bilateral quiet standing after unilateral total knee arthroplasty, Gait Posture. 41 (2015) 769–773. https://doi.org/10.1016/j.gaitpost.2015.02.005.
[173] M. Scholes, S. Stadler, D. Connell, C. Barton, R.A. Clarke, A.L. Bryant, P. Malliaras, Men with unilateral Achilles tendinopathy have impaired balance on the symptomatic side, J. Sci. Med. Sport. 21 (2018) 479–482. https://doi.org/10.1016/j.jsams.2017.09.594.
[174] M.G. Benedetti, M. Coli, L. Campanacci, M. Manfrini, Postural control skills,

proprioception, and risk of fall in long-term survivor patients treated with knee rotationplasty, Int. J. Rehabil. Res. 42 (2019) 68–73. https://doi.org/10.1097/MRR.0000000000000331.
[175] Y. Ivanenko, V.S. Gurfinkel, Human Postural Control , Front. Neurosci. . 12 (2018) 171. https://www.frontiersin.org/article/10.3389/fnins.2018.00171.
[176] M.L. Madigan, B.S. Davidson, M.A. Nussbaum, Postural sway and joint kinematics during quiet standing are affected by lumbar extensor fatigue, Hum. Mov. Sci. 25 (2006) 788–799. https://doi.org/10.1016/j.humov.2006.04.004.
[177] R.J. Doyle, E.T. Hsiao-Wecksler, B.G. Ragan, K.S. Rosengren, Generalizability of center of pressure measures of quiet standing, Gait Posture. 25 (2007) 166–171. https://doi.org/10.1016/j.gaitpost.2006.03.004.
[178] C. Caballero, D. Barbado, F.J. Moreno, What COP and Kinematic Parameters Better Characterize Postural Control in Standing Balance Tasks?, J. Mot. Behav. 47 (2015) 550–562. https://doi.org/10.1080/00222895.2015.1014545.
[179] O. Levin, A. Van Nevel, C. Malone, S. Van Deun, J. Duysens, F. Staes, Sway activity and muscle recruitment order during transition from double to single-leg stance in subjects with chronic ankle instability, Gait Posture. 36 (2012) 546–551. https://doi.org/10.1016/j.gaitpost.2012.05.009.
[180] F.B. Horak, Postural orientation and equilibrium: What do we need to know about neural control of balance to prevent falls?, in: Age Ageing, Oxford Academic, 2006: pp. 7–11. https://doi.org/10.1093/ageing/afl077.
[181] F. Smithson, M.E. Morris, R. Iansek, Performance on clinical tests of balance in Parkinson's disease, Phys. Ther. 78 (1998) 577–592. https://doi.org/10.1093/ptj/78.6.577.
[182] G. Nilsson, E. Ageberg, C. Ekdahl, M. Eneroth, Balance in single-limb stance after surgically treated ankle fractures: A 14-month follow-up, BMC Musculoskelet. Disord. 7 (2006) 1–8. https://doi.org/10.1186/1471-2474-7-35.
[183] E. Ageberg, D. Roberts, E. Holmström, T. Fridén, Balance in Single-Limb Stance in Patients with Anterior Cruciate Ligament Injury: Relation to Knee Laxity, Proprioception, Muscle Strength, and Subjective Function, Am. J. Sports Med. 33 (2005) 1527–1537. https://doi.org/10.1177/0363546505274934.
[184] F.A. Hazime, P. Allard, M.R. Ide, C.M. Siqueira, C.F. Amorim, C. Tanaka, Postural control under visual and proprioceptive perturbations during double and single limb stances: Insights for balance training, J. Bodyw. Mov. Ther. 16 (2012) 224–229. https://doi.org/https://doi.org/10.1016/j.jbmt.2011.02.003.
[185] R. Collings, J. Paton, S. Glasser, J. Marsden, The effect of vision impairment on dynamic balance, J. Foot Ankle Res. 8 (2015) A6. https://doi.org/10.1186/1757-1146-8-S1-A6.
[186] T. Robert, V.M. Zatsiorsky, M.L. Latash, Multi-muscle synergies in an unusual postural task: Quick shear force production, Exp. Brain Res. 187 (2008) 237–253. https://doi.org/10.1007/s00221-008-1299-7.
[187] W.-C.C. Yang, C.-H.H. Cheng, H.-K.K. Wang, K.-H.H. Lin, W.-L.L. Hsu, Multi-muscle coordination during a challenging stance, Eur. J. Appl. Physiol. 115 (2015) 1959–1966. https://doi.org/10.1007/s00421-015-3158-0.
[188] L.A. Kelly, S. Kuitunen, S. Racinais, A.G. Cresswell, Recruitment of the plantar intrinsic foot muscles with increasing postural demand, Clin. Biomech. 27 (2012) 46–51. https://doi.org/10.1016/j.clinbiomech.2011.07.013.
[189] J.A. Pruszynski, I. Kurtzer, J.Y. Nashed, M. Omrani, B. Brouwer, S.H. Scott, Primary motor cortex underlies multi-joint integration for fast feedback control, Nature. 478 (2011) 387–390. https://doi.org/10.1038/nature10436.
[190] L.H. Ting, J.L. McKay, Neuromechanics of muscle synergies for posture and movement, Curr Opin Neurol. 17 (2007) 622–628. https://doi.org/10.1016/j.conb.2008.01.002.
[191] G. Grimby, M. Börjesson, I.H. Jonsdottir, P. Schnohr, D.S. Thelle, B. Saltin, The "Saltin-Grimby Physical Activity Level Scale" and its application to health research, Scand. J. Med. Sci. Sports. 25 (2015) 119–125. https://doi.org/10.1111/sms.12611.
[192] H.J. Hermens, B. Freriks, C. Disselhorst-Klug, G. Rau, Development of recommendations for SEMG sensors and sensor placement procedures, J. Electromyogr. Kinesiol. 10 (2000) 361–374. https://doi.org/10.1016/S1050-6411(00)00027-4.
[193] N. Benjuya, I. Melzer, J. Kaplanski, Aging-Induced Shifts from a Reliance on Sensory Input to Muscle Cocontraction during Balanced Standing, Journals Gerontol. - Ser. A Biol. Sci. Med. Sci. 59 (2004) 166–171. https://doi.org/10.1093/gerona/59.2.m166.
[194] S. Baudry, G. Lecoeuvre, J. Duchateau, Age-related changes in the behavior of the muscle-tendon unit of the gastrocnemius medialis during upright stance, J. Appl. Physiol. 112 (2012) 296–304. https://doi.org/10.1152/japplphysiol.00913.2011.

[195] E. Kurz, O. Faude, R. Roth, L. Zahner, L. Donath, Ankle muscle activity modulation during single-leg stance differs between children, young adults and seniors, Eur. J. Appl. Physiol. 118 (2018) 239–247. https://doi.org/10.1007/s00421-017-3764-0.
[196] R. Creath, T. Kiemel, F. Horak, R. Peterka, J. Jeka, A unified view of quiet and perturbed stance: Simultaneous co-existing excitable modes, Neurosci. Lett. 377 (2005) 75–80. https://doi.org/10.1016/j.neulet.2004.11.071.
[197] R.J. Peterka, Sensorimotor integration in human postural control, J. Neurophysiol. 88 (2002) 1097–1118. https://doi.org/10.1152/jn.2002.88.3.1097.
[198] T.A.L.L. Wren, G.E. Gorton, S. Õunpuu, C.A. Tucker, Efficacy of clinical gait analysis: A systematic review, Gait Posture. 34 (2011) 149–153. https://doi.org/10.1016/j.gaitpost.2011.03.027.
[199] V. Agostini, S. Rosati, C. Castagneri, G. Balestra, M. Knaflitz, Clustering analysis of EMG cyclic patterns: A validation study across multiple locomotion pathologies, in: 2017 IEEE Int. Instrum. Meas. Technol. Conf., IEEE, 2017: pp. 1–5. https://doi.org/10.1109/I2MTC.2017.7969746.